SOME STUDIES ON TRANSPORT PHENOMENA IN PRESENCE OF A BLUFF BODY

Thesis submitted by

SUDHIR CHANDRA MURMU

Doctor of Philosophy (Engineering)

Department of Mechanical Engineering,

Faculty Council of Engineering & Technology

Jadavpur University

Kolkata, India

2019

JADAVPUR UNIVERSITY

KOLKATA-700032

<u>**INDEX NO**</u>. 20/14/E

1.	**Title of the thesis:**	**Some Studies on Transport Phenomena in Presence of a Bluff Body**
2.	**Name, Designation & Institution of the Supervisor/s:**	Dr. Himadri Chattopadhyay Professor Department of Mechanical Engineering Jadavpur University Dr. Amitava Sarkar Professor(Retired) Department of Mechanical Engineering Jadavpur University

3. **List of publication:**

    1 **Sudhir Chandra Murmu**., Himadri Chattopadhyay, Transport Phenomena around bluff body at varying inlet turbulent intensity, *Heat transfer research*, *accepted*.

    2 **Sudhir Chandra Murmu,** Himadri Chattopadhyay, Effect of different bluff bodies on heat transfer enhancement in a channel flow- *Progress in Computational fluid dynamics - Under Review*.

    3 **Sudhir Chandra Murmu,** Himadri Chattopadhyay, Augmentation of heat transfer in a channel using a triangular prism with varying inlet turbulent intensity, Journal of enhanced heat transfer- *Under Review.*

4. **List of Patents:**   Nil

5. **List of Presentations in National / International :**

    1. S. C. Murmu, H. Chattopadhyay, A. Sarkar, "Numerical simulation of flow and heat transfer around circular cylinder" 1st International ISHMT-ASTFE Heat and Mass Transfer Conference, 17-20 December, 2015, ISRO, Kerala.

2. S. C. Murmu, H. Chattopadhyay, A. Sarkar, **"**Numerical simulation of flow and heat transfer around triangular prism**",** 6th International & 43rd National Conference on Fluid Mechanics and Fluid Power, 15-17th December,2016,MNNIT Allahabad, Uttar Pradesh.

3. S.Saha, S.C. Murmu, A. Chatterjee, H. Chattopadhyay, "Transport phenomenon around a diamond shape bluff body",6thInternational and 43rd National Conference on Fluid Mechanics and Fluid Power, Dec 15-17,2016,ISBN 978-93- 5267-408-4MNNIT Allahabad, India.

4. S.Saha, A.Chatterjee, H. Chattopadhyay," Augmentation of heat transfer a channel in presence of a diamond shape bluff body "National Conference on Advances in Thermal Engineering, Dec 23-24,2017 Jadavpur university, Kolkata, India.

5. S. C. Murmu, H. Chattopadhyay, **"**Transport phenomena over bluff bodies at varying inlet turbulent intensity**",** Computational Science Symposium, 16-18 March 2017, IISC, Bangalore.

CERTIFICATE FROM THE SUPERVISORS

This is to certify that the thesis entitled **"Some Studies on Transport Phenomena in Presence of a Bluff Body"** submitted by **Shri Sudhir Chandra Murmu** who got his name registered on 20th August 2014 for the award of Ph.D. (Engg.) degree of Jadavpur University is absolutely based upon his own work under the supervision of *Dr. Himadri Chattopadhyay*, Professor, Department of Mechanical Engineering, Jadavpur University & *Dr. Amitava Sarkar (Retired)* Professor, Department of Mechanical Engineering, Jadavpur University and that neither his thesis nor any part of the thesis has been submitted for any degree/ diploma or any other academic award anywhere before.

Signature of Supervisor with seal   **Signature of Supervisor with seal**

Seal of the Supervisor   **Seal of the Supervisor**

को अद्धा वेद क इह प्र वोचत्कुत आजाता कुत इयं विसृष्टिः ।
अर्वाग्देवा अस्य विसर्जनेनाथा को वेद यत आबभूव ॥

(Rig-Veda, Mandal 10)

*(But then who can say where the creation started and where from?
Even the Gods came after that.)*

Dedicated to
My family

<u>ACKNOWLEDGEMENT</u>

ABSTRACT

Transport phenomena around bluff bodies have been a subject of considerable research interest. Heat transfer characteristics inside a channel in presence of bluff body and effect of turbulence level on transport process around bluff bodies encompassing laminar and turbulent regime covering a Reynolds number range of 10-2,00,000 along with turbulence intensities varying from 5% to 40% are studied in this work. Here bluff bodies of five different shapes are considered, namely a) Circular cylinder, b) Square cylinder, c) Equilateral triangular prism, d) Diamond and e) Trapezium shape bluff bodies.

The effect of turbulence intensity on the transport phenomena over two-dimensional bluff bodies is investigated. The governing equations of continuity, momentum, and energy equations are solved along with transition SST Model for the closure of turbulence. The simulation results are validated with experimental correlations that show good agreements. This work demonstrates that the transition SST Model can effortlessly bridge all flow regimes for predicting the heat transfer. The study quantifies the effect of inlet turbulence intensity on enhancing heat transfer from the bluff bodies. The drag and pressure coefficients are found to be unaffected by inlet turbulent intensity.

An operative study of different bluff bodies is incorporated in this work. The bluff bodies are taken triangular prism, diamond and trapezoidal shaped bodies with the identical hydraulic diameter D, which is further the non-spatial length scale. The flowing medium i.e., the air is considered to have a constant Prandtl number (0.71). This work explains that transition SST Model can effortlessly link all flow regimes for predicting the heat transfer. The study quantifies the effect of inlet turbulence intensity on improving heat transfer from different bluff bodies.

As part of the present work, an attempt has been made to study the augmentation of heat transfer on a channel wall in the presence of the bluff body of different shapes. Heat transfer enhancement in a channel in presence of bluff bodies of different shape has been numerically investigated in the turbulent flow regime with Reynolds number ranging from 100-2,00,000. The hydraulic diameter of the bluff body (Three different shapes namely Triangular Prism (TP), Diamond and Trapezoidal considers in this work) is taken as characteristic length. The inlet turbulent intensities are varied from 5% to 40%. The aspect ratio between channel to the bluff body is fixed at 4. The velocities and pressures were

predicted using a semi-implicit pressure linked equations (SIMPLE) scheme. The results show that in the presence of triangular prism, heat transfer in a channel is augmented by around 10%. The presence of TP enhances heat transfer all through the downstream region. The analysis shows that the amount of enhancement increases with inlet turbulent intensity. The study quantifies the effect of inlet turbulence intensity on enhancing heat transfer from all other bluff bodies. Augmentation is associated with higher values of the skin friction coefficient on the channel wall. The Augmentation is also expressed as a percentage increased of heat transfer from a similar system without the diamond bluff body. For trapezoidal bluff body different configurations as (a) large edge of trapezium facing the flow (b) small edge facing flow and (c) trapezium is symmetrically placed is considered. Results show that the small edge facing upstream show better heat transfer performance. The thermohydraulic efficiency for three bluff bodies is also computed.

Research Publications from this Thesis

- *Journals*

1. **Sudhir Chandra Murmu**., *Himadri Chattopadhyay, Transport Phenomena around bluff body at varying inlet turbulent intensity, Heat transfer research, accepted.*

2. **Sudhir Chandra Murmu**, *Himadri Chattopadhyay., Numerical simulation of flow and heat transfer over bluff body at varying inlet turbulent intensity, Heat Transfer Research - Under Review.*

3. **Sudhir Chandra Murmu**, *Himadri Chattopadhyay, Effect of different bluff bodies on heat transfer enhancement in a channel flow- Progress in Computational fluid dynamics - Under Review.*

4. **Sudhir Chandra Murmu**, *Himadri Chattopadhyay, Augmentation of heat transfer in a channel using a triangular prism with varying inlet turbulent intensity, Journal of enhanced heat transfer- Under Review.*

- **Conferences**

1. S. C. Murmu, H. Chattopadhyay, A. Sarkar, "Numerical simulation of flow and heat transfer around circular cylinder" 1st International ISHMT-ASTFE Heat and Mass Transfer Conference, 17-20 December, 2015, ISRO, Kerala.

2. S. C. Murmu, H. Chattopadhyay, A. Sarkar, "Numerical simulation of flow and heat transfer around triangular prism", 6th International & 43rd National Conference on Fluid Mechanics and Fluid Power, 15-17th December,2016,MNNIT Allahabad, Uttar Pradesh.

3. S.Saha, S.C. Murmu, A. Chatterjee, H. Chattopadhyay, "Transport phenomenon around a diamond shape bluff body",6thInternational and 43rd National Conference on Fluid Mechanics and Fluid Power, Dec 15-17,2016,ISBN 978-93- 5267-408-4MNNIT Allahabad, India.

4. S.Saha, A.Chatterjee, S.Murmu, *H. Chattopadhyay, " Augmentation of heat transfer a channel in presence of a diamond shape bluff body "National Conference on Advances in Thermal Engineering, Dec 23-24, Jadavpur university, Kolkata, India.*

5. S. C. Murmu, *H. Chattopadhyay, "Transport phenomena over bluff bodies at varying inlet turbulent intensity", Computational Science Symposium, 16-18 March 2017, IISC, Bangalore.*

6. S. C. Murmu, *H. Chattopadhyay, Augmentation of heat transfer in a channel using a triangular prism with varying inlet turbulent intensity", December 27-30, 2017, BITS Pilani, Hyderabad,.*

7. S. C. Murmu, H. Chattopadhyay, "Numerical simulation of flow and heat transfer around trapezoidal shape bluff body", 1st International Conference on Mechanical Engineering, 4th - 6th January, 2018, Jadavpur University, Kolkata.

8. S.C. Murmu, *H. Chattopadhyay, "Numerical simulation of flow and heat transfer around trapezoidal shape bluff body, 5th International Conference on Computational Methods for Thermal Problems, $9^{th} – 11^{th}$ July, 2018, IISC Bangalore, India*

TABLE OF CONTENTS

List of figures

List of Tables   *Page no.*

Nomenclatures

Abbreviations

RANS Reynolds Averaged Navier-Stokes

SST Shear Stress Transport

Symbols

a transitional model constant

A transitional model constant

C_{a_1}, C_{a_2} intermittency constant

C_{e_1}, C_{e_2} intermittency constant

C_d drag coefficient

C_f Skin friction coefficient

C_p Pressure coefficient

D Diameter of the bluff body, m

E model destruction terms

F_1, F_2 blending functions in SST model

F_{onset} transition onset

f Friction factor

H Height of the computational domain, m

h heat transfer coefficient w/m^2-k

k thermal conductivity, w/m-k

L Length of computational domain, m

Nu Nusselt number based on diameter

$\overline{Nu}$ Average Nusselt number

p pressure, Pa

P model production term

Pr Prandtl number

Re Reynolds number based on bluff body diameter

R_{θ_c} critical Reynolds number

S absolute value of the shear strain rate, s^{-1}

SST shear stress transport

TI turbulence intensity

T_s bluff wall temperature, K

T_∞ free stream temperature, K

U_∞ free stream velocity, m/s

x_i tensor coordinate direction

x, y, z Cartesian coordinates

Greek symbols

α thermal diffusivity, m^2/s

β_1, β_2 SST model constants

μ dynamic viscosity. kg/m-s

κ turbulent kinetic energy, m^2/s^2

ν kinematic viscosity, m^2/s

σ Prandtl-like diffusivities

γ intermittency

η thermo-hydraulic performance parameter

ω specific rate of turbulence dissipation, s^{-1}

Π intermittency adjunct function

ρ density, kg/m^3

Θ dimensionless temperature

Θ azimuthal angle, degree

τ wall shear stress, N/m^2

Ω vorticity magnitude

Subscripts

avg   average

eff   effective property

i, j   tensor notations

turb   turbulent

x, y, z   Cartesian coordinates

Chapter

1

Introduction

1. 1. Background

Flow around a bluff body in ducts and channels have been investigated intensively by many researchers both experimentally and numerically. Over the decade's meticulous research efforts have been carried out to a broader understanding of the fluid flow and heat transfer past bluff bodies of various cross-section geometries. Most of the effort is dedicated to analyzing the complex flow physics and thermo-fluid transport phenomenon for circular, square and rectangular shaped bodies. Fluid flows are classified as external flow and internal flow, depending on whether the fluid is flowing over the surface or in the conduit. External flow generally shows a very different character concerning internal flow. A bluff body (i.e. external flow) is one in which the length in the flow direction is close or equal to the length perpendicular to the flow direction. Otherwise, a body is referred to as bluff and a significant pressure drag is associated with it. In general, the value of the Reynolds number is large for heating, cooling systems for nuclear power plants. However, in lines, offshore structures, buildings, chimneys, stints, grids, screens, and cables, in both air- and water-flow where recently a lot of emphases is being given, Re can be relatively low. In specific terms, the flow around circular cylinders shows various important physical phenomena, such as separation of flow, vortex shedding and also the shifting of flow from laminar to turbulence. It is the shape of the bodies which determined the form of flow and the energy transformation and flow characteristics.

1.1.1 Drag force

A body moving through a fluid experience a drag force, which is usually divided into two components :(a) frictional drag, and (b) pressure drag. Frictional drag comes from friction between the fluid- and the surface over which it is flowing. This friction is associated with the development of the boundary layers, and it scales with Reynolds number. Pressure drag comes from the eddying motions that are set up in the fluid by the passage of the body. This drag is associated with the formation of a wake, which can be readily seen behind a passing boat, and it is usually less sensitive to Reynolds number than the frictional drag. Formally, both types of drag are due to viscosity (if the body was moving through an inviscid fluid there would be no drag at all), but the distinction is useful because the two types of drag are due to different flow phenomena. Frictional drag is important for the attached flows (that is, there is no separation), and it related to the surface area exposed to the flow. Pressure drag is important for separated flows, and it related to the cross-sectional area of the body.

1.1.2 Bluff bodies and streamlined bodies

When the drag is dominated by viscous drag, then it is called streamlined, and when it is dominated by pressure drag, then the body is called a bluff body. Whether the flow is viscous-drag ruled or pressure drag ruled depends completely on the format of the body. A streamlined body views alike a fish, or an airfoil at small angles of attack, whereas a bluff body looks like a brick, a cylinder, or an airfoil at extensive angles of attack. For streamlined bodies, frictional drag is the controlling origin of wind resistance. In the case of the bluff body, the ruling source of drag is pressure drag. For a given frontal region and velocity, a streamlined body will continually have an inferior resistance compare to a bluff body. Pressure drag and frictional drag which is based on the pressure variation between the upstream and downstream facial of the substance. Fig 1.1 illustrates a bluff body and streamlined body.
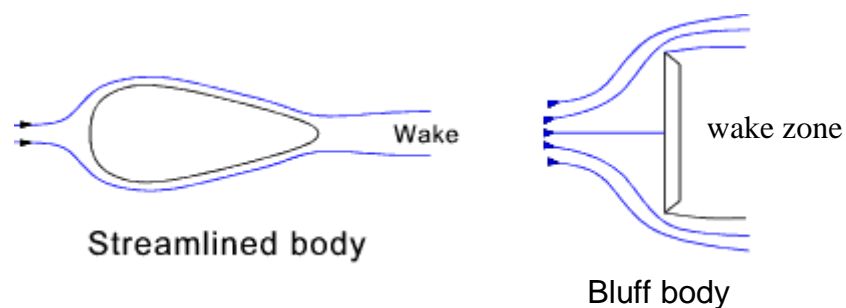
Figure 1.1: Streamline and bluff body

Especially bluff body can be characterized as a body that, as a result of its shape, has divided flow over a significant section of its surface. A valuable feature of the bluff body flow is that there is really powerful communication between the vicious and in viscous domains. Break-up may happen either from a sharp corner or from a maintained surface. Forecast of break-up point from a constant surface is specifically tough the formate of the adjacent wake zone. Further, the separation location may change in feedback to pressure gradients to appoint by unsteady flow features in the wake. Normally bluff bodies induce flow disengagement at the location where the velocity at the border of the edge layer is higher than the free stream velocity. This leads to a huge ratio of shedding of circulation which in shift leads to a big drag also due to the production and shedding of a comprehensible whirlpool, wide unsteady forces may grow, especially in a direction across to the flow direction. Spheres, cylinders, triangular prism, etc. are treated bluff bodies because at wide Reynolds number the drag is governed by the pressure fall in the wake. Circular cross-

division members are a universal shape used in offshore design and therefore it is fortunate that the circular cylinder is further the most thoughtful bluff body structure. Currently, the unstable viscous flow past bluff bodies and the effect vortex shedding has been the centre of attention of plentiful numerical investigation and experimental analyses. The variation of the drag coefficient with Reynolds number is shown in figure 1.2 and the corresponding flow structures are shown in figure 1.3. We noticed that as the Reynolds number rises the difference of drag coefficient (based on cross-sectional area) drop, and over a wide area in Reynolds number, it is approximately consistent.
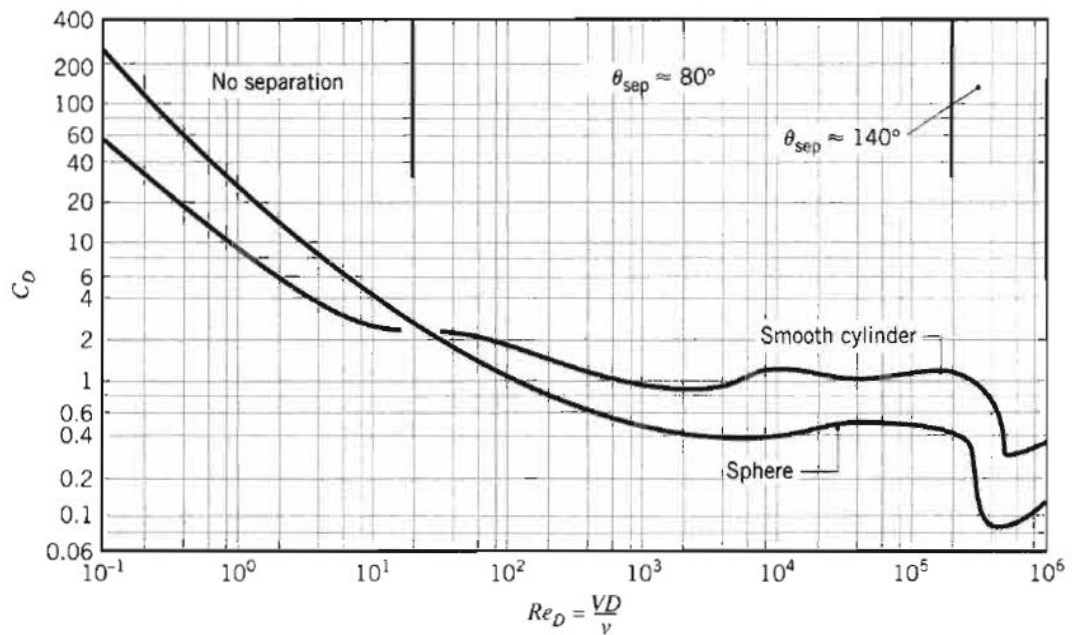
Figure 1.2: Drag coefficient as a function of Reynolds number for smooth circular cylinders and smooth spheres (Incorpera, 2006)
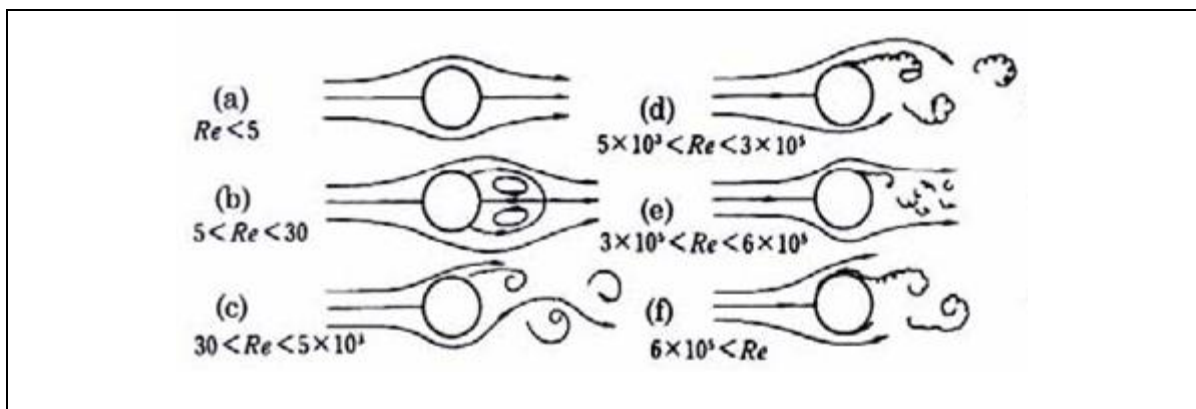
Figure 1.3: Flow arrangement at various Reynolds numbers over circular cylinder (Incorpera, 2006)

1.1.3 Aerodynamic body and bluff body

Aerodynamic bodies are those characterized by thin boundary layers completely attached over their whole surface, which leave behind them generally thin and steady wakes containing vorticity. The aerodynamic forces acting on these bodies may be evaluated through the potential flow-boundary layer procedure. Conversely, bluff bodies are characterized by a more or less precocious separation of the boundary layer from their surface, and by wakes having significant lateral dimensions and normally unsteady velocity fields.

1.1.4 Application of bluff bodies

On the engineering application, there are several devices in mechanical, civil and another engineering, where circular and cylindrical structures are used. Cylinder-like structures are found in both alone and a group, in the designs for heat exchangers for locomotive, cooling system for nuclear power plants, offshore structures, building chimneys, power lines, grids, screens, and cables, in both air and water as the flowing medium. Tube banks of different cross sections are also often encountered.

1.1.5. External flows

External flows are characterized as the flows deeply involved in an unbounded fluid. A body immersed in a fluid experience a resultant force due to the communication between the body and fluid ambiance. In few cases, the body shift in a static fluid medium (like the movement of an airplane) while in few occasion, the fluid passes around a fixed article (such as the motion of wind over a replica in an air channel). In several cases, one can fix the coordinate system in the body and treat the condition as the flow past a static body at a uniform velocity U_∞, well-known as upstream/free-stream velocity. Though, there are significant cases where the flow is not uniform. Even, the flow in the proximity of the object can be irregular in the case of a steady, consistent upstream flow. For cases, when air blast over a towering building, various velocities are sense at the highest and lowest portion of the building. But, the unstableness and non-consistency are of lesser significant somewhat the flowing nature on the surface of the body is greater valuable. The pattern of the body (like cutting-tip, blunt or streamline) influence the design of external flow. For the study viewpoint, the bodies are normally classified as, two-dimensional objects (infinitely lengthy

and fixed cross-section), axi-symmetric bodies and three-dimensional objects. In such a flow border coating grow openly without restraint set by adjoining surfaces. Appropriately there will consistently exist an area of the flow outside the boundary layer in which temperature, velocity, and/or consolidation slop are trivial. For example fluid movement around a flat plate (this may be inclined or parallel to the free flow velocity) and flow around arc facial e.g. a cylinder, airfoil or turbine blade, sphere.

Many attracting phenomena happen in an external viscous flow past an item. For a given structure of the object, the features of the stream depend much actively on deliberate parameters like size, orientation, speed, and fluid properties.

1.1.6. Flow Separation

The appearance of the fluid viscosity sluggish down the fluid fragment much adjacent to the solid facial and create a lean lazy-moving fluid coating called a boundary layer. The stream velocity is zero at the surface to gratify the no-slip boundary condition. Indoors the border layer, flow momentum is quite low since it knowledge a substantial viscous stream resistance. Thus, the boundary layer stream is sensible to the outer pressure slop (while the shape of a pressure force acting upon fluid fragments If the pressure reduce in the direction of the stream, the pressure slope is spoken to be favourable. In this circumstance the pressure force can help the fluid motion and there is no stream delay. However, if the pressure is rising in the direction of the flow, an conflicting pressure slop situation as so it is called exist More to the existence of a substantial viscous force, the fluid fragments now have to shift against the rising pressure force. That's why, the fluid fragments could be interrupted or turned around, causing the bordering fragments to shift abroad from the surface. This phenomenon is called the boundary layer separation.

1.1.7. Bluff body wake

Consider a fluid particle flows within the boundary layer over the circular cylinder. From the pressure allocation calculated in a previous experiment, at the stagnation point, the pressure is a highest and uniformly diminishing along the frontal part of the cylinder. The flow hold connects in this favourable pressure zone as expected. Still, the pressure beginning to raise in the back half of the cylinder and the fragment presently knowledge an opposing pressure slopes. Therefore, the flow split from the surface and developing a highly turbulent zone following the cylinder which called the wake. The pressure interior the wake zone debris low

as the flow split and a profiting pressure force (pressure drag) is formed. Many researchers investigate the wake characteristics behind the bluff body. Some of works are describe below.

Dutta et al.(2004) studied the impact of coordination on the wake of a square cylinder at laminar region. The experimental research of flow past a square cross section of cylinder at Reynolds number range of Re=97-187 is stated. Cylinder coordination of 0^0-60^0 with regard to the mean flow has been treated. Two part hotwire anemometry has been take-up for calculations of velocity. The cylinder's wake has been anticipated with a pulsed laser coat to know the flow formation. Calculations have been performed at the near wake, mid wake and far wake of the cylinder. The impact of coordination and Reynolds number on drag coefficient, Strouhal number, time average and rms velocity allocation, collapse of velocity oscillations and power spectra are of concern. The drag coefficient and Strouhal number are comparing to the angle of cylinder. A variation in the cylinder adjustment experienced to an initial arrival of quasi-periodicity and therefore, three dimensionality, unpaid to the irregular kind of the wake. The structure of the mean velocity portrait, oscillations and the rate of collapse display a active reliance on the cylinder adjustment in the adjacent wake, however dependency decrease in the far wake. In a group of angle considered, the wake of a cylinder whose orientation is 22.5^0 with regard to the incoming flow is unusually energetic and display powerful three-dimensionality.

Samani and Bergstrom (2015) had performed the influence of a solid wall on the wake design of an infinite cylinder of square cross-section when it is placed in proximity to the wall. Three different values of the gap ratio were considered, namely g=D 0,0.5 and 1, also to the reference case of a cylinder in a free stream with no wall. The Reynolds number which based on the cylinder width and free stream velocity was Re =500. A coarse-grid Large Eddy Simulation was employ to anticipate the resolved-scale velocity and pressure fields.

An experimental analysis into logical design in the wake behind a circular disk was performed by **Lee et al.(1992)**. The spectral study and a conditional phase averaging method are used. In order to help clear up the form of the wake design, the velocity fluctuations were split into two manners: positive (+ve) mode and negative (−ve) mode, and the conditional averaging method was used to each mode individually. The wake exhibits a predominant vortex-shedding frequency and the corresponding Strouhal number is about 0·138. The phase angle between velocity fluctuations in the wake at the shedding frequency, measured by two hot-wires, changes very little for circumferential angular separations Ψ, below ±70° and

changes very quickly through 180° near Ψ = 90°. On average, vortices are shed alternately from diametrically opposite sides of the disk. Negative mode velocity fluctuations are dominant at small angular separations between the reference probe and the measurement probe. The probability of occurrence of the −ve mode decreases steadily and that of the +ve mode starts to increase with increasing angular separation between the probes and becomes dominant at Ψ = 180°. At Ψ = 90°, the two modes, which have velocity fluctuations that are 180° out of phase with each other, occur equally, and hence the velocity fluctuations cancel each other when they are averaged together in a conventional phase-averaging way.

Forbes et al. (2017) studied a progression of the computational methods in reproducing experimental data for a generic sports utility vehicle (SUV) geometry and an assessment on the influence of fixed and rotating wheels for this geometry. Initially, comparisons are made in the wake structure and base pressures between several CFD codes and experimental data. It was shown that steady-state RANS methods are unsuitable for this geometry due to large scale unsteadiness in the wake caused by separation at the sharp trailing edge and rear wheel wake interactions. unsteady RANS (URANS) offered no improvements in wake prediction despite a significant increase in computational cost. The detached-eddy simulation (DES) and Lattice–Boltzmann methods showed the best agreement with the experimental results in both the wake structure and base pressure, with LBM running in approximately a fifth of the time for DES. The study then continues by analysing the influence of rotating wheels and a moving ground plane over a fixed wheel and ground plane arrangement. The introduction of wheel rotation and a moving ground was shown to increase the base pressure and reduce the drag acting on the vehicle when compared to the fixed case. However, when compared to the experimental standoff case, variations in drag and lift coefficients were minimal but misleading, as significant variations to the surface pressures were present.

1.1.8. Vortex Shedding

The boundary layer split from the surface forms a free shear layer and is highly changeable. This shear layer will ultimately revolve into a various vortex and separate from the surface (a phenomenon called vortex shedding). Additional kind of flow inconsistency appear while the shear layer whirlpool shed from both the highest and lowest surfaces connect along one another. They shed alternatively from the cylinder and produce a continues vortex design (known as Karaman vortex street) in the wake. The whirlpool shedding take place at a various frequency and is a function of the Reynolds number. The dimensionless frequency of

the whirlpool shedding, the shedding Strouhal number, St = f D/V, is almost identical to 0.21 when the Reynolds number is greater than 1,000.

1.1.9. Vortex-Induced Vibrations

When whirlpool shed from the cylinder, unbalanced pressure allocations establish between the top and bottom surfaces of the cylinder, producing an fluctuating aerodynamic loading (lift) on the cylinder. This unsteady force can induce important vibrations on a design, particularly if the "resonance "situation is connect. The best popular example is the breakdown of bridge in 1940 under the action of wind-induced vibrations. It is trust that natural whirlpool shedding frequency trailing the bridge matches one of the sonorous method of the bridge and eventually lead to a disaster vibration that damage the bridge.

Hydraulic diameter

For flow through non circular pipes the Reynolds numbers is based on the hydraulic diameter. It is expressed as given below.

$$D_h = \frac{4A}{P}$$

A cross sectional area and P   wetted perimeter of the cross section

Hydraulic diameter is mainly employ for computation for turbulent flow. Hydraulic diameter is further utilizing in calculation of heat transfer in internal flow problems. In figure 1.5 some geometry and their formulas are given below.
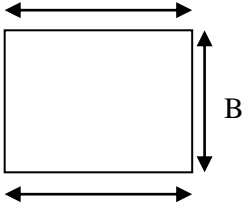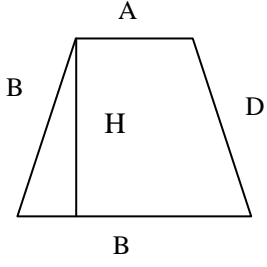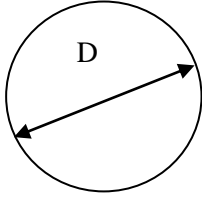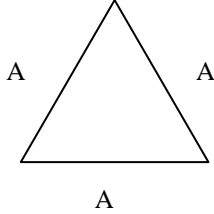
Type of Geometry	Hydraulic diameter
	Square $$D_h = \frac{4B^2}{4B} = B$$
	Trapezium $$D_h = \frac{(A + B) \times H}{2(A + B + C + D)}$$
	Circular $$D_h = \frac{4(\pi D^2)}{4\pi D} = D$$
	Equilateral triangle prism, $$D_h = \frac{A}{\sqrt{3}}$$

Figure 1.4: Formula of hydraulic diameter for different geometry

1.2 Thesis Organization

The present thesis comprises of seven chapters.

- In chapter **1**, a brief introduction has been given about the difference between the bluff body and stream line body, its applications, the flow field, and its classifications.

Also details about the hydraulic diameter of circular, square and rectangular ducts and their formulae are enumerated.

- *Chapters 2 includes* an extensive literature review of the entire thesis. This section is divided into four parts. This consists of a literature survey of numerical simulation around bluff body, vortex flow around bluff body and augmentation on the channel wall. Based on the literature survey objectives were itemized in the final part of chapter two.

- *Chapter 3* deals with the mathematical modeling of the computational method which is utilized for a current research task. The transition SST mode which can simulate laminar, transition and turbulent regions seamlessly, is described. Parameters applied to evaluate performance such as global and local distributions of Nusselt number and drag coefficient are described.

- *Chapter 4* deals with the analysis of transport phenomena around different shapes bluff bodies. This analysis further covers the effect turbulence intensity on heat transfer covering a large range of Reynolds number containing laminar, transition and turbulent regimes. Also, the TI effect on drag value and pressure coefficient is studied here.

- The next *Chapter 5* deals with augmentation on a channel wall in the presence of a bluff body. The bluff bodies are again considered of different shapes. Comparative performance analysis in bringing out enhancement is demonstrated.

- *Chapter 6* briefly describes the conclusions drawn from the analysis done in this study. The limitations and future scope pertaining to this work is finally highlighted.

<u>**CHAPTER 2**</u>

LITERATURE REVIEW

The subject of heat transportation with numerical simulation and vortex flow around the bluff body has been introduced in Chapter 2. In this section, a detailed state-of-art is presented.

2. STATE OF ART

In this section, attention is focussed on two aspects of bluff body flow studies. One is related to transport phenomena around bluff bodies. The other one is about enhancement of heat transfer in ducts in channel in presence of bluff body. Thus the first one involves looking at the detailed distribution of transport coefficients around the bluff body and in case of augmentation, focus is shifted to the channel wall which is affected by the presence of the bluff body.

2.1 Literature review on transport phenomena around bluff body

2.1.1 Studies on numerical simulation around bluff body

Distribution of local pressure and skin friction around a smooth circular cylinder in cross-flow has been studied by **Achenbach (1968)** with a large range of Reynolds number up to Re=5×10^6. The higher Reynolds number achieved in test channel which could be pressurized up to 40 bar. Experiments were carried out to measure the local pressure and skin friction distribution around the cylinder. The total drag, pressure drag, and friction drag were computed. Utilizing skin friction allocation the location of the separation point, transition point or separation bubble can be bounded. This results showed three different category of flow: sub-critical flow, where the boundary layer separates laminarly, critical flow, where a separation bubble, followed by a turbulent reattachment, happen and supercritical flow, in which an instantaneous transition from laminar to turbulent boundary layer is found at a critical gap from the stagnation point.

The experimental study of transport process in the near wake of a circular cross-section of a Reynolds number, Re=1, 40,000 by **Brian(1983).** The wake of flow was measured using X-array hotwire probes which were mounted on a pair of rotating arm. These hotwire approach raised the relative velocity component on the axis of the probe. For generating an intermittency signal an analog circuit was used and incorporated a fast surface pressure sensor to produce a phase signal integrate using the vortex shedding technique. The

protections of turbulence signify that turbulent energy was formed at the largest scale of the flow and soon after relocated by a cascade technique to a lower scale. The outcome of this experiment is that sizeable fractions of the turbulent energy are formed mainly at intermediate or even short scales near saddle in the flow decoration and are later transported to and gather at a centre whose larger scale may be carefully visible in uniform spectra or interrelation.

The computations of incompressible high Reynolds number flow over a circular cylinder with surface roughness were studied by **Kawamura et al. (1985)** in which Navier Stokes equations with the finite difference method was integrated. A statement coordinate setup was used so as to distribute the enough number of grids point in the wake and boundary layer region. The computations were done at Reynolds number, Re=1,200 and the corresponding results were compared with experimental results which showed reasonably good agreement. The computations series found out on the flow over the circular cylinder with surface roughness. In this computation, the height of roughness was 0.5% of the diameter. No turbulence model was applied for the Reynolds number ranges from 1,000-1,00,000. The sudden decline of the drag coefficient was noticed close at Re=20,000. This signifies that the critical Reynolds number is captured in the current computation.

Nakamur and Ozono (19987) made a study on the work of the effect of free flow disturbance on the mean pressure allocation ahead the break-up droplet develop on a flat plate with rectangular best-side calculus. It was examined experimentally in a wind tunnel with disturbance generating grids. Attention was located on discovery the impact of turbulence scale. The ratio between the turbulence scale and plate thickness was around 0.5 to 24 for two values of TI of around 7 and 11.

It was observed that the major impact of free-flow disturbance decreased the break-up droplet. It gradually decreases with increasing turbulence intensity. The average pressure allocation along the decrease break-up droplet is unresponsive to altering the turbulence scale up to a scale ratio of about 2. Furthermore, an increase in the scale ratio it asymptotes towards the smooth-flow allocation. Which ultimately shows no meeting between disturbance and circular current shedding (the impinging-shear-layer fluctuation) in the average pressure allocation.

The numerical simulation of flows around cylinders with rectangular cross-section of different width -to height ratios of 0.4 to 8 which corresponding Reynolds number range from 100 to 1.2×10^3 which is performed by **Okajima et al.(1990).** It was observed that a few

impressive phenomena by which a flow over the cylinder with a B/H ratio of 2 was completely detached from the superior edge at the Reynolds number at about Re=800, with the B/H ratio of 2.8, a fully detached flow changed to an substitute reattachment flow at the Re=1.2×10³, and two ingredient with various Strouhal frequencies arrived in a flow field around the cylinder with the B/H ratio of 6 at the Re=800. Specifically, the flow arrangement critically modified when the B/H ratio is 2.8 and 6 about Re=500 to 1.2×10³. During the numerical simulation, the part with a large Strouhal frequency was induced through the vortices detached from the following edges and that the small Strouhal element was due to the fluctuations of flow up the edge surfaces guide by the change of detaching bubble.

Norberg (1993) performed an experimental investigation of the flow over rectangular cylinders at angles of attack 0⁰-90⁰. Pressure forces and moments for cylinders with side ratios B/A = 1, 1.62, 2.5 and 3 (shortest side A = 20 ram) were approximated from analysis of static pressure allotment at midspan. Strouhal numbers and wake frequencies were determined from hotwire measurements in the close to wake regions (A = 4 and 20 mm). The free stream turbulence intensity was less than 0.06%, blockages less than 5% and aspect ratios L/A greater than 50 were used in this work with Reynolds number ranging from Re=400-30,000 (Pressure calculation about Re=30,000).

Drag coefficient and Strouhal number are plotted against H/D in figure 2.1. A normal agreement with past analysis was found (Nakaguchi, 1968, Bearman, 1972 Nakamura1975, Knisely, 1990, Courchesne, 1979, Igarashi1, 1987). The most important characteristic is that in the range H/D=0-1, drag value undergoes a convincing turnover while the Strouhal number changes slightly through the reverse are true in the range H/D=2-3. The drag value reaches the maximum at nearby H/D=0.6
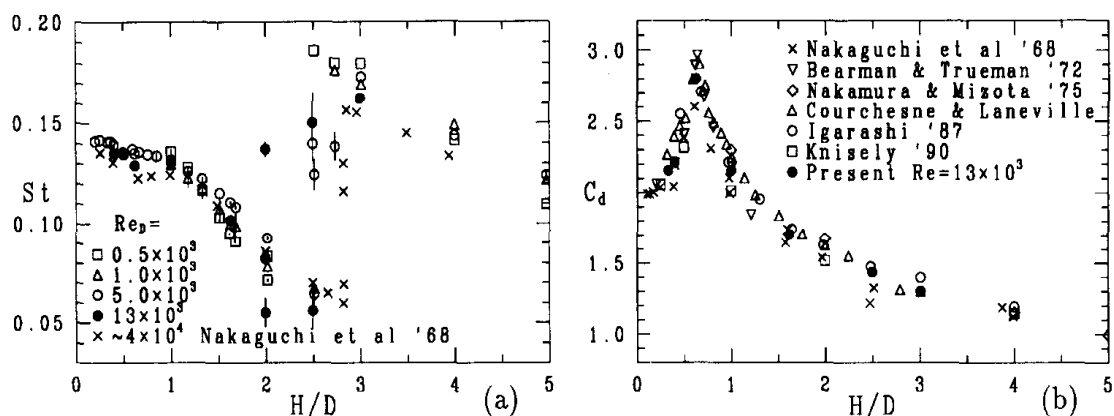
Figure 2.1. Strouhal number (a) and drag coefficient (b) vs *H/D* at low free stream turbulence, Norberg (1993)

Kondjoyan and Daudin (1995) showed the effect of free stream turbulence intensity on heat and mass transfer at a surface of a circular cylinder and an elliptical cylinder. Turbulence intensity ranging from 1.5 to 40% with Reynolds number ranging from 3,000 to 40,000 on transfer coefficients has been measured for a circular cylinder in cross-flow. The effect of turbulence intensity is important as the influence of velocity and it seemed to be independent of the pressure gradient and the degree of turbulence isotropy. It also showed that the heat transfers were much less affected by the cylinder axis ratio than by the air flow properties. It confirmed that the local transfer coefficient was much higher at the stagnation point of a circular cylinder than elsewhere at the surface.

An experimental analysis was performed to study the effect of free stream turbulence on surface pressures on a flat plate with rectangular cross section by **Li et al. (1995)** applying turbulence producing grids. The measured mean and crest pressure coefficients, standard deviation, pressure coefficients were reported and explained.

A comprehensive review of the impact of three-dimensionality on the lift and drag of nominally two-dimensional cylinders is performed by **Mittal and Balachandar(1995).** It has been admitted that two-dimensional numerical computations of flow around two-dimensional bluff bodies at Reynolds number for which the stream is basically three dimensional, starts to defect guess of the drag and lift coefficient.

In appropriate, for flow past a natural flat plate (International Symposium on Nckzsteady Fluid Dynamics, edited by J. A. Miller and D. P. Telionis, 1990, pp. 455-464) and circular cylinders [J. Wmd Eng. Indus. Aerodyn. 35,275 (1990)], it was observed that the CD value measured from two-dimensional computation was undoubtedly greater than what was obtained from experiments. Further the study showed that three-dimensional simulation of flows influence to exact guess of drag [J. Wind Eng. Indus. Aerodyn. 35, 275 (1990)]. The fundamental reason for this difference is that the surface pressure allocation achieves from two-dimensional computations does not match up with that get from experiments. In this study, the two and three-dimensional results of flow past circular and elliptical cylinder was uniformly distinguished to identify the accurate reason for the defective prediction of the lift and drag by two-dimensional simulations. This study also showed a detailed way of how the oscillations affect the mean pressure distribution and the aerodynamic forces on the body.

Convective heat transfer and pressure loss aspect in the rectangular tunnel with a staggered bunch of drop-structure pin fins in the mixed flow of air was experimentally investigated by

Chen et al. (1997). The effects of plans of pin fins on heat transfer and opposition were explained and the row-by-row differences of the average Nusselt numbers were given. By way of the heat/mass transfer similarity and the method of naphthalene sublimation, obtained the gain in film coefficients on pin fins and edge walls of the tunnel have been gain accordingly. The complete average heat transfer coefficients of pin fin tunnels were determined and the opposition coefficients were further examined.

A CFD study on the unsteady flow field past a square cross-section of two-dimensional cylinders was inspected by **Murakami et al. (1995).** The precision of the numerical simulation results was checked from different viewpoints. In the early part of the work, the comparison of the outcome of large eddy simulation (LES) for 2D and 3D simulations were represented. The LES results obtained from 3D simulation admit well with the experimental results, but the outcomes obtained from 2D computation were different from those located on 3D simulation including from those disposed of experiments. In the second part of the work verification of 3D LES simulations for the study of periodic and hypothetical oscillations, was done with corresponding specific experimental results. The LES computation results were further compared with those obtained from the Reynolds-averaged Navier-Stokes equations model (RANS) including those from experiments. Lastly, 3D LES simulation results of unsteady pressure field and wind force performing on the fluctuating square cylinder were conferred.

Li et al. (1997) carried out an experimental study to analyze the heat transfer and pressure drop nature in rectangular duct along a staggered bunch of shortened elliptical pin fins in an air's cross flow. By applying the heat and mass transfer similarity and the naphthalene sublimation approach, the mean heat transfer coefficients on pin fins and the base plate of the channel were reported, commonly. The total mean heat transfer coefficients and resistance coefficients of pin fins were found out. The empirical results showed that the heat deportation of a channel with elliptic pin fins was slightly bigger than that with circular pin fins while the struggle of old much lessened than that of the recent in the Reynolds number ranging from 1,00 to 10,000.

The analysis of the flow around rectangular cylinders was numerically predicted by **Nathan Steggel (1998).** The viscous flow around rectangles defined by after body length, B, and cross-stream dimension, A, was analyzed by a hybrid discrete vortex approach. For uniform flow conditions the effects of varying the side ratio, B/A, the angle of incidence, a, and the

Reynolds number, Re, were all considered. Pulsating flow results were recorded for rectangular cylinders with B/A values of 0.62, 1.0, 2.0 and 3.0, a B/A=1.0 cylinder inclined at 45° and a circular cylinder.

At a settled Reynolds number, Re=200, the alternation of drag coefficient with side ratio display CD increasing with decreasing B/A ratio. This variation with the accepted result at higher Reynolds number, $10^4 \leq Re \leq 10^5$, for which a maximum drag happened close to B/A=0.6. A peak was seen in both the Strouhal number and lift coefficient near to B/A=0.30. This is made clear by the after body elimination of the shear layer interaction. In the case of the square cylinder, results are granted for the alternation of drag coefficient and Strouhal number with Reynolds number, $50 \leq Re \leq 5 \times 10^3$. The analysis showed the good agreement with experiment. This study also presented a detailed view of how the oscillation take place.

The 'lock-in' natures under pulsating flow were shown to be extremely dependent on body geometry. All the cylinders were shown to display an asymmetric resonant mode within which the shedding frequency was controlled at half the forcing frequency and the mean forces increased. Several different shedding designs were predicted across this asymmetric synchronization range. A 'quasi-symmetric' mode was also seen for few cylinders characterized by near wake symmetry and a substantial reduction in mean forces. A pseudo-phase lag was defined which relates a moment of the life cycle to a moment of the forcing oscillation. Change across the synchronization range of each cylinder was considered and the change was found to be greater at lower forcing amplitude.

Scholten and Murray (1998) has studied unsteady heat transfer and velocity profile of a cylinder in cross-flow for Low free-stream turbulence. A method was developed for making simultaneous measurements of time-resolved velocity, using laser Doppler anemometry, and local heat flux, using a hot film sensor, at the surface of a cylinder in cross flow. The results that they found are the magnitude of fluctuations in heat transfer at the front of the cylinder is very small.

The 2D simulation at low-Reynolds-number flow around a square cylinder at incidence of 0^0-45^0 was numerically investigated by **Sohankar et al. (1998)**. The low Reynolds numbers were applying (45-200) so that the flow purely laminar. A Von Kármán vortex sheet was observed behind the cylinders with a periodicity which was good agreement with experiments. Also presented reported the Strouhal number and drag, lift and moment coefficients.

Fred et al. (1998) studied the pressure field over a rectangular prism using an advanced turbulence creation technique with constant turbulence intensity. Applying jets blowing parallel to the vital flow and impediment, the method produced a turbulent flow of variable scales. The effect of turbulence on the aero elastic stability of long-span bridges was reported here. The necessary scales of the incident flow had a meaningful impact on the flow form that happen in changes in rms, mean and contradictory peak pressure allocation. The fluctuating scale showed that scales had meaningful effects on the flow form. Up to critical value, growth of integral scale, with the related decreased in small scale content essential to keep up the constant turbulent intensity, changed mean, rms and bad crest pressure distribution. The crest of this allocation moved closer to the leading edge and the shapes of the distributions grow narrower on either side of the crest.

Unsteady turbulent adjacent wake of a rectangular cross section of a cylinder in tunnel flow was performed experimentally by using a laser Doppler velocimetry (LDV) which was analyzed by **Nakagawa et al. (1999).** The time-averaged and phase-averaged stats were calculated for the cylinder which having different width to height ratios, b/h. It was observed that the turbulent intensities on the centre line of the channel have their maxima adjacent to the back stagnation point of a recirculation domain. The profile of consistent vorticity and streamline created precisely the shed vortices from the cylinder was noticed during the flow visualization. The natures of the flow field was explained and a meaningful donation of the understandable form to the flow field was explained. Additionally, the turbulent kinetic energy budget was investigated.

Taylor, Ian J. (1999) showed the bluff body flow fields and aero elastic stability using a discrete vortex method. A two-dimensional discrete vortex method was developed to simulate the unsteady, incompressible flow field and aerodynamic loading on bluff bodies. The method was validated successfully on a range of simple bluff geometries, both static and oscillating, and was further validated on a wider range of problems including static and oscillating suspension bridge deck sections. The results were compared with experimental data and showed good qualitative and quantitative agreement, and also compared favorably with other computational methods. Most notably, the method was used to study the aero elastic stability of a recent bridge deck, with accurate predictions of the critical flutter velocity. A thorough literature review is presented, considering the nature of bluff body flows and the aero elastic phenomena associated with the unsteady flow field. Analytical methods was considered for studying these phenomena and other computational methods are reviewed. The basis of the method was the discretization of the vorticity field into a sense of

vortex particles, which were transported in the flow field that they collectively induce. In the method presented herein, the time evolution of the system of particles was calculated by solving the vorticity transport equation in two stages: employing the Biot-Savart law to calculate particle velocities and random walks to simulate flow diffusion. The Lagrangian approach to the calculation avoided the necessity for a calculation grid and therefore removed some of the problems associated with more traditional grid-based methods. These included numerical diffusion and difficulties in resolving small scale vortical structures. In contrast, vortex methods concentrated in areas of vorticity and provided high-quality representations of these small scale structures. Dispensing with a calculation mesh also eased the task of modelling a more arbitrary range of geometries. In particular, vortex methods were well suited to the analysis of moving body problems. The vortex method presented herein was originally developed to study dynamic stall on pitching aerofoils. The necessary modifications to enable the method to be used as a tool to study bluff body flow fields were presented. These included improvements to the modelling around sharp comers and an empirical procedure to account for three-dimensional effects in the wake. Also, a more efficient algorithm for the velocity calculation was implemented, reducing the computational operation count from $O(N_2)$ to $O(N+MogN)$. The procedure used a zonal decomposition algorithm, where the velocity influences of a group of vortex particles can be calculated using a series expansion. Results of the validation exercise were firstly presented for a range of simple bluff geometries to give confidence in the results before moving on to more complex geometries. These results include the effect of incidence on the aerodynamic loading for a stationary square cylinder, and also a study of the effect on aspect ratio for rectangular cylinders. This included the limiting case of a flat plate. Vortex lock-in was studied on a square cylinder undergoing a forced transverse oscillation, for a range of frequencies and amplitudes. The results in each of these cases were in good agreement with experimental data. The flutter instability on recent bridge design and also on the original Tacoma Narrows bridge section was considered. Predictions of the flutter derivatives and the critical flutter velocity on each section indicated the capability of the method to analyse the stability of bridge sections. A study of flow control devices, which were used to increase structural stability has been made, demonstrating how the vortex method could potentially be used as part of a design process to investigate a range of possible designs. It was anticipated that future work on the vortex method will include a link to a structural solver to give a full aero elastic model that can be used to analyse the flow around a wide range of geometries.

Another work, the turbulent wake behind a square cylinder was numerically investigated by **Saha et al. (2001).** The problem in this study was considered as two dimensional and Reynolds number are taken Re= 20,000. Two approaches were highlighted in terms of time-averaged flow, Strouhal number and aerodynamic forces. Simulations were done through direct solution and calculation by using the turbulence model. The time-averaged drag value and rms fluctuation which was obtained by direct calculation were higher than the results coming out by the turbulence model. The time-averaged drag value was decreasing with increase the shear parameter up to assured value. After that, it increased further increasing the shear parameter. The diversely lift coefficient increases with increased in the shear parameter. It is observed that the Strouhal number decreases with an increase in shear parameter though rms value of lift and drag coefficient increased with the shear parameter

The unsteady incompressible flow simulation of drag crisis past a circular cylinder was found out by **Singh et al. (2001)**. The 2-D Navier Stokes equations were solved with a finite element method in which Streamline Upwind/Petrov-Galerkin (SUPG) and Pressure-Stabilizing/Petrov-Galerkin (PSPG) for large Reynolds number(Re=10^5-10^6) were applied to compute drag crisis. The mean drag value was compared with experimental values. It was seen that flow at Re=10^6 separates much later from the surface of the cylinder compared to the Re=10^5. Also, the wake was narrower in the case of Re=10^6 compare to the Re=10^5. The time-averaged flow field displayed a continuing bubble just downstream of the flow separation point for the Re=10^5 where as it was not observed at Re=10^6.

E(k) was computed by summing $\bar{E}$(K)over a slim shell over k. Fig 2.2 displays the effect of several bands of k over energy spectra. The invariable change of E(k) is seen when the number of bands within the range of 200-300. But when the number of bands has crossed the range of 2,000, the spectrum converts oscillatory. Both gradients are seen when a number of the band is around 300.
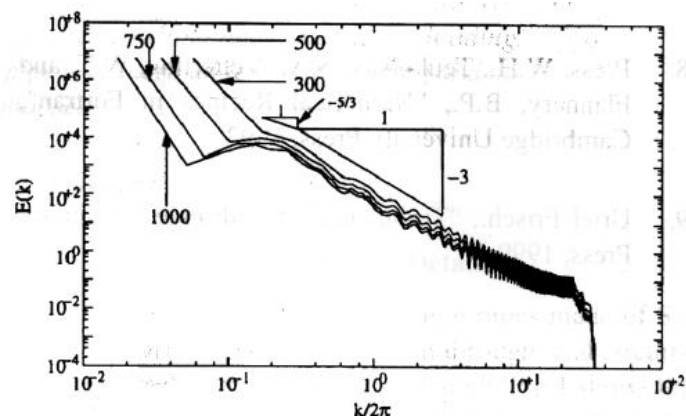
Figure 2.2: Effect of number of band of k over energy spectra at Re=10^6(**Singh et al. (2001).**

21

Figure 2.3 show the comparison of energy spectra for two different Reynolds numbers (Re=10^5 and10^6). It is observed that flow displays the characteristics of 2D turbulence. The energy casced is shown at k^{-3}. A reverse energy cascade is observed which varies according to $k^{-5/3}$. Seeing that no turbulence model is being used and the resolution is not neat enough to solve the Kolmo-gorov scale. So this proposes that the numerical dissipation received by the stabilization terms is not sufficient to drag out the energy at broad wavenumbers and that's why a proper turbulence model is required.
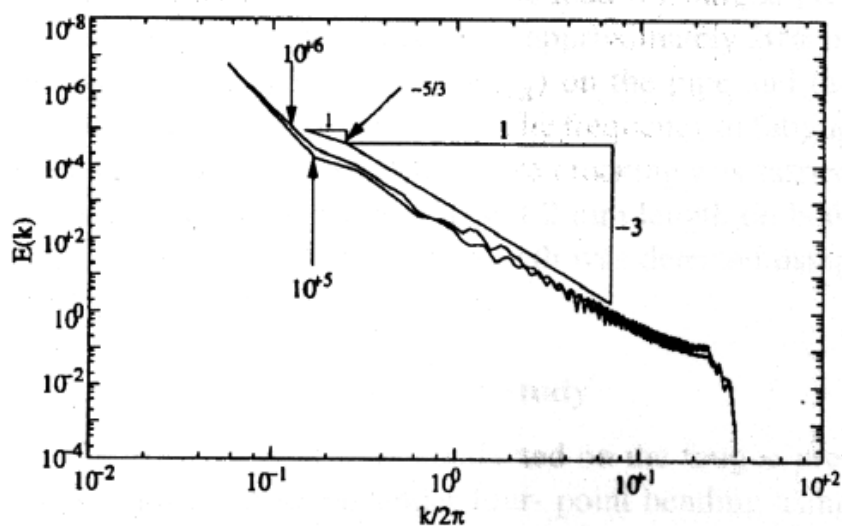
Figure 2.3: Comparison of energy spectra at different Reynolds number (**Singh et al.(2001).)**

Large eddy simulation was applied for the flow over a bluff body to display that it is attainable to get correct results in a rough grid simulation, which was carried out by **Krajnovic et al. (2002).** The defective decision was to satisfy through the employment of a one equation subgrid range model. In this place, two one equation sub grid models were applied for modelling the subgrid-scale stress tensor. The turbulent stress and time averaged velocities were calculated and distinguished with the experimental results which showed good agreement with each other. Universal quantities like drag coefficient, lift coefficient, and vortex shedding frequency were reported. The relocation of turbulent energy and reversal transmission of energy was forecast. Comprehensible structure and other flow appearance were further investigated. The results display excellent agreement with the results of the experiments.

Sohankar et al. (2002) observed that the large eddy simulation of flow and heat transfer around square cylinder along one side covering the upcoming flow at Reynolds number. Three distinct sub-grid scale model were namely the Smagorinsky, the standard dynamic, and

a dynamic one-equation model, used in this study. An incompressible finite volume code that was established on a fractional step technique and a non-staggered cell arrangement were used. Strouhal number .mean and rms value of lift and drag were calculated. The results which were found out by dynamic one equation provide the superior agreement with experiments compare to the other two sub grid model.

The turbulent characteristics of the flow around a bluff body of a circular cylinder in the near wake and the near wall upstream domain with the Reynolds number of 1, 40,000 were analysed by **Djeridi et al. (2003).** The geology of average and turbulent velocity fields engaging a moderate blockage and aspect ratio was provided to use the modern outcome for direct comparisons with realizable 3D-Navier Stokes computation. Two experiments were used using PIV and LDV techniques respectively where both supply a purify grid of survey points and the flow structure was examined by these two techniques. **Nakaguchi et al. (1968)** investigated an experimental study on aerodynamics drag of rectangular cylinders with Reynolds number up to Re=6×10^4. It showed that the drag value change significantly accompanying the d/h ratio of rectangles and that the C_d value was maximum of about 2.6 for d/h of 2/3 compared, that C_d value was 2.0 for the cases of flat plate and square cylinder. The Strouhal number of the vortex shedding was remained nearly constant for d/h up to 1.0, again moderately decreased for larger values of d/h and then increases unexpectedly at d/h ratio of about 2.0, where the flow reconnect on the sideways surface of the cylinder.

Gupta et al. (2003) numerically investigated the two-dimensional steady flow of a power-law fluid past a square cylinder in a plane channel. The momentum and energy equation solved with the finite difference method. The rheological and kinematic ambiance were considered power law index n=0.5-1.4, Re=5-40 and Peclet number, Pe=5-400. Using the fixed blocakge ratio the constant heat flux and the isothermal condition was investigated. Drag coefficient and Nusselt number value for both individual and overall was marginally upper unity in shear-thinning fluids and marginally below unity in case of dilatants fluids. Reynolds number effect on flow arrangement was approximately the same which notice for Newtonian fluids is.

The laminar flow over a square cross-section of a circular cylinder seated inside a plane channel (β=1/8) was carried out by **Breuer et al. (2002).** In this work, two distinct numerical approaches i.e. lattice-Boltzmann automata (LBA) and a finite volume method (FVM), were applied.. So to restrict the way to 2D computations, the biggest Reynolds number was selected of Re=300 based on the highest inflow velocity and chord length of the cylinder. The

lattice a Boltzmann automaton was developing on the D2Q9 model and the single recreation time technique called the lattice-BGK method. The finite volume code based on an incompressible Navier -Stokes solver for inconsistent non-rectangular and frame fitted grid was used. The two numerical techniques were a second-order skill in slot and time. Proper computing was performed on grids accompanying various resolutions. The outcomes of the both methods were checked out and analysed in detail. There magnificent agreement was created between LBA and FVM computations. The global quantity like drag coefficient, Strouhal number, and recirculation length was reported.

Catalano et al. (2003) illustrated, numerical simulation of the flow around a circular cylinder at high Reynolds number. Large Eddy simulation was used with wall modelling for high Reynolds numbers in the supercritical regime. An understandable wall stress model was engaged to supply exact boundary conditions to the large eddy simulations. The results were correlated with those obtained from steady and unsteady RANS solutions with experimental result's data. The LES simulations results were appreciably more authentic than the RANS results. They catched the deferred boundary layer separation and shortened drag coefficients regular with experimental calculation after the drag crisis. The mean pressure allocation was anticipated fairly good at $Re_D=5\times10^5$ and 10^6. However, the Reynolds number confidence was not captured and therefore results became lesser authentic at increased Reynolds number.

Swirling flow past a cross section of a square cylinder placed in a channel was computationally studied by **Kim et al. (2003)** with large eddy simulation (LES). The major objective of this investigation was to broadly check the experimental results of Nakagawa et al. [Exp. Fluids 27(3) (1999) 284] with Large Eddy Simulation and to analyze the appearance of flow past a square bluff body bounded in a channel in comparison with the regular one in a vast region. The simulation results obtained were in good agreement with experiment both collectively tentatively. Karman vortex shedding was observed. The mean drag and fluctuation lift force were increased significantly by the vortices. The rolled up vortex was connected with the interrelated Karman vortex, they develop a counter-rotating vortex couple. Table 1 shows that at the same Re, the drag force, lift fluctuation and Strouhal number is larger in the case of square cylinder confined in a channel compared to the square cylinder in an infinite domain.

Table 1

Comparison of characteristics of wakes for simulations with the two conditions, Re ¼ 3000

	Confined in a channel (20% blockage ratio)	Infinite domain
St	$0.124(f\frac{h}{U_b})$	$0.125(f\frac{h}{U_m})$
C_{Dmean}	2.76	1.97
C_{Drms}	0.49	0.43
C_{Lrms}	2.06	1.15
L_r/h	0.67	0.96

Here, L_r the recirculation length behind the square cylinder, and C_{Drms} and C_{Lrms} represent RMS fluctuations of C_D and C_L, respectively. U_b is the mean stream wise velocity at the cylinder location. C_D and C_L based on U_m.

Further the comparisons of St and C_D mentioned above which are summarized in Tables 2.

Table 2

Comparison of Strouhal numbers

	Author	St
Confined channel	Nakagawa et al. [8] ($f\frac{h}{U_b}$)	0.13
	Present($f\frac{h}{U_b}$)	0.124
Infinite domain	Okajima [6] ($f\frac{h}{U_m}$)	0.126
	Present($f\frac{h}{U_m}$)	0.125

Figure 2.4 shows distribution of the mean wall shear stress on the channel wall along the plate. It is seen that the maximum value obtained at x/h=-0.8 where the flow accelerated because the reduction of cross sectional area and maximum occur at the location where flow separation takes place to produce vortex counter rotating across the Karman vortex shed from the square bluff body. The gradient of the mean stream wise velocity on the channel wall become lower compare to the other location.
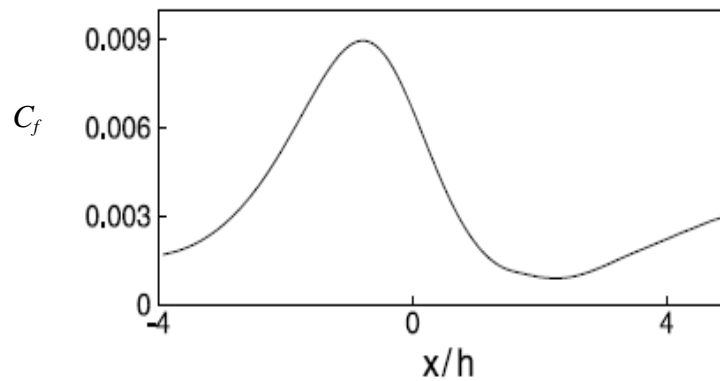
Figure 2.4: Mean shear stress along the square cylinder [Kim et al.(2003)]

Figure 2.5 shows the distribution of turbulent kinetic energy along with the centre line of the square cylinder. It is clearly observed that the magnitude of fluctuation is increased towards the cylinder and flow is undoubtedly affected by the cylinder.
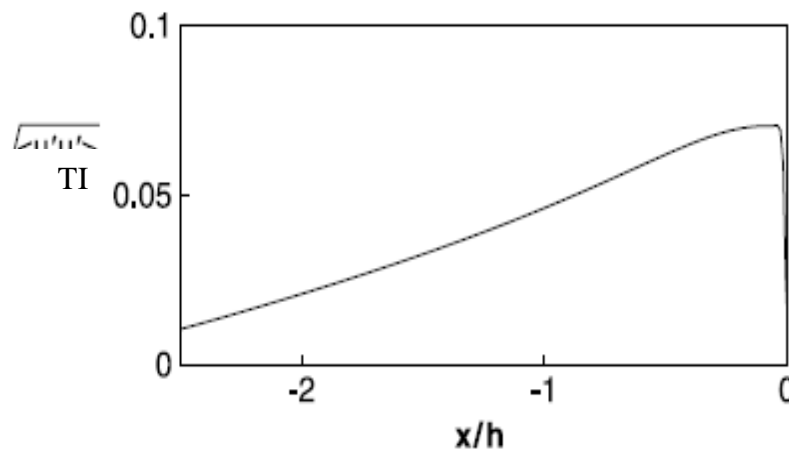
Figure 2.5: Distribution of turbulent kinetic energy upstream of the square cylinder along the centre line [Kim et al.(2003)]

Figure 2.6 shows the comparison of turbulence intensity with that over a square bluff body at infinite zone at fixed Reynolds number. It is noticed that the contour pattern of the maximum zone is varied. In infinite domain, the local maximum zone of stream wise velocity fluctuation rear both trailing edges which are shown in Fig.11(a), don't exist. So it is proposed that the channel has a perfect effect on high stream wise turbulent fluctuation in the normal direction in the close wake zone.
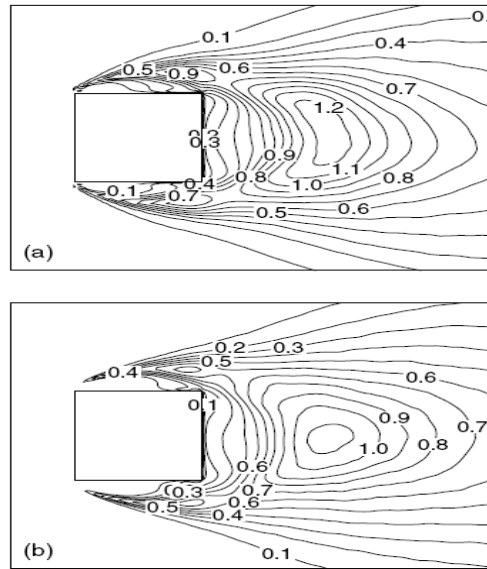
Figure 2.6: Comparison of turbulence intensity ($\left.U'_i U'_i\middle/U^2_m\right.$) increment: 0.1): (a) square

cylinder in the channel and (b) square cylinder in an infinite domain **[Kim et al.(2003)]**.

The momentum and forced convection heat transfer nature for an incompressible and constant free stream flow of power law liquids over a square cylinder were performed by **Paliwal et al. (2003).** The momentum and energy equations were discretized with a finite difference method. Power law index, n=0.5-1.4 was used so that housing both shear thinning and shear thickening behavior and Reynolds number Re=5-40, Peclet number Pe=5-400 were used in this study. Only one blockage ratio was considered ($\frac{L}{H} = \frac{1}{15}$) for all computations. The shear thinning cut down the size of the wake region but it also setback the wake formation and shear thickening behaviour.

Isaev et al. (2004) carried out numerical computing of the parameters of unsteady -state flow and heat transfer under the circumstance of a laminar crosswise stream of viscous incompressible fluid past a circular cylinder with Reynolds number up to, Re=14. The forming of Karman vortex was treated, including the cyclic heating of the close and distant wake following the heated cylinder. The major concentration was given to investigate the nature of the basic attribute of flow and heat transfer and allocation of friction, pressure, and coefficient of heat transfer on the surface of the cylinder, The three-dimensionality of vortex shedding from a trapezoidal bluff body using a direct numerical simulation method at Re$_d$=250 which was analysed by **Najjarand Balachandar (1998).** Numerical procedures presently applied in this work was classified into two categories. The first one was a direct

numerical simulations method which was used to solve the Navier-Stokes equation directly, and the second one was averaging of the Navier-Stokes equation. Flow around triangular prism had received significant attention from researchers.

Sanitjai and Goldstein (2004) studied the local and average heat transfer by forced convection from a circular cylinder. Reynolds number ranging from 2,000 to 90,000 and Prandtl number from 0.7 to 176 were considered. Their results were interested for subcritical flow. The local heat transfer measurement indicated three flow regions including the laminar boundary layer region, reattachment of the shear layer region and periodic vortex flow region. In each region, the average heat transfer was calculated and correlated with the Reynolds number and the Prandtl number. Also, the Nusselt number in each region depends on the Reynolds number and the Prandtl number. An empirical correlation was developed for predicting the overall heat transfer from the cylinder in these three regions.

Application of a modified k-ε model for predicting the aerodynamic characteristics of rectangular cross-section cylinders of infinite and different breadth to depth ratios ranging from B/D=0.6-8.0 were studied by **Shimada et al. (2001).** In spite of employing two dimensional numerical method, a physically fairly smooth, cyclic vortex shedding was achieved, uniform in the high Reynolds number range .The same phenomena can not be obtained by common 2-D study which does not include a turbulence model. The different conventional aerodynamic appearance was favorably obtained, especially including the discontinuity in Strouhal number at the retracting portion of B/D=2.8 and 6.0. Also, the drag coefficient and mean surface pressure distribution were in reasonably good agreement with the experimental results and the 3D study for the same range of B/D ratio. The prediction of force and pressure variations with the available RANS model were capable of performing to examine the periodic components and not hypothetical components. The total fluctuations in lift force and surface pressure were significantly miscalculated in few cases, distinguished with those deliberate in experiments and computed from the 3D examination.

Sharma and Eswaran (2004) showed the flow structure and heat transfer characteristics of an isolated square cylinder in cross flow. It was investigated numerically for both steady and unsteady periodic laminar flow. The problem considered two-dimensional where Reynolds numbers of 1 to 160 with a fixed Prandtl number of 0.7. The isotherm pattern, heat transfer from the cylinder and the effect of vortex shedding on the cylinder was discussed. The

correlations of heat transfer between Nusselt number and Reynolds number were presented for boundary condition of uniform heat flux and constant cylinder temperature.

Three-dimensional computational analysis of the flow around the cross-section of rectangular cylinders with different side ratios of D/H, from 0.2 to 2.0, was performed by **Rokugou et al. (2003)** for Reynolds number of 1000 with using a multi directional finite difference method. It was observed that simulation results were a good agreement with experimental results. The study presented the fluid dynamics nature of rectangular cross section replacement between high pressure and low-pressure mode of the base pressure for D/H=0.2-0.6. Privately showed that this development was induced by the modification of the flow arrangement around a rectangular cylinder.

Singh and Mittal et al. (2004) studied numerically the flow past a circular cylinder with resolving the unsteady incompressible two dimensional Navier-Stokes equations by way of steady finite element organization with Reynolds number of Re=100. It was realised that the flow expanded significant three-dimensional characteristics. Thus, two-dimensional simulations had tendency to decline well short of predicting the flow correctly at high Reynolds number. In the present computations, the frequency of the shear layer vortices good agrees with the fluctuation noticed by a different investigator from the experimental analysis. The major aim of this paper was to find out a probable relationship between the drag crisis (abrupt deficit of drag at) and the imbalance of the detached shear layer. The transition point is situated much closer to the point of flow separation at a critical Reynolds number. The lag of flow separation correlates with shortening of the wake, increase in Reynolds shear stress close the shoulder of the cylinder and important decline in the drag and base suction coefficient. As in two-dimensional isotropic turbulence, E(k) change as for wave numbers greater than the energy does scale and as for inferior wave numbers. The current simulations propose that the shear layer vortices play a bigger act in the transition boundary layer from laminar to turbulent.

The numerical simulation of flow around triangular prism situated vertically on a level with moderate aspect ratio using the Large-eddy simulation method was studied by **Camarri et al. (2006).** The outcomes were compared with available and fresh experimental statistics to achieve proof on the physical source of the velocity oscillation interior and over the wake. Both the numerical and the experimental velocity signs were studied through time–frequency approach placed on the wavelet and Hilbert transform to define the time alternation of the

amplitude and frequency of the various distinguishable oscillating parts. It shoed that the numerical simulation, related to a Reynolds number that is one rule of magnitude lesser than in the experiments, supply values of the rms wake oscillation that are in excellent reconciliation with those achieved from the hot-wire calculation. Moreover, it admitted the form of the top adjacent wake to be defined and provided valuable clues on the dynamics of the vorticity designs emerge from the free edge of the body and on their feasible contact with the wake oscillating flow range.

Dalal et al. (2006) observed a numerical simulation of unconfined flow past a triangular cylinder. Reynolds number taken was in the range of 10 to 250. A finite volume method, 2nd order correct in space and time, applying non-staggered settlement of the variables with momentum initiation for the coupling of pressure velocity was developed. The phenomena of vortex shedding were found to be identical to the cylinder of the square cross-section with no second ramification in the range of Reynolds number studied. An analysis of the time-averaged coefficient of drag, rms of lift coefficient and Strouhal number were discussed.

The flow over the bluff body from moderate to high Reynolds number which was performed by **Sohankar et al. (2006).** Large eddy simulation was applied to study the uniform flow over a square section cylinder where Reynolds number varying from 1,00 to 5×10^6. Smagorinsky and a dynamic one-equation model were used. The Strouhal number, the mean lift and RMS values of the drag coefficient were reported here. This showed that there is good agreement with the experimental results.

The two-dimensional flow over an infinitely long circular cylinder was analyzed numerically by **Posdziech et al. (2006)** using the spectral element method. Precise analysis of the reaction of resolution and enlargement of the computational territory on drag and lift forces, Strouhal number, and base pressure coefficient were carried out in the laminar region. The asymptotic outcome was achieved by raising the length of the computational territory to assort thousand of cylinder diameters. it was observed that in comparison to the Strouhal number, the base pressure coefficient, and the force coefficients were fully dependent on the decision and even greater on the size of the computational territory. The Reynolds number communications were compared to computational and experimental info from the literature. The database was favorable both for confirmation of computational codes and calculation proofs where the partition of physical appearance and effect of experimental plans were regularly a free question.

Turbulent flow past a circular cylinder at the critical regime was studied by **Benim et al. (2007)**. The flow was considered as an incompressible flow. Numerical simulation over a circular cylinder was done by using a RANS model (Transition SST model) up to Reynolds number 10,000-5, 00,000. For the velocity -pressure coupling, the SIMPLEC scheme and low turbulence intensity (0.01%) were used in this study. The major parameter non-dimensional wall distance y^+ value was calculated as $y^+=(y/\nu)(\tau_w/\rho)^{0.5}$ where, y, ν, τ_w, p represents the cell to wall distance, kinematic viscosity, wall shear stress, and density receptively. The drag co efficient value which was obtained in the present simulation, compared with the measured value from the literature.

Benim et al. (2011) simulated flow around a cylinder using RANS, URANS as well as LES and found that LES predict the drag coefficient closer to experimental results. The Reynolds numbers for the study were (Re) 2500, 5000 and 25,000 and the Prandtl number was identical to 0.7 for whole computations. For Re=2500 and Re= 5000 three-dimensional URANS (3D URANS) and Large Eddy Simulations (LES) were also performed. In the RANS and URANS computations, the Shear Stress Transport (SST) model was used as the turbulence model. The Wall-Adapting Local Eddy-Viscosity (WALE) subgrid-scale model was used in LES. It was predicted that the heat transfer at the channel wall can be enhanced by the triangular prism, where the forecast features depend on the modeling method employ. URANS and LES predicted mainly enough higher Nusselt values compare to RANS, and, thus, point out enough powerful heat transfer enhancement by the triangular prism. It was explained that the impact of the unsteady movement of the understandable whirlpool design behind the prism, which was primarily liable for the heat transfer enhancement cannot be sufficiently described by a RANS model, and an unsteady approach (URANS/LES) was necessary for a superior forecast. The compared 2D URANS and 3D URANS and realized that, three-dimensional impact in large scales can further play few acts, depending on the Reynolds number, which could fairly be proved for Re =2500. The forecast crest time-averaged Nusselt numbers in the downstream zone of the prism by LES produced to be much higher than those of URANS, due to small but intense vortical design in the wall proximity, that was solved by LES. Still, more downstream, LES and URANS converged and displayed a fairly identical asymptotic attitude.

While **Ding et al. (2004)** applied to mesh free method to analyze the flow field over a cylinder, the lattice Boltzmann method was applied by "Shueet al. (2005)" for rotating cylinders successfully.

Two and three-dimensional numerical heat transfer modelling from different circular cylindrical particles was performed by **Motlagh and Hashemabadi (2008)** with the commercial CFD software, FEMLA. In this work, four distinct positions (a) infinite cylinder in cross-flow, (b) cross-flow on a finite cylinder with different aspect ratio in a rectangular duct,(c) axial-flow on a finite cylinder and d) axial-flow on a finite cylinder with upstream turbulence were used. All body forces were neglected and the standard κ–ε turbulence model has been used for calculation of eddy viscosity of flow. The computation results were validated with experimental data and also experimental correlations from different research papers and showed reasonably good agreement with each other.

The 2-D flow around a porous expanded trapezoidal cylinder using a finite volume method, based on the body-fitted, non-orthogonal grids and multi-block technique was analyzed by **Chen et al. (2009).** The Brinkman-Forcheimmer lengthy model was employed to control the flow in the porous medium zone. At it's junction, a shear stress bounce that contains the inertial impact was enforcing, together with a constancy of common stress. The current model was verified by comparing with the for the flow over a tight circular cylinder. Outcomes for flow over absorbent extend trapezoidal cylinder were granted with flow structure for various Darcy number, 10^{-2} to 10^{-7}, porosity ranging from 0.4 to 0.8, and corresponding Reynolds number Re=20 to 200. The flows grew from steady to unsteady intermittent whirlpool shedding state. The early coefficient β had a greater notable impact, whereas the second coefficient β1 had a much low impact, consistent for Re = 200. The impact of the porosity, Reynolds number and Darcy number on drag and lift coefficients, and the length of circulation region or shedding cycle were investigated.

Rajani et al. (2009) have investigated the numerical simulation of laminar flow past a circular cylinder in various laminar flow regimes. In this work, the implicit pressure-based finite volume method was used for time accurate computation of incompressible flow with second-order accurate convective flux discretization scheme. Skin friction coefficients, recirculation wake length at the invariant flow regime, Strouhal frequency of vortex shedding mean and rms value of the oscillating aerodynamic coefficient for cyclical flow regime. The complicated flow structure of the cylinder wake was also fairly captured by the current forecast procedure.

In fig 2.7 the surface pressure and skin friction coefficient are presented for three different Reynolds numbers. For all the Reynolds number the measurement data and simulation results

are a good agreement to each other in the drive flow zone which is covering the front part of the cylinder. These differences may be usually due to the incorrect guess of the location of the variable flow separation point on the cylinder surface. The differences may also be attributed to the three-dimensional fluctuation of the wake with the spanwise direction at Reynolds number Re=200 and Re=300.

(a) $Re = 100$

(b) $Re = 200$

(c) $Re = 300$
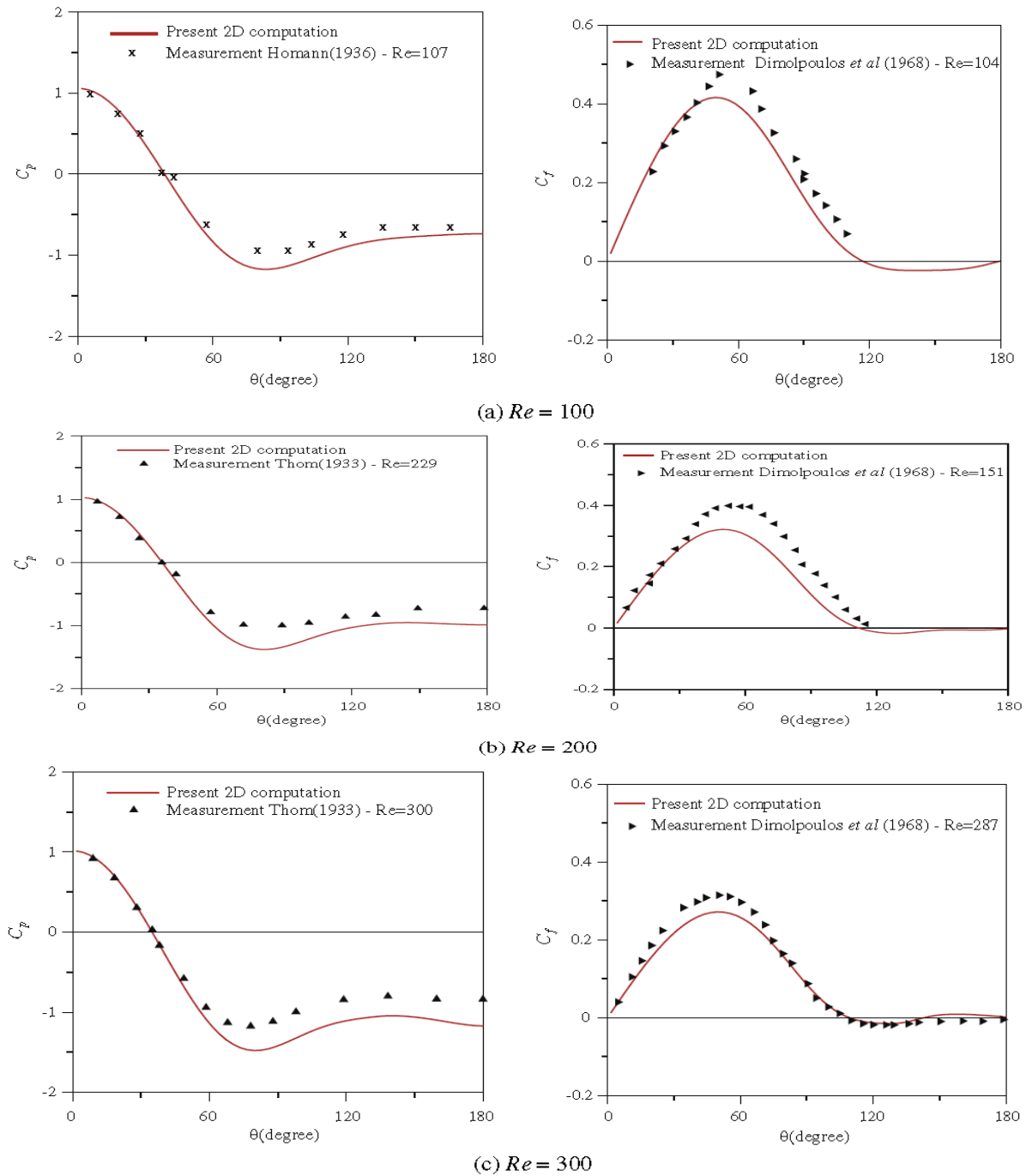
Figure 2.7: Distribution of surface pressure and skin friction around the cylinder at different Reynolds number (Rajani et al., 2009)

The three dimensional effect of Transitions on flow past a square cylinder at low Reynolds number ranging from 100-325 was investigated by **Saha (2009).** The flow is find out two dimensional at Re 160 and three dimensional at Re 163.5. The transition effect on the instantaneous flow and root mean square fluctuations were quite significant while the time-averaged flow did not show any noticeable variation.

Mannini et al.(2010) studied the unsteady RANS modeling of flow past a rectangular prism with fineness ratio(cord to thickness) of 5.0.The flow was two dimensional with Unsteady Reynolds-Averaged Navier-Stokes equation are used. The study considered with various Reynolds numbers ranging from 20×10^3 to $1,850\times 10^3$, Mach number of 0.1, and angle of attack of 0^0 and 4^0. The focus of this work was to judge the capability of the computationally efficient two-dimensional URANS calculations to see the features of complex separated flow around such type of geometry. Another goal was to investigate the Reynolds number effects noticed in wind-tunnel experiments with using numerical simulation.

Sen et al. (2010) analysed the flow past a square cross section of cylinder at laminar region. A balance finite-element organization was engaged to discretize the equation of incompressible fluid stream. The values of laminar segregation Reynolds number (Re_s) and separation angle (θ_s) were predicted. Further, the change of separation angle with Reynolds number was presented. It was observed that the steady break-up starts at Re=1.15.Opposed to the favourite assumption that break-up originates at the back sharp edge, it was found to emerge from the low specific location, that is θ_s=180^0 $Re = Re_S$ .Separation angle came nearer the limit of 135^0 at $Re \succ 5$. The length of break-up droplet raise almost linearly with rising Reynolds number. The C_d was changed as $Re^{-0.66}$ .Flow nature at $Re \ll 40$ was also conferred for elliptical cylinders of aspect ratios 0.2, 0.5, 0.8 and 1 (circle) having the identical characteristic magnitude as the square and main axis align common to the free-stream.

The developments in enhanced heat transfer were experimentally and theoretically presented by **Bergles et al. (2011)**. This study give an outline of the modern state of this essential technology for past ten years representative development in each division of enhancement approach are point out and communicated. The argument was classified into the literature, passive enhancement approach, progressive enhancement techniques, and composite improvement approach. The modifications of enhancement in the study were invariably being

advanced and they were being used in modern purpose. Much of the attempt was guided in the direction of micro scale even nanoscale.

Berrone et al. (2011) studied the numerical simulation of flow past rectangular cylinder by two different numerical methods, a final volume method(FVM) and adjusting final element method(AFEM). 2D simulations using rectangular and square cylinder with width to height ratio is 5 was carryout for various Reynolds number in order to consider various flow regimes, namely the steady, the periodic and turbulent flow. Strouhal number, drag coefficient and then recirculation length was distinguished. A reasonable excellent agreement between the FEM and FVM calculations, including with the available literature results, were obtained. Appropriate results of this work are the cross confirmation of an adjusting FE method and famous open source FV code.

The flow nature in the near wake of two exact side-by-side circular cylinders placed close to a perfectly grown turbulent boundary layer were performed by **Chen et al. (2011)** with experimentally utilizing the particle image velocimetry (PIV) and the pressure sensor. The Reynolds number which based on the diameter of the cylinder (D) was 1,696.The boundary layer thickness of 6.6 D, the cylinder midpoint to midpoint layout (T) varying from T/D=1 to 1.906,the gap layout between the inferior cylinder and the wall(G) varying from G/D-0 to 1.811 were considered in the analysis. To analyze the effect of varying the gap ratios of T/D and G/D on the wake stream, different wake nature like averaged streamlines, vorticity contours, Reynolds stress and additional crucial flow characteristics as well as Strouhal number and length scale were examined for various ratios T/D and G/D. Grant to these wake features, five key flow arrangement were analyzed.

The two dimensional convective heat transfer around a triangular cylinder in an air cross flow was analyzed by **Zeitoun et al. (2011)**. Equilateral triangular cylinder of different side dimensions and configurations were examined in laminar conditions.

The effect of adding/opposing buoyancy on the two-dimensional upward flow and heat transfer around a heated/cooled cylinder of square cross section was numerically studied by **Chatterjee and Mondal (2012)**. The influence of adding/opposing buoyancy and the blockage parameters of 2% and 25% was studied for Reynolds and Richardson numbers ranging from 50 to 150 and -1 to 1 respectively.

You and Kwon (2012) have investigated the performances of the numerical simulation around a circular cylinder using different turbulent models at a critical Reynolds number regime. The Reynolds number and turbulence intensity were 8.5×10^5, 0.7% respectively. RANS model(Transition SST Model), Hybrid RANS/LES model (SAS model), a correlation-based transition model were used to simulate the laminar-turbulence transition inside the boundary layer and the unsteady vortex shedding in the wake region.

The flow and heat transfer characteristics inside a rectangular channel enclosed with drop shaped pin fins were experimentally and numerically analyzed by "Wang et al. (2012)".Three different shaped pin fin, i.e., circular, elliptical and drop shaped fin accompanying the identical cross-sectional area were distinguished in a staggered arrangement. The Reynolds number which based on the hydraulic diameter was varied from 4,800 to 8,200. The heat transfer enhancement was less in the case of dropped shaped pin fin compare to the circular pin fins. Figure 2.8 shows the pressure loss coefficient against the different Reynolds number for the channel with various pin fin collection. Even though there was an obvious dissimilarity between experimental and computational results. For the particular performance, the specific friction loss in drop-shaped pin fin was inferior to that of elliptical and circular pin fins, which signified that the drop-shaped pin fin was the more favorable compared to the other.
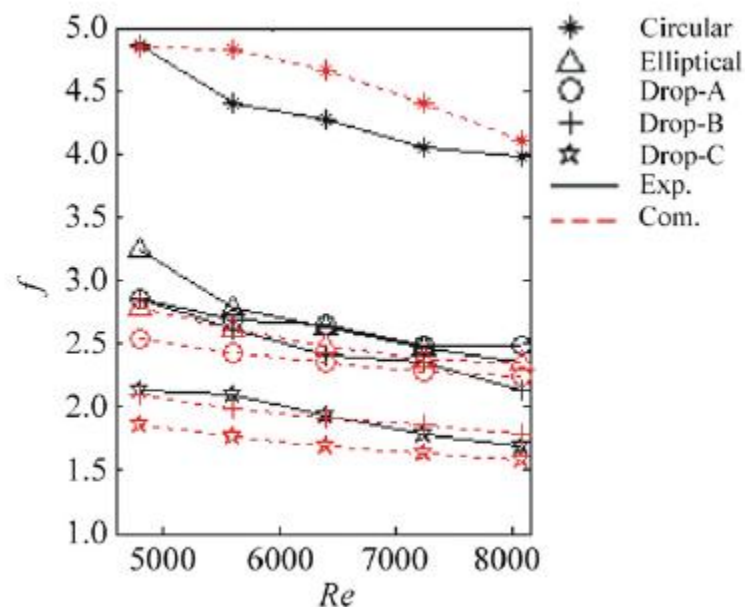
Figure 2.8: Pressure loss coefficient vs Reynolds number [Wang et al.(2012)].

Figure 2.9 shows the average Nusselt number against the Reynolds number for the channel with various pin fin bunch. Though there was a higher relative error of 10%-20% between the experimental and computational results, the relationship between convective heat transfer capacities to the pin shapes are admitted well The elliptical pin fins seemed to decrease the Average Nusselt number by about 20% compare to the circular pin fins at Reynolds number of 4,800-8,200. In the case of drop-shaped pin fins, the reduction of average Nusselt number compare to the circular pin was about 24% for drop A, 26% for drop B, and 27% for drop C.
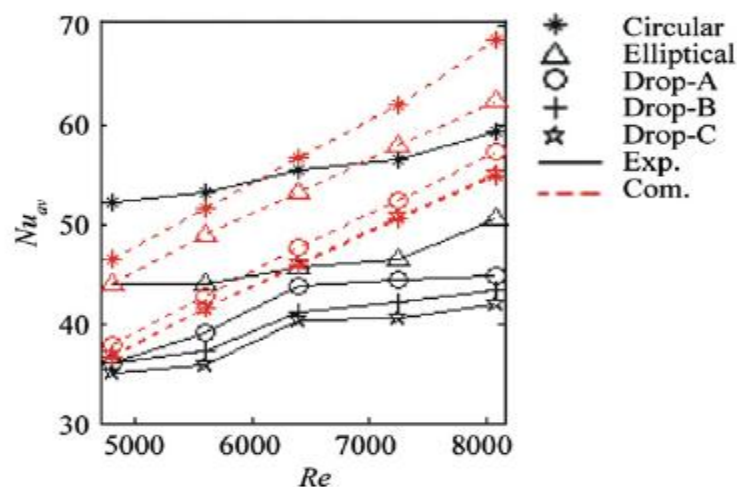
Figure 2.9:Variation of averaged Nuuselt number with Reynolds number [Wang et al.(2012)].

You and Kwon (2012) have investigated the performances of various turbulent models for the flow simulation around a circular cylinder at a critical Reynolds number regime. The investigation considered Reynolds number and turbulence intensity of 8.5×105, and 0.7% respectively. Hybrid RANS/LES model (SAS model), a correlation-based transition model, (γ- Reθ model) and a fully turbulent RANS model (Transition SST model) were utilized to simulate the laminar-turbulence transition inside the boundary layer and the unsteady vortex shedding in the wake region. A vertex-focus finite-volume approach was adopted to discretize the incompressible Navier-Stokes equations and an unorganized mesh method was employed to discretize the calculating territory. The inviscid fluxes were judged by utilizing second-order Roe's FDS and the viscous fluxes were calculated based on the central differencing scheme. A dual-time stepping technique and the Gauss-Seidel iteration were applied for unsteady time integration. To minimize the calculation costs, the parallelization plan employing METIS and MPI libraries was adopted. The unsteady features and time-averaged amount of the flow range were compared between the turbulent models. The

computational results were further compared with experimental results. At the critical regime, turbulent models have exhibited dropout various results owed to the distinct capability of every model to forecast different flow characteristics like laminar-turbulent transition, unsteady vortex shedding.

In this work, the 2-D numerical investigation was performed by **Ai et al. (2013)** for unsteady high Reynolds number flows over a soft circular cylinder in the supercritical and upper-transition flow regimes, particularly $8.21 \times 10^4 < Re < 1.54 \times 10^6$. The measurement was carried out employing resolve the two dimensional Unsteady Reynolds-Averaged Navier-Stokes (URANS) equations with a k -ε turbulence model. The determined data were formed flow design coefficients of drag and lift, including Strouhal numbers. The judgment was in favourable agreement with the earlier written result, which also provides us with an excellent understanding of the flow across cylinders of various high Reynolds numbers. At the same time, an efficient measure was given to regulate the lift force on a cylinder.

Chatterjeeet al. (2013) performed to investigate the laminar forced convection heat transfer for flow past a semicircular cylinder in an unconfined medium. The numerical simulation was done for two-dimensional unsteady flow. In this study, the Reynolds numbers were in the range of 50-150 with a fixed Prandtl number (Pr=0.71).In this work two different configurations of the semicircular cylinder were considered; one when the curved surface facing the flow and the other when the flat surface facing the flow. For numerical computation, a finite volume-based technique was used.

The experimental and Numerical analysis of flow around a fixed circular cylinder at Reynolds number 1,00,000 were performed by **Islam and Hassan (2013).** The Favre-averaged Navier-Stokes equation was used and solved by the finite volume procedure. Numerical surveillance was compared with experimental data's and with the research performance of other scientists. Various flow phenomena e.g. flow partition, pressure allocation over the surface, drag, vortex shedding, etc. were also calculated at various boundary circumstances. A short comparison between the 2D and 3D numerical studied including the character of vorticity allocation and impact of surface roughness were broadly considered. In the case of a polished cylinder, the partition angles for 2D or 3D numerical computation were found to be about 80~90° in one side of the cylinder from the challenging stagnation mark. The drag coefficients for polished surface are 0.771 and 0.533 for 2D and 3D numerical studies respectively and successive variation in drag due to introducing surface

coarseness was explained. The critical surface coarseness was beginning to be approx 0.004 along with the drag coefficient of 0.43. However, the wake design was unclear seeable, and they were not as regular as in Karman street.

Rodríguez et al. (2013) performed the direct numerical simulations of the flow over a sphere in the wake of turbulence. The numerical simulation was performed in the sub-critical regime of Re=3,700 and Re=10,000 which was based on the free stream velocity and diameter of the sphere. Simulations were done on unstructured grids obtained by the constant step rotation about the axis of a two-dimensional grid. This Poisson equation was resolved using the Fourier diagonalization method. The principal features of the flow containing power spectra of a set of elected monitoring probe at dissimilar positions were described and explained clearly. The turbulent enumeration had been provided clearly.

The fluid flow past an obstruction of a circular cross-section in the unsteady flow regime was numerically solved by **Golani and Dhiman (2014)**. Here, the effect of Reynolds number on Strouhal number, drag and lift coefficients, heat transfer nature of a heated circular cylinder was examined for Reynolds number ranging from Re=50-180 and Prandtl number =0.7(air) in the unstable unsteady mix flow. The numerical computation was performed with finite volume method(FVM) which was based on the commercial CFD solver Fluent(version 6.3). A particularized flow arrangement was conferred by the approach of spontaneous streamline, vorticity magnitude, velocity magnitude, and pressure contour. The current results are a good agreement with experimental data available for a circular cylinder in the literature. The average Nusselt number raised with raising Reynolds number. When The Reynolds number increases, the vortex shedding frequency, drag value increases, though, the rms lifts and rms drag coefficients increases with Re.

A. Alonzo-García et al. (2014) studied the Large Eddy simulation flow around a smooth polished circular cylinder and U-Grooved shape circular cylinder with the Reynolds of 1,40,000. It was a nearby transition in the middle of subcritical and critical flow regimes. The numbers of the cell were 2.6 million and 20.7 for the case of smooth and U-grooved circular cylinder correspondingly. Hexahedral cells were used with extra filtering in close the wall region to get y^+ value less than 5. The governing equation of the RANS model was solved using commercial CFD software Ansys Fluent V.12.1.In the case of U-grooved cylinder, drag co-efficient, recirculation length, development of a wake created by secondary vortices were observed reasonably by the LES model.

Numerical analysis of flow around a square cross-section cylinder was presented by **Islam et al. (2014)** with the multi-relaxation-time lattice Boltzmann methods at low Reynolds numbers. Time-trace study of drag and lift coefficients, vorticity contours visualizations, power spectra study of lift coefficient, phase diagrams and streamlines were reported here. The global quantities like Strouhal number, drag coefficient, mean drag coefficient, root mean square values of drag and lift coefficients were determined and compared with the strong solve experimental result and numerical data's available in the open article. The Reynolds numbers affected global quantities.

Saeedi et al. (2014) studied the direct numerical simulation to perform the turbulent wake behind a surface mounted square cylinder bluff body. The aspect ratio and Reynolds number were considered for the study were 4 and 12,000 respectively(based on the free flow velocity and bump side length) in a developing boundary layer. In the case of high Reynolds number and high aspect ratio of the cylinder, the wake was broad spread trailing the cylinder and display complicated and dynamic vortex action. The side and travel vortex shedding arrangements at various frequencies, systematic structures downstream of the obstruction, the production rate and transportation of turbulent kinetic energy, the rapid pressure distribution in the wake zone was carefully examined. To justify computational results, the first and second order stream data's achieve from the simulations were thoroughly compared against accessible wind-tunnel calculation data.

Large eddy simulations of the flow around a circular cylinder with Reynolds number ranging from 2.5×10^5 to 6.5×10^5 were carried out by **Lehmkuhl et al. (2014).**It was admitted that flow spent a circular cylinder at critical Reynolds number combines flow partition, turbulence transition, reconnection of the flow, and more turbulent partition of the boundary layer. The study showed that how the pressure allocation changes as the Reynolds number increases in an irregular manner that, happens early on one side of the cylinder and next on the alternative side to complete the drop in the drag up to 0.23 at Re=6.5×10^5. These differences in the pressure sketch were followed by the presence of a short recirculation droplet, noticed as a little plateau in the pressure, and placed around $\phi=105^0$ which was measured from the stagnation point. The power spectra for the velocity variation were calculated. The study of the resulting spectrum exhibit the footmark of Kelvin-Helmholtz uncertainty in the entire range. It was found that the ratio of these imbalance frequencies to the basic vortex shedding frequency agrees well the scaling suggested by Prasad and Williamson ["The instability of

the separated shear layer from a bluff body," Phys. Fluids 8, 1347 (1996); "The instability of the shear layer separating from a bluff body," J. Fluid Mech. 333, 375–492 (1997)].

Liu et al. (2015) studied the computational analysis of the effect of particles on the adjacent wake over a circular cross section of a cylinder at a moderate Reynolds number with a direct numerical simulation (DNS) technique. High-order finite-deference proposal was used to clarify for the quantity fluid properties, and a Lagrangian method maintains to record the sole particles The individual-stage flow was resolved and justified with the prior experimental result. U and V-shaped states were noticed in the adjacent wake, which was regular with the experimental data's. The drag force from the circular cylinder increases by particles and restrain the circular current shedding frequency.

The effect of a solid wall on the wake dynamics of a square cross-section of an infinite cylinder was studied by **Samani et al. (2015)** when it was located in closeness to the wall. Three different gap value ratios were studied namely g/D=0,0.5 and 1. The Reynolds number, which based on the cylinder width and free stream velocity was Re=500. Large Eddy simulation was used to predict the determine scale-velocity and pressure fields, and further to produce the input info for the convenient Orthogonal Decomposition studies. When the cylinder was placed to the wall, it imported active asymmetry into the adjacent -wake, which was unmistakable in the readjustment of the upper and lower redistribution cells, including the improvement of an insignificant recirculation region on the base wall itself. For every cut ratio, the systematic structure relate with early three POD approach were analyzed and the results were correlated with a case of an infinite cylinder in a free flow. For the two minimal gap ratio, both the energy allocation between the POD modes and the flow arrangement correlated with the systematic structures for every mode were powerfully influenced by the existence of the wall.

The turbulent flow around a square cylinder using the DNS method was studied by **Trias et al. (2015).** The results of time averaged flow and statistics of turbulent were discussed together with experimental data which were showing good agreement. Comparison of the turbulent statistics in the wall region which indicates that the transition zone was well captured.

Experimental and numerical analysis was performed to examine the effect of nozzle shape on unconfined jet impingement heat transfer from a heated circular cylinder by **Singh et al. (2015).**Air was considered as a working fluid where Prandtl number was fixed 0.71. The

41

surface of the heated cylinder was maintained at a constant heat flux. The circular, rectangular and square nozzles were selected with the same hydraulic diameter for comparative analysis. The ratio between hydraulic diameters of the nozzle to the diameter of a heated cylinder was maintained at 0.2 for the parametric study. The non-dimensional distance between the rear side of the nozzle and the cylinder was varied from 4 to16. Reynolds number was considering ranging from 10,000 to 25,000. For a fixed Reynolds number, the mass flow rate through the various nozzle was different. So a diametric analysis was also carried out to notice the effect of nozzle shape for different constant mass flow rate. The heat transfer rate from the cylinder was higher in the case of a rectangular nozzle.

Spanwise correlations in the wake of a circular cylinder and a trapezoid placed inside a circular pipe using hotwire anemometer were studied by **Venugopal et al. (2015)**. Results were considered for Reynolds number 1, 00,000. Three blockage ratio of 0.14, 0.19 and 0.28 are used in the present study. The coefficient of correlation is seen to enhance with the increase in blockage ratio. The trapezium bluff body holds a high correlation length compared to the circular cylinder. It was observed that increase in blockage ratio enhanced the correlation coefficient and also observed that the concurrent effect of curvature, upstream turbulence, and low aspect ratio cut down the correlation co efficient undoubtedly as compared to confined and unconfined flow. Vortex shedding for trapezoid with a blockage ratio of 0.28 was observed to be lower compared to a circular cylinder and all other blockage ratios.

Yagmur et al. (2015) carried out Experimental and Numerical study of Flow Structures over Cylindrical Bluff Bodies. The major goal of this work was to perform experimentally and numerically the flow field in the wake region of various bluff bodies, like a square cylinder, circular cylinder, triangular cylinder located horizontally perpendicular to the consistent flow. Particle Image Velocimetry method was used for experimental study in an open water tunnel with the Reynolds number range of 5,000 to 10,000. The large eddy simulation model is used and the experimental results were compared with the simulations results. It was observed that the experimental results were good agreement with simulations results in sense of the spontaneous and time-averaged flow field design of vorticity, velocity element stream wise direction and streamline topology. Also, the geometries drag coefficient was computationally determined. Profile of the time-averaged stream wise velocity for Re=10000 explains that the stagnation point over the proportion plane shift more upstream for all cylinders in agreement

with Re=5000. The highest drag coefficient value allowed for the square cross-section cylinder as 1.78 due to the sharp-edged geometry.

Experimental and numerical study of heat transfer from a heated whirl horizontal cylinder in Pacific air about its axis was investigated by **Elghnam (2013).**The rotating cylinder diameter was taken at 50mm. The computation was performed by using the finite volume method(FVM) based computational fluid dynamic solver FLUENT. The heat transfer's results aware defined in terms of non-dimensional parameters like Reynolds number, Nusselt number, Grashof number (Gr). The experimental analysis was performed for Re=1880-6220 and Grashof numbers range from, Re=14,285-7,14,285, while the computational measurements were performed for Reynolds number ranging from Re=0-1,00,000 and Grashof numbers range of Gr=100-10,00,000. The impact of rotation on heat transfer nature was given in terms of the local and averaged Nusselt number, streamlines, isotherm arrangement. The outcome correlated as :$Nu = 0.022Re^{0.821}$ and showed very strong with the data available for air in published work.

The main focal point of the present investigation was on the computational prediction of the drag crisis which is based on CFD methods**. Wen et al. (2017)** investigated the drag crisis phenomena that occur between the sub-critical and supercritical Reynolds number. In this work, blocked structure meshes with polished grids close the cylinder surface and in the downstream were applied. Both 2D and 3D computation were performed using the different turbulence models, including the SST with LCTM, the DES model, and the LES, the SST $k - \omega$ model, the $k - \varepsilon$ model. Different Reynolds numbers between Re=$6.31\text{x}10^4$ and $7.57\text{x}10^5$ were used for the validation. The averaged drag force, the RMS of lift force and the Strouhal number were compared with experimental data. The studies marked that standard 2D and 3D RANS methods were weak to capture the drag crisis phenomenon. Though the Large Eddy Simulation method can address the doubt.

The Strouhal numbers which are found out in this work were compared with experimental data from de Wilde et al. [6] and the ITTC report [15] shown in figure2.10. The predicted Strouhal numbers normally followed a similar pattern to that of the experimental results and increased gradually as increasing the Reynolds number. Though, the Strouhal numbers were over-predicted at the sub-critical Reynolds numbers and were under-predicted at the super-critical Reynolds numbers. Strouhal numbers by 2D and 3D RANS with SST k−ω model were smaller.
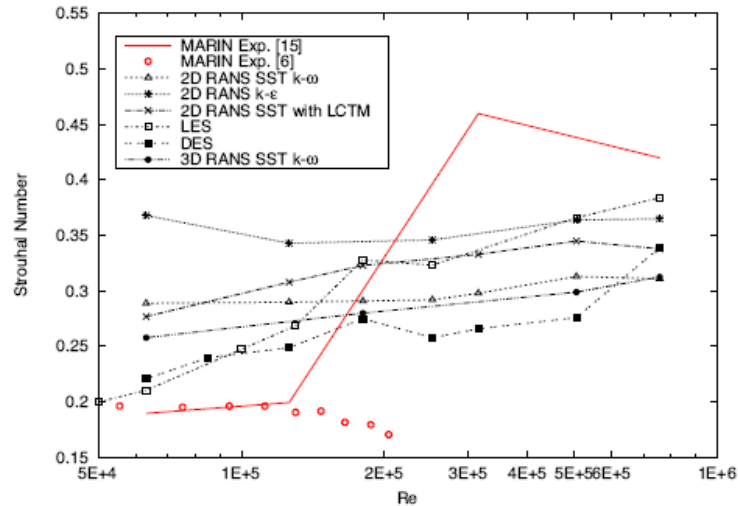
Figure 2.10: Variation of Strouhal number with Re. (Wen et al.(2017)

Moreover, figure 2.11 compares the spectra which were achieved from the lift forces predicted by 2D and 3D RANS models with the SST k − ω turbulence model and by the LES model. The study were carried out for two Reynolds numbers, (a) Re = 6.31×10^4 and (b)Re = 7.57×10^5. It was clearly visible that the spectra by the RANS models all have a single crest at Re=$6.31x10^4$ and Re=$7.57x10^5$(right). This suggests that the vortices flow predicted by the RANS models thickened at a single frequency at any Reynolds number. The spectrum predicted by LES at Re = 6.31×10^4 had a single narrow crest, where the spectrum is more spreading at Re = 7.57×10^5. The spectra pattern obtained from the LES simulation was consistent with that described in the work of de Wilde and Huijsmans [6], although that from the RANS solution was not. The variations in the spectral patterns were attention due to turbulence modelling.
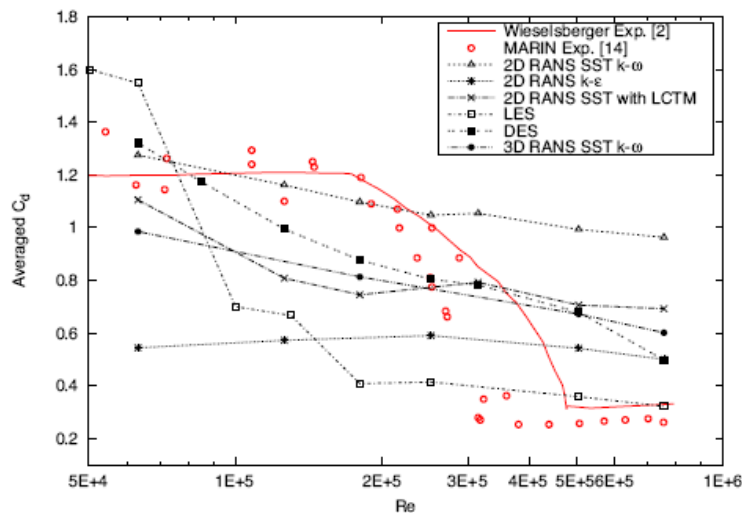
Figure 2.11: Variation of averaged drag coefficients vs Re [Wen et al. (2017)]

Dutta et al. (2004) studied the impact of coordination in the wake of a square cylinder at the laminar region. The experimental research of flow past a square cross-section of the cylinder at Reynolds number range of Re=97-187 is stated. Cylinder coordination of 00-600 with regard to the mean flow has been treated. Two-part hotwire anemometry has been take-up for calculations of velocity. The cylinder's wake has been anticipated with a pulsed laser coat to know the flow formation. The calculation has been performed in the near wake, mid-wake and far wake of the cylinder. The impact of coordination and Reynolds number on drag coefficient, Strouhal number, time average, and rms velocity allocation, the collapse of velocity oscillations and power spectra are of concern. The drag coefficient and Strouhal numbers are compared to the angle of the cylinder. A variation in the cylinder adjustment experienced an initial arrival of quasi-periodicity and therefore, three-dimensionality, unpaid to the irregular kind of the wake. The structure of the mean velocity portrait, oscillations and the rate of collapse display an active reliance on the cylinder adjustment in the adjacent wake, however dependency decrease in the far wake. In a group of angle considered, the wake of a cylinder whose orientation is 22.50 with regard to the incoming flow is unusually energetic and display powerful three-dimensionality.

2.1.2 Studies on vortex flow around bluff body

One of the universal conditions where computational techniques are of vast support to engineers and scientists is in the design of different fluid stream phenomena. These technologies have enhanced to specific the extent that complete airplane construction is presently achievable [(Rogers et al. (2001), Shang et al. (2004), Fujii et al. (2005)]. Still, in the territory of wind engineering, computational fluid dynamics (CFD) is alone just start to be used for the construct of aerodynamic design for air effects, like long-span bridges, because of the challenges of complicated design, large- Reynolds numbers and the communication of bluff bodies with the boundary layer of atmosphere. So, modeling is generally based on an important matrix of air channel study which is carried out to support in the assurance of the optimum aerodynamic structure which gives the area of realistic restriction for the specific design in an inquiry. The specific attention of these analyses is to reduce or check aero flexible inconsistency containing bluff body sparkle and whirlpool-induced fluctuations, including to resolve buffeting loads (look, such as [Davenport(1962), King (2003)]. So, the Strouhal number is frequently one of the extreme valuable criteria to be achieved for flows over these bluff bodies.

Roshko (1954) presents three experiments on the flow past a circular cylinder at very high Reynolds number Re=10^5 -10^6. The drag value increases from its low hypocritical value to a value of 0.7 at and then shift constantly. Vortex shedding occurs at Reynolds number Re>3.5×10^5along with Strohaul number 0.27.

The vortex shedding around a circular cylinder in the critical regime where the Reynolds number ranging from 10^5 to 7.5×10^5 is performed by **Bearman(1968).** The Reynolds number which based on the diameter of the cylinder. Restricted-band vortex shedding has been noticed up to Re=5.5×10^5, namely strong inside the critical regime. Strouhal number arrive the surprisingly high value of 0.6 at this Reynolds number. Spectra of the velocity oscillations calculated in the wake are granted for assorted Re values.

Hakozaki et al. (1982) perform experimental work on the vortex shedding frequency different rectangular cross-section cylinder were regulate in an air tunnel and in a water container. The results exhibit that how Strouhal number change with a cylinder's width to height ratio within the Reynolds number range of 70 -20,000. There is observed to stay a convincing range of Reynolds number with the width to height ratios of 2 and 3 where flow arrangement unexpectedly varies with an abrupt stop in Strouhal number. The variations in flow design corresponding to the stop of Strouhal number have been proved by way calculation of velocity allocation and flow determinations. These results are correlated with those of alternative researchers. The experimental results show reasonable good agreements with the other simulation results.

The forced convection heat transfer for considering the axial flow of air on the external surface of a whirling cylinder which is studied by **Smyth and Zurita (1994)**. The study was two dimensional along an grant for a rotating segment of velocity over the cylinder. The outcome exhibit that an exponential law interact the numerical statistics strong with an exponent of 0.8, like is gain for turbulent flow spent a flat plate. The data were correlated with that feasible for mix flow, orbit never turns into dominant sufficient to create the Nusselt number autonomous of the blasting Reynolds number.

A numerical analysis of vortex shedding for two-dimensional time-dependent flow about rectangles in the infinite territory. The numerical approach applies for third order upwind divining for convection and Leith kind of temporal differencing. An undertake the use of minimizing order scheme and its imperfection are further represent. The Reynolds number reign is ranging from 100 to 2800. Another parameter is like the angle of attack, upstream

velocity profile, rectangle dimension are varied. The introduction and consecutive improvement of the vortex shedding aspect are examined. The equity of vortices is found to be firmly dependent on Reynolds number, while are a drag, lift, Strouhal number. Calculated Strouhal numbers correlated strongly with those gain from a wind tunnel analysis for Reynolds numbers less than 1000.

Aerodynamic aspects and flow arrangements over a rectangular cylinder with a portion of different depth/breadth ratios have been studied by **Tamura and Itoh (1996).** The arrangement of the cyclic vortex shedding in the wake discharge of cylinders is delicately affected by the form of after body of the cylinder. Sometimes the Strouhal number is bounce due to the alteration of the depth/breadth ratio of the cylinder. In this work, the detached flow over a cylinder along different sectional configuration is solved with finite difference method of the incompressible Navier-stokes equations. The mechanism of the changeable and extreme variation in vortex shedding is examined, over the analogy between the numerical simulation and experimental data. Here further take into attention the attitude of the detached shear layers from the cylinder and their following vortex development method in the adjacent wake.

The wake flow fluctuations due to vortex shedding were characterized experimentally for the case of a triangular prism of moderate aspect ratio having two different cross-section (equilateral and isosceles with 90°apex angle), placed vertically on a plane by **Buresti et al. (1998).** The choice of a triangular shape for the cross sections of the prism was mainly dictated by the low Reynolds number dependence of the geometry (due to the presence of shape edges fixing the boundary layer simulation), and by the possibility of obtaining quite different flow conditions by varying the orientation of the models to the wind; furthermore, a very limited number of data existed in the literature for this body shape.

Two-dimensional numerical computations of the Benard-von-Karman fluctuation following trapezoidal shape bluff body has been performed by **Kahawita and Wang (2000)** using the spline method of fractional steps. For critical Reynolds number, i.e. Re/Re_c <2, the computational results approve the experimentally noticed action recorded by Goujon Durand et al. (Phys. Rev. E 1994), especially the highest magnitude of the velocity component fluctuate accompanying the crucial frequency follows reasonably strong the scaling laws and the location. The impact of the trapezoidal body on the critical Reynolds number value and on the vortex shedding is shortly explained. It arrives that the impact of the trapezoidal height

(H) is the commanding impact on the Strouhal number value when distinguished with the effect of shorter trapezoidal base width B.

Flow nature in the adjacent wake of a circular cross-section of a cylinder placed near to a completely grown turbulent boundary layer is studied experimentally with PIV technique by **Wang and Tan (2007).** The Reynolds number which based diameter of the cylinder is 12,000 and circumstance boundary layer thickness is δ=0.4 D. Particularized of vorticity and velocity territory in the wake zone are given for different gap altitude (S) between the circular cylinder and the surface, accompanying S/D varies from 0.1-1.0. The outcome declares that at, the flow is described through the repeated, Karman-like circular current shedding from the uppermost and under the face of the cylinder. For short and transitional cut ratios, the wake flow grows definite irregularity around the centreline of the cylinder. Still, few flow batch, like the convection velocity of the discard circular current, Strouhal number, maintain approximately fixed and practically free of S/D.

Rajani et al. (2009) have investigated the numerical simulation of laminar flow past a circular cylinder in various laminar flow regimes. In this work, the implicit pressure-based finite volume method is used for time accurate computation of incompressible flow with second-order accurate convective flux discretization scheme. Skin friction coefficients, recirculation wake length at the invariant flow regime, Strouhal frequency of vortex shedding mean and rms value of the oscillating aerodynamic coefficient for cyclical flow regime. The complicated flow structure of the cylinder wake is also fairly captured by the current forecast procedure.

In figure 2.12 the surface pressure and skin friction coefficient are present in three different Reynolds number. For all the Reynolds number the measurement data and simulation results are a good agreement to each other in the drive flow zone which is covering the front part of the cylinder. These differences may be associate usually to the incorrect guess of the location of the variable flow separation point on the cylinder surface. The differences may also be attributed to the three-dimensional fluctuation of the wake with the spanwise direction at Reynolds number Re=200 and Re=300.
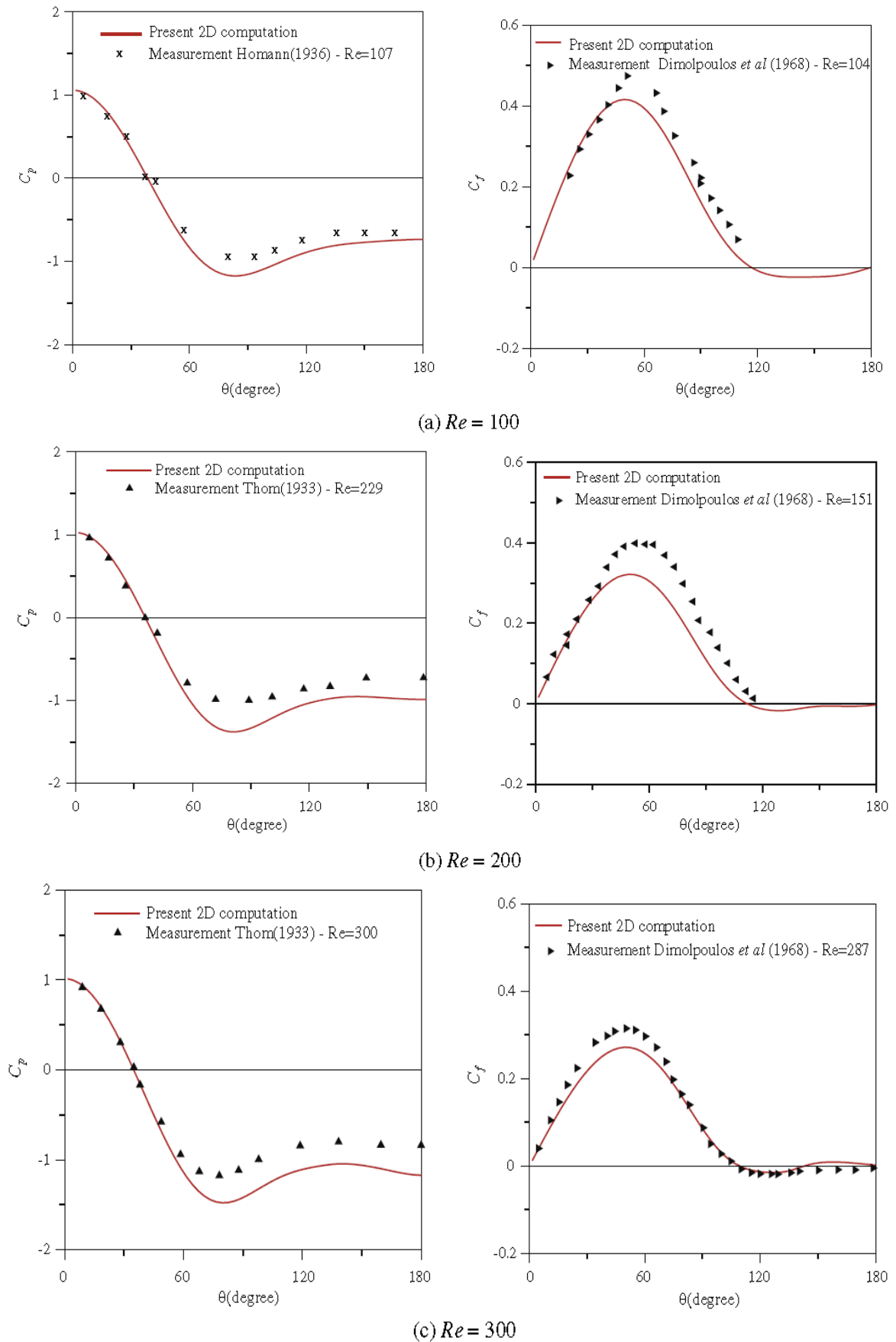
(a) $Re = 100$

(b) $Re = 200$

(c) $Re = 300$

Figure 2.12: Distribution of surface pressure and skin friction around the cylinder at different Reynolds number (Rajani et al., 2009).

49

The vortex dynamics in the cross-section of circular cylinder wake was analyzed by **Williamson et al. (1996),** seeing that the analysis of fluctuating flow phenomena by "Berger and Wille (1972)" in this journal past twenty years ago, there had a surge of activity about bluff body wake. New approaches in an experiment, laser-induced fluorescence, and Particle-Image Velocimetry are sincerely being applied to wakes but certain of the new invention has come from concerned use of the classical process. These advanced evolutions and discoveries of the different new approaches in wakes are given in this survey.

Figure 2.13 shows the transition to three-dimensionality in the wake can smoothly be described along regarding the Strouhal -Reynolds number. It is observed that the transition, originally stated by **Roshko (1954),** associated with two discontinuous changes "(Williamson 1988b)".The first interruption the frequency of Strouhal decrease from the laminar curve to one interrelated to a mode A3-D shedding, at close Re=180-190. The mentioned interruption is most erotic and the exact Recruit depends on whether the flow speed is increased or decreased and on the experimental arrangements, as shown below. When Re increased close to 230-260, there is another interruption in Strouhal number, demonstrate a new mode B. This break may be a conflict with the first in that it is not most erotic, and rather incorporate a gradual transfer of energy from mode A to mode B, as one enlarged Reynolds number.
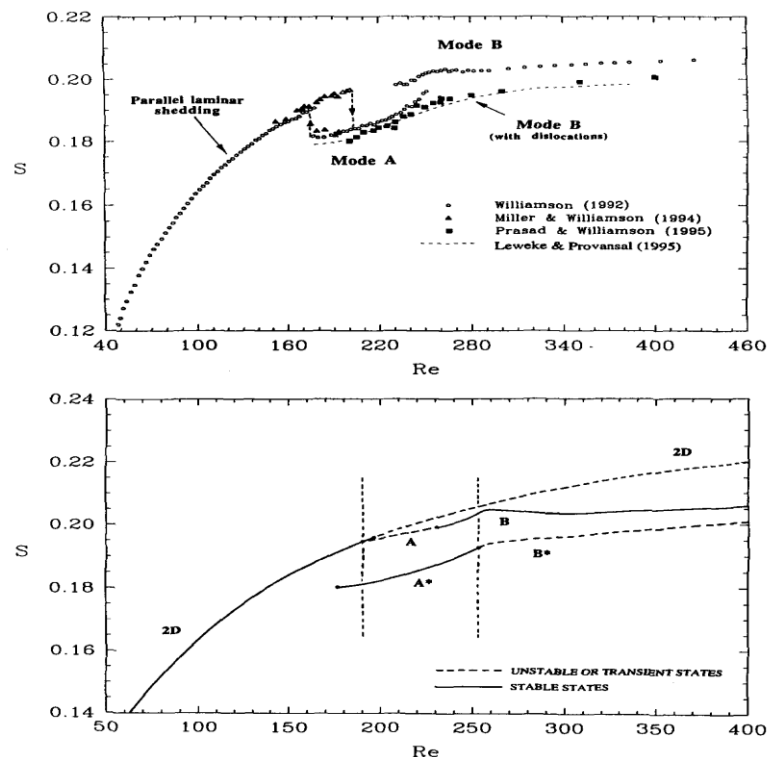

Figure 2.13: Strouhal-Reynolds number relation on laminar and **3-D** transition reign. *(a)*The transition reign is describe by two different stop in the measured wake specification, **as** Re is

rise, and possibly cleverly explained with citation to this S-Re plan. *(b)* A fresh analysis of the Strouhal contour; the top contour conform to short scale inconsistency only (like A, B), the bottom one conform to these inconsistency linked with infrequent vortex displacement (like A*, **B***)**.** The normal wake transition pursue the order *(2D* + **A*** + B). (plan from **Williamson 1995a.)**

In the transition zone, velocity fluctuation profile in the wake is distinctly different from those associated with the laminar regime which is shown in figure 2.14. Such as the turbulent flow profile at Re=183, shows a vast proportional peak in the center plane of the wake as noticeable from the two lower side crest for the Reynolds number Re=52, generally correlate with the two rows of laminar vortices sail downstream. "Williamson (1992a)" exhibit that the presence of vortex disorder produces this large central crest in the profile, in addition to the slow decay of oscillating velocity downstream of the bluff body in fig 6b.the intermittent irregularity which is originally found by Roshko (1954), are shown in figure 2.13(c).
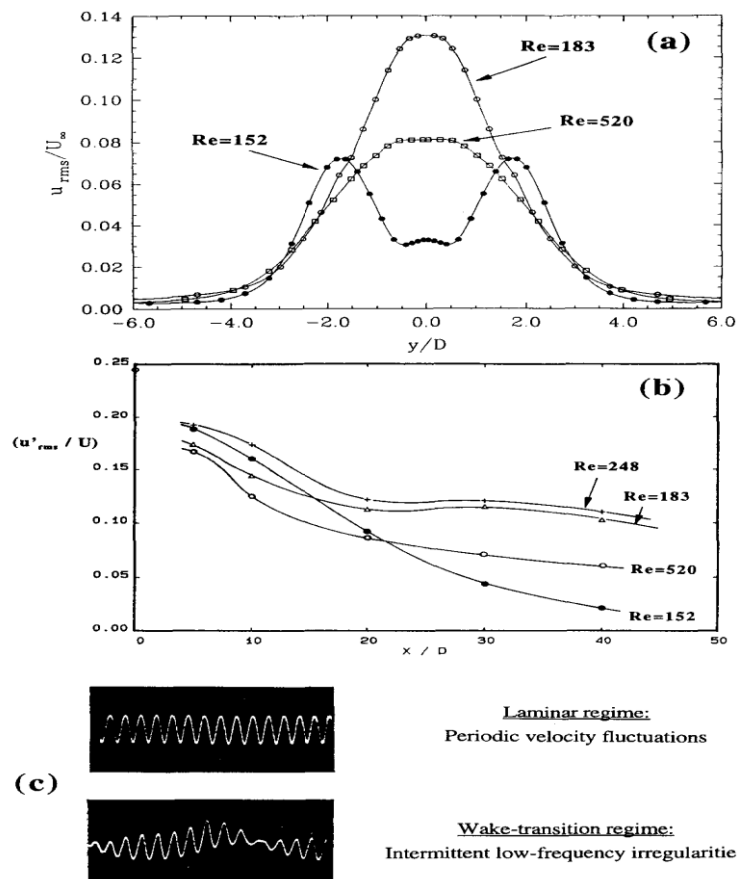

Figure 2.14: Velocity study in the transitional wake. **(a)** The rms velocity oscillation profile measure in both the laminar reign (Re = **152)** and more in the wake-transition reign (Re = 183), at **x / D = 10.** (b) next collapse of normalized rms velocity oscillation, display the

exactly various ratio of break-down in the laminar reign (Re = **152)** vs the transition reign (Re = **1,83,248).** (plan from Williamson 1995a.) **(c)**small-frequency infrequent velocity oscillation sketch and next breakdown plan display in **(a)** and (b). Specific massive variation inconsistency were initial observed.

The three dimensional inconstancy of the wake of the square cylinder bluff body was investigate by **Robichaux et al. (1998)**. Floquet steadiness study is engaged to draw out the various modes of three dimensional inconstancy. It is seen that the three dimensional transition method for a square cylinder is identical to that of a circular cylinder. Especially the long wavelength(mode A) three dimensional disruption which becomes inconsistent early at Reynolds number of around 161, take the place of by a short wavelength(mode B) three dimensional disruption that becomes inconsistent at a Reynolds number of about Re=190.In adding, a third intervening wavelength mode is also seen to convert into unstable condition at a Reynolds number of about 200. Different mode A and B, the middle wavelength manner is sub-harmonic accompanying a duration of twice the shedding cycle of the two dimensional base condition. The space-time similarity of three models are investigate in detail.

Thompson et al. (2001) studied the physical nature of primary transition in bluff body wakes. Based on various suggested mechanism, the probability classification as an elliptical uncertainty is reconstruct in this article. The details of transition Floquet study shows the fair confirmation of the increase elliptic uncertainty in the build vortex centre chased by amplification by the powerful strain field in the hyperbolic zone between the developed and shed vortices. Actually, it arrive that the wake instantly trailing the cylinder display noticeable signs of a coordinated elliptic uncertainty as found long ago for connecting anti-rotating vortices. More downstream, later the vortices have been drop into the wake, the uncertainty again raise in the nucleus.

The impact of coordination on the wake of a square cylinder at laminar region is performed by **Dutta et al.(2004)**. The experimental research of flow past a square cross section of cylinder at Reynolds number range of Re=97-187 is stated. Cylinder coordination of 0^0-60^0 with regard to the mean flow have been treated. Two part hotwire anemometry has been take-up for calculations of velocity. The cylinder's wake has been anticipate with a pulsed laser coat to know the flow formation. Calculation have been performed at the near wake, mid wake and far wake of the cylinder. The impact of coordination and Reynolds number on drag coefficient, Strouhal number, time average and rms velocity allocation, collapse of velocity

oscillations and power spectra are of concern. The drag coefficient and Strouhal number are compare to the angle of cylinder. A variation in the cylinder adjustment experienced to an initial arrival of quasi-periodicity and therefore, three dimensionality, unpaid to the irregular kind of the wake. The structure of the mean velocity portrait, oscillations and the rate of collapse display a active reliance on the cylinder adjustment in the adjacent wake, however dependency decrease in the far wake. In a group of angle considered, the wake of a cylinder whose orientation is 22.5^0 with regard to the incoming flow is unusually energetic and display powerful three-dimensionality.

Liu et al. (2011) investigate a two-dimensional (2-D), whirlpool particle technique is carried out, and computation of flows over different bluff bodies are conferred, with a thorough investigation of the flow over rectangular cylinders. Then long-time simulations of flows around the square and rectangular cylinders with low to moderate Reynolds numbers are carried out. The arise Strouhal–Reynolds number connection is correlated with experimental and simulation results in the study of literature. For rectangular cylinders, the familiar stepwise difference between the chord-based Strouhal number and the chord-to-thickness ratio is a repeat. Then the flow field surveys and compared with the experimental investigation. More studies with recognizing vortices supply fresh judgment inside the shedding method which leads to the stepwise difference of chord-based Strouhal numbers and the frequency vault.

Literature survey suggests that the effect of inlet fluctuation on the transport process over bluff bodies are not covered comprehensively. Only one experimental work "Kondjoyan and Daudin, (1995)"documents the effect of turbulent intensity on the circular and elliptic cylinder and no such studies have been performed for the square cylinder. Hence investigations of inlet fluctuations in the form of prescribed turbulent intensity are undertaken in this work covering both the laminar and turbulent regimes.

2.2 Studies on augmentation of heat transfer in a channel wall in presence of bluff body

Augmentation of heat transfer is a subject of considerable interest to researchers as it leads to savings in energy and cost. A bluff body can be defined as a body that as a result of its shape has separated flow over a substantial part of its surface. An important feature of a bluff body flow is that there is a very strong interaction between the viscous and

inviscous regions. If we consider that at the moment of starting the flow is attached then the adverse pressure gradient that this flow imposes on the boundary layer will be too great to sustain the attachment.

Edwards and Alker (1974) found that the delta winglets provided a higher overall heat transfer enhancement, compare to cube placed on a plate'. Experimental investigation of Doi et al. (1977) showed that the heat transfer is locally enhanced in the region where neighbouring vortices impose a flow toward the surface and heat transfer locally decreases where the vortices impose flow away from the surface.

The incompressible laminar flow and heat transfer in a 2-D channel with a built-in triangular prism were computationally analysed by **Abbasi et al. (2002).** They showed that the use of a triangular prism could enhance the heat transfer to the channel walls. Heat exchangers have several industrial and engineering applications. The design procedure of heat exchangers was quite complicated, as it needs exact analysis of heat transfer rate and pressure drop estimations apart from issues such as long term performance and the economic aspect of the equipment. The major challenge in designing a heat exchanger was to make the equipment compact and achieve a high heat transfer rate using minimum pumping power.

Chattopadhyay (2007) numerically carried out the turbulent flow and heat transfer around a triangular prism in a channel in the turbulent flow regime up to the Reynolds 40,000. The aspect ratio between the channel wall to the prism element was 4.0. The Navier–Stokes equation along with the energy equation was resolved to apply the SIMPLE method and the standard k–ε model was preferred for turbulence stoppage. A structured grid was used at the entrance and exit domain, the area close to the prism element was discretized by using an unstructured triangular mesh. The results showed that in the presence of a triangular prism, heat transfer in a channel was enhanced by around 15%. The augmentation in heat transfer is connected to the vortex development downstream of the prism element.

The numerical solutions of a viscous uniform approach flow past square and diamond cylinders, with and without rounded corners was carried out by **Dalton et al. (2003).** The Reynolds number was in the range of 250-1,000. This unsteady viscous flow problem was solved by the 2-D Navier–Stokes equations in vorticity and stream-function form on body-fitted coordinates. The finite difference method was used. Central-difference

schemes, Second-order Adams-Bash forth were used to discretize the vorticity transport equation and a third-order upwinding scheme was used to represent the nonlinear convective terms. For an efficient mesh system for the flow a grid generation technique was used. The average in-line force coefficients and Strouhal number and agree well with previous numerical and the experimental value. The evolutions of vortex shedding and vortex structures were illustrated by vorticity contours. Rounding the corners of the diamond and square cylinders produced a noticeable decrease on the lift and drag coefficients.

Techniques for heat transfer augmentation are relevant to several engineering applications. These studies demonstrated heat transfer enhancement and can be conveniently categorized in passive and active techniques by **Webb et al. (2005)** and **Bergeles (1983)** which either harness flow energy or utilize an external source of energy to augmentation the heat transfer respectively. The flow past bluff, rigid bodies such as rectangular cylinder studied by **Valencia(1995),** inclined square cylinder by Yoon et al. (2009), triangular cylinder by Chatterjee et al. (2012). Biswas et al. (1992) and Hiravennavar et al. (2007) on a channel.

Benim et al. (2011) investigated computational analysis of turbulent forced convection in a channel with a triangular prism using cascade of modelling strategies Reynolds Averaged Numerical Simulations (RANS) and two-dimensional Unsteady RANS (2D URANS) were used for the Reynolds numbers of (Re) 2,500, 5,000 and 25,000.and the Prandtl number of 0.7 in all computations'. For Re ¼ 2500 and Re ¼ 5000 three-dimensional URANS (3D URANS) and Large Eddy Simulations (LES) were also performed. For the RANS and URANS computations, the Shear Stress Transport (SST) model was used as the turbulence model.

number of 40,000.

The confined flow and heat transfer across a triangular cylinder in a channel was thoroughly investigated by **Srikanta et al. (2010)**. Reynolds number of 1-80 and Prandtl number of 0.71 were considered for a fixed blockage ratio of 0.25. The governing Navier-Stokes and energy equations along were solved by using a commercial CFD solver FLUENT (6.3). the temperature and flow field is shown by isotherm and streamlines, respectively. Average Nusselt number, mean drag coefficient, wake length/recirculation length, etc. were reported here. The transition to a transient is found

to lie between Re=58 and Re=59. The average Nusselt number and the wake length increase with increasing the value of Reynolds number, though, the mean drag coefficient decreases with increasing the value of the Reynolds number. Also, simple correlations for average Nusselt number, wake length, mean drag coefficient are obtained for the range of above Reynolds number.

Zheng and Zhang (2011) investigated the flow fields in vortex flow sensors with a circular cylinder and trapezoidal cylinder bluff bodies'. Also, the characteristics of two flow fields were compared by numerical simulations while the mechanism of vortex shedding was analyzed in detail.

Finally, the reason, which leads to different vortex shedding frequency and affects the relationship between Reynolds number and Strouhal number, was specified as the size of the wake flow region behind the bluff body where the vortex generated. Steady and unsteady forced convection flow and heat transfer past a long expanded trapezoidal bluff body were investigated for the air as working fluid for Re = 1–150. The wake length increases as the Reynolds number increases in the steady flow regime ($1 \leq$ Re ≤ 47). However, heat transfer, as well as Strouhal number, increases with the increasing value of the Reynolds number.

The maximum augmentation in heat transfer for the expanded trapezoidal cylinder concerning the tapered trapezoidal cylinder was found to be approximately 146% by **Dhiman and Ghosh (2013).** Heat transfer enhancement in duct flow by using an inclined vortex generator was numerically investigated for the air as working fluid for Reynolds number, Re = 1–150. The wake length rises when the Reynolds number rises in the steady flow regime $1 \leq Re \leq 47$ The changeover from a steady regime to the unsteady regime happens between Re = 47 and 48. The total drag coefficient reduces with the rising value of Reynolds number up to Re = 90 and then it rises along with Reynolds number. Though, heat transfer including Strouhal number rise with the rising value of the Reynolds number. The highest enhancement in heat transfer for the enlarge trapezoidal cylinder with honor to the tapered trapezoidal cylinder was found to be almost 146%. On the alternative side, pressure decline displays an augmentation of nearly 97% for the enlarge trapezoidal cylinder when compared with the tapered cylinder. Simple correlations of wake length, average Nusselt number, and Strouhal number, drag, with Reynolds number were further entrenched.

Yoon et al. (2009) investigated a square cylinder located on the centreline of laminar channel flow, which was subject to a constant heat flux on the lower channel wall. As the cylinder was inclined with some angle of attack concerning the main flow direction, flow characteristics change downstream of the cylinder and significantly affect heat transfer on the channel wall.
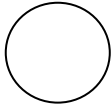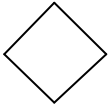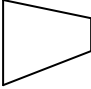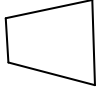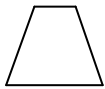
In summary, the state of art survey focuses on transport phenomena around the bluff body as well as possibility of heat transfer augmentation in confined channels by introducing bluff bodies. Lietrature survey shows that there is very less amount of work on the effect of inlet turbulence intensity in both the cases. So a combination of different shapes of bluff body in tandem with inlet turbulence was used in this work.

2.3 Objective of the Thesis

After a comprehensive survey of literature, the objective of this thesis has been set to address certain unexplored issues involving transport phenomena around bluff bodies. This work is mainly concerned about the following points:

i.   To study transport phenomena around bluff bodies at all flow regimes with varying turbulent intensity at the inlet.

ii.   To compare the performance of different bluff bodies e.g. circular cylinder, square cylinder, triangular prism, a diamond in heat transfer enhancement in a channel.

iii. To study the effect of Turbulence Intensity on heat transfer around bluff bodies and also enhancement on channel walls.

iv.   To study the heat transfer at different confinement ratio and also without confinement.

In this work different shapes of bluff bodies have been considered. They are (1) Square cylinder, (2) Circular cylinder, (3) Triangular prism, (4) Diamond, 5(a) Large edge facing Trapezium, (b) Small edge facing Trapezium, (c) Symmetrically placed which are shown in below.

Square cylinder	Circular cylinder	Triangular prism	Diamond
Large edge facing trapezium	Small edge facing trapezium	Symmetrically placed trapezium	

CHAPTER- 3

MATHEMATICAL MODELING

3.1 Introduction

This work addresses a numerical review of heat transfer enhancement using different shapes bluff bodies.

This chapter describes the technique with which the solutions were achieved. In most of the literature cited in chapter 2, the flow regime has been independently assessed based on whether the flow is laminar or turbulent. Here in this work, Reynolds-averaged Navier–Stokes equation (RANS) based approach is used to analyze flow construction of laminar, turbulent and also while in the transition from laminar to turbulent.

Since the working fluid, air, is assumed to be Newtonian, the flow of the fluid can be described by the Navier-Stokes equations. Therefore, the heat transfer and fluid flow under consideration are governed by the Navier-Stokes and energy transport equations. The working fluid is considered to be incompressible, and thermal radiation, chemical reaction, and compression work are negligible. The Navier-Stokes equations, developed by Stokes and Navier, represent the general behavior of the fluid. They are continuity, momentum and energy equations.

3.2 Transition Shear Stress Transport (SST) turbulence model

The predictions of turbulent flows can be based on the time-averaged properties of turbulence. The process of time-averaging gives rise to fluctuating temperature and velocities in the conservation equations. These small-scale turbulent fluctuations do not have to be directly simulated. To achieve this, the Navier-Stokes equations are rendered tractable by employing the Reynolds Averaged Navier-Stokes (RANS) equations.

Within the frame work of a RANS approach, the momentum and energy equations are closed by a turbulent viscosity hypothesis, where the turbulent viscosity is obtained via the Transitional SST model of (Menter et. al. 2002), allowing a seamless modelling of all three flow regimes by a single formulation. The turbulence model requires the solution of the transport equations of three quantities, namely the turbulence kinetic energy (κ), the specific dissipation rate (ω), the intermittency (γ) and the momentum thickness Reynolds number

(Re$_{\theta t}$). Thus, with the three components of the momentum equation, the pressure correction equation (replacing the continuity equation) and the energy equation, the total number of field equations to be solved results in nine.

Abraham et. al. (2009) used transition SST model to predict the heat transfer characteristics in all flow regimes i.e., laminar, intermittent and turbulent. The authors used one set of Reynolds averaged conservation equations for mass, momentum and energy with two supplementary equations for turbulent viscosity and effective thermal conductivity and another set for turbulence containing equations to solve turbulent kinetic energy, specific rate of turbulence dissipation and intermittency. This intermittency will help in predicting laminar to turbulent transition. The same Transition-SST model was used for predicting heat transfer in all flow regimes for various heat transfer problems effectively, namely parallel plate channels (Minkowycz et. al. 2009), Internal flows (Abraham et. al., 2010 and Abraham et. al., 2011), diverging conical ducts (Sparrow et. al., 2009), and synthetic jets (Abraham and Thomas 2009).

As the pressure correction scheme, the SIMPLE scheme is used. For the discretization of the convective terms, the Second Order Upwind scheme is used for the momentum and energy equations, and the second Order Upwind scheme for the transport equations of the turbulence quantities. The convergence criteria for continuity, momentum and energy are set at 10^{-4}, 10^{-5}, and 10^{-7} respectively. The convergence criterion for the four turbulence quantities was also fixed at 10^{-4}.

3.3 Governing Equations

The three dimensional governing equations of continuity, momentum and energy equations are solved using transition SST model modified and proposed by **Abraham et. al. (2009)**. The flow is steady, incompressible Ansys Fluent 16.2 is used to solve the following governing equations.

Continuity equation

$$\frac{\partial u_i}{\partial x_i} = 0 \qquad \text{i=1,2} \tag{3.1}$$

Momentum equation

$$\rho\left(u_i\frac{\partial u_j}{\partial x_i}\right) = -\frac{\partial p}{\partial x_i} + \frac{\partial}{\partial x_i}\left((\mu + \mu_{turb})\frac{\partial u_i}{\partial x_i}\right) \quad \text{j=1.2}$$

(3.2)

Energy equation

$$\left(u_i\frac{\partial\Theta}{\partial x_i}\right) = \frac{\partial}{\partial x_i}\left(\left(\alpha + \frac{v_{turb}}{\Pr_{turb}}\right)\frac{\partial\Theta}{\partial x_i}\right)$$

(3.3)

The values of turbulent Prandtl number ($\Pr_{turb}$) are taken from "Abraham et. al. (2009)". The laminar to turbulent modelling provided by the following equations for K and ѡ.

$$\frac{\partial(\rho u_i\kappa)}{\partial x_i} = \gamma.P_\kappa - \beta_1\rho\kappa\omega + \frac{\partial}{\partial x_i}\left(\left(\mu + \frac{\mu_{turb}}{\sigma_\kappa}\right)\frac{\partial\kappa}{\partial x_i}\right)$$

(3.4)

$$\frac{\partial(\rho u_i\omega)}{\partial x_i} = A\rho S^2 - \beta_2\rho\omega^2 + \frac{\partial}{\partial x_i}\left(\left(\mu + \frac{\mu_{turb}}{\sigma_\omega}\right)\frac{\partial\omega}{\partial x_i}\right) + 2(1-F_1)\rho\frac{1}{\sigma_{\omega2}\omega}\frac{\partial\kappa}{\partial x_i}\frac{\partial\omega}{\partial x_i}$$

(3.5)

where $\mu_{turb} = \dfrac{a\rho\kappa}{\max(a\omega, SF_2)}$

(3.6)

The working equations for the intermittency and intermittency adjunct function Π adopted [2002, 2009] are given below.

$$\frac{\partial(\rho\gamma)}{\partial t} + \frac{\partial(\rho u_i\gamma)}{\partial x_i} = P_{\gamma,1} - E_{\gamma,1} + P_{\gamma,2} - E_{\gamma,2} + \frac{\partial}{\partial x_i}\left(\left(\mu + \frac{\mu_{turb}}{\sigma_\gamma}\right)\frac{\partial\gamma}{\partial x_i}\right)$$

(3.7)

$$\frac{\partial(\rho\Pi)}{\partial t} + \frac{\partial(\rho u_i\Pi)}{\partial x_i} = P_{\Pi,t} + \frac{\partial}{\partial x_i}\left(\sigma_{\Pi,t}(\mu + \mu_{turb})\frac{\partial\Pi}{\partial x_i}\right)$$

(3.8)

The equations (3.4), (3.5), (3.7) and (3.8) are the additional equations which are solved along with regular equations of continuity (3.1), momentum (3.2) and energy (3.3) for calculating velocities, pressure, temperature, turbulent kinetic energy, specific turbulent dissipation and intermittency (γ). The state of transition will depend on intermittency parameter (γ) which varies from 0 to 1. Near 0 value of γ determines the state as laminar, while the value near 1

determines the flow as turbulent. The term Π is again required for calculation of term F_1 in eqn. (3.5). The details are available in "Menter et al (2002)".

In equation (3.7) the transition sources are describe as follows:

$$P_{\gamma 1} = C_{a1} F_{length} \rho S \left[\gamma F_{onset} \right]^{c_{\gamma 3}} \tag{3.9}$$

$$E_{\gamma 1} = C_{e1} P_{\gamma 1} \gamma \tag{3.10}$$

Where S is the absolute value of shear strain rate, F_{length} is an empirical correlation which supervision the length of the transition zone, and C_{a1} and C_{e1} grasp the values of 2 and 1, accordingly. The desvastation/relaminarization sources are described as follows:

$$P_{\gamma 2} = C_{a2} \rho \Omega \gamma F_{turb} \tag{3.11}$$

$$E_{\gamma 2} = C_{e2} P_{\gamma 2} \gamma \tag{3.12}$$

Where Ω is the vorticity magnitude. The transition onset is regulated by the following functions:

$$\text{Re}_V = \frac{\rho y^2 S}{\mu} \tag{3.13}$$

$$R_T = \frac{\rho k}{\mu \omega} \tag{3.14}$$

$$F_{onset1} = \frac{\text{Re}_V}{2.193 \text{Re}_{\theta c}} \tag{3.15}$$

$$F_{onset2} = \min \left(\max \left(F_{onset1}, F_{onset1}^4 \right), 2.0 \right) \tag{3.16}$$

$$F_{onset3} = \max \left(1 - \left(\frac{R_T}{2.5} \right)^3, 0 \right) \tag{3.17}$$

$$F_{onset} = \max \left(F_{onset2} - F_{onset3}, 0 \right) \tag{3.18}$$

$$F_{turb} = e^{-\left(\frac{R_T}{4} \right)^4} \tag{3.19}$$

$Re_{\theta c}$ is the critical Reynolds number where the intermittency first starts to raise in the boundary layer. This happen upstream of the transition Reynolds number $\overline{Re}_{\theta t}$ and the difference between the two must be achieve from an empirical correlation. Both the F_{length} and $Re_{\theta c}$ interrelationship are tasks of $\overline{Re}_{\theta t}$.

The constants for the intermittency equation are:

$C_{a1} = 2;\ \ C_{e1} = 1;\ \ C_{a2} = 0.06;\ \ C_{e2} = 50;\ \ C_{\gamma 3} = 0.5;\ \ \sigma_{\gamma} = 1.0$

Previous work on slot jet impingement (Kadiyala and Chattopadhyay, 2017, Pal et al., 2018) and duct flow (Bhattacharya et al., 2017) has reported successful deployment of the method employed here.

Skin friction coefficient is also an important parameter, which is a non-dimensional form of wall shear stress and visualizes the type of flow adjacent to the wall.

$$C_f = \left(\frac{\tau}{\dfrac{1}{2} \times \rho \times U^2} \right) \tag{3.20}$$

The governing equations along with appropriate closures were solved to obtain time-averaged flow and temperature fields. The solution procedure of Patankar and Spalding (1972) implemented in Ansys Fluent 16.2 was adopted. The details of the solution procedure including choice of discretization schemes and convergence criterion are discussed in the following chapters.

For all the computations carried out, special attention was paid to the Y^+ value. The Y^+ parameter was controlled in addition to the grid independency check. The value of Y^+ was kept within 1 - 4. For achieving this, sufficiently fine grids were employed. Y^+ is a non-dimensional wall distance obtained by non-dimensionalizing the distance to the wall via the wall shear stress, viscosity, and density. Figure 3.1 shows the variation of Y^+ values around the bluff body wall.
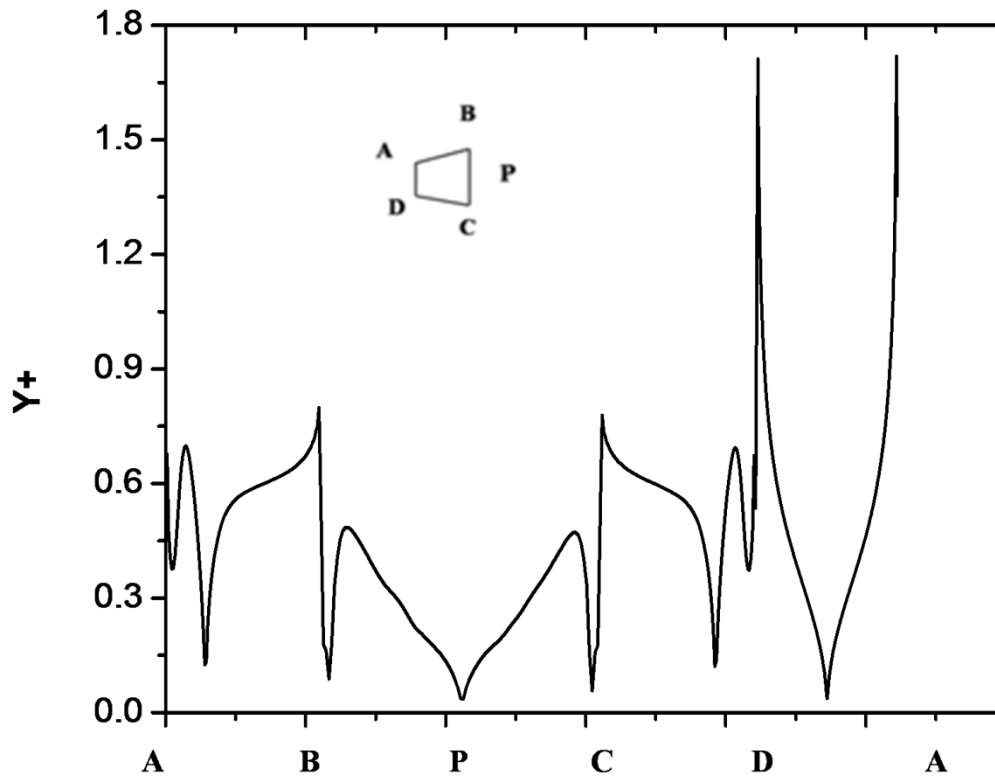
Fig.3.1:Variation of Y$^+$ values

The Nusselt number was calculated according to the following way,

$$Nu = \frac{hD_i}{K} \qquad (3.21)$$

Where, k is the thermal conductivity of air and h is the convective heat transfer coefficient

The Reynolds number based on the hydraulic diameter of the object is given by,

$$Re = \frac{\rho v D_i}{\mu} \qquad (3.22)$$

The friction factor is evaluated by,

$$f = \frac{2}{\frac{L}{D}} \frac{\Delta P}{\rho u_\infty{}^2} \qquad (3.23)$$

Where, ΔP is the pressure drop across the test section and *v* is the mean air velocity of the duct channel.

"Fan et al. (2012)" defined the thermal enhancement factor, η, as the ratio of the heat transfer coefficient of an augmented surface, f to that of a smooth surface, f₀, at an equal pumping power:

$$\eta = \frac{Nu}{Nu_0} / (\frac{f}{f_0})^{0.33}$$ (3.24)

The viscous and pressure forces acting on the both cylinder are used to calculate the drag coefficients. The drag coefficient is given by:

$$C_d = \frac{F_d}{\frac{1}{2}\rho U_\infty^2 d}$$ (3.25)

Where F_d is the drag force acting on the cylinder.

Average Nusselt number is obtained by integrating this value over the surface of the cylinder, which is defined as (for circular cylinder):

$$Nu = \frac{1}{\pi}\int_0^\pi Nu(\theta)d\theta$$ (3.26)

The Nusselt number which can be found by the local temperature gradient:

$$Nu = \frac{\partial T}{\partial z}$$ (3.27)

The pressure co-efficient is defining as:

$$C_P = \frac{P - P_\infty}{\frac{1}{2}\rho U_\infty^2}$$ (3.28)

Chapter

4

Transport phenomena over different shapes bluff body

4.1 Introduction

This chapter explains the simulation of a series of transport phenomena around the bluff body. The research was performing to address the effect of turbulence intensity on different shapes bluff bodies. The results are validated with correlation findings of "Zukauskas (1978)" and "Whitaker (1976)" and with computational results of "Dhiman and Shyam (2011)" and "Dalal et al. (2008)".Among the more discovery of this study, pressure coefficient and surface Nusselt number distribution on the different bluff body surface, the effect of TI on drag coefficient and intermittency at the exit plane are reported here.

4.2 Computational domain

The work considers the forced convection cross flow around five bluff bodies, i.e., a circular, and square cylinder, equilateral triangular prism, diamond and small edge facing trapezoidal cylinder as shown in figure 4.1. While the hydraulic diameter of all bluff bodies is keeping same as D. The non-dimensional distance between the inlet plane and the front surface of the cylinder is 15D and the non-dimensional distance between the rear surface of the cylinder and exit plane is 35D with the total non-dimensional length of the computational domain 50D. The ratio of the width of the cylinder to the vertical distance between the upper and lower walls, H=10D has been used in this work. The problem is considered to be two-dimensional. Air is considered as a working fluid for which Prandtl number of 0.71.
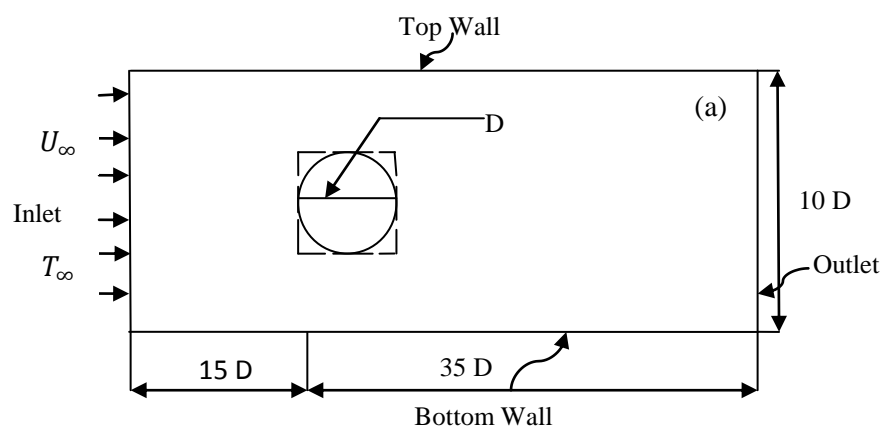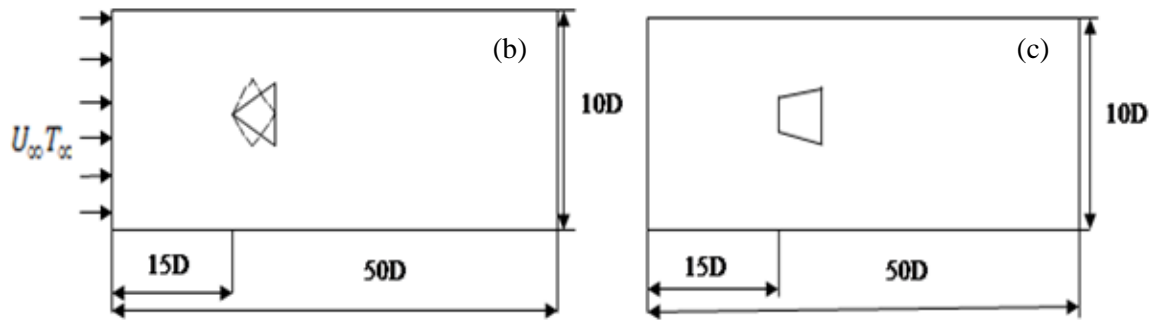
Figure 4.1: Computational domain for flow around a bluff body (a) circular and square cylinder, (b) equilateral triangular prism and diamond cylinder, (c) small edge facing trapezoidal cylinder

4.3 Boundary condition

Fluid approaches to the cylinder with inlet velocity of U_∞ and temperature of the inlet fluid is T_∞ where the cylinder constant surface temperature is maintained about T_s =398 K. The fluid is defined to be air with constant physical properties (Pr=0.71) with an inlet temperature of 298K. The top and bottom walls are assumed symmetrical where the first derivative vanishes. The domain size is fixed and the fluid properties are also considered to be constant thus the variation of Reynolds number is done by changing the inlet velocity.

4.4 Solution procedure

The two-dimensional governing equations of continuity, momentum, and energy equations are solved using the Transition SST model proposed by Abraham et. al. (2009) were discussed in chapter 3. The governing equations are discretized on a non-uniform structured grid using a finite volume method. The governing equations were solved using commercial CFD software ANSYS FLUENT 16.2. The momentum equation was discretized with second-order accurate QUICK scheme by Leonard (1990) for achieving the desired level of accuracy and the energy equation was solved using third-order MUSCL by Van Leer (1979) The solutions were assumed to converge when the scaled residual was below 10^{-5} for momentum, 10^{-5} for continuity and 10^{-8} for energy equations. The interpolation of the gradients of and temperature used the third-order accurate scheme and the gradients for intermittency (γ), turbulent kinetic energy, specific dissipation rate, and momentum thickness was done second order accurate upwind scheme.

After performing a rigorous check for grid independence, adequate numbers of cells were used. The number of cells for the square cylinder case is 210 x 325 and for the circular cylinder, a triangular mesh with 55,000 cells were used. It was found that further refinement of grids does not lead to an appreciable change in results such as drag coefficient and Nusselt number distribution. The number of nodes is 157,368 for the case of TP. Structured meshes are used throughout the domain. The number of nodes is 348,080 and 502,200 for the case of diamond and trapezium respectively. Wall y^+ of the surface of the bluff bodies varies from 0.1 to 5 which are within the recommended limit. The profiles of parameters like Nusselt number and skin friction coefficient were calculated and compared for three levels of grids and finally, a grid size is taken which results in a profile where the values are within 1-2% of the extrapolated profile obtained from three grid levels. A part of the grid is shown in figure 4.2. In the proceeding section, validation with available experimental data from literature is also discussed.

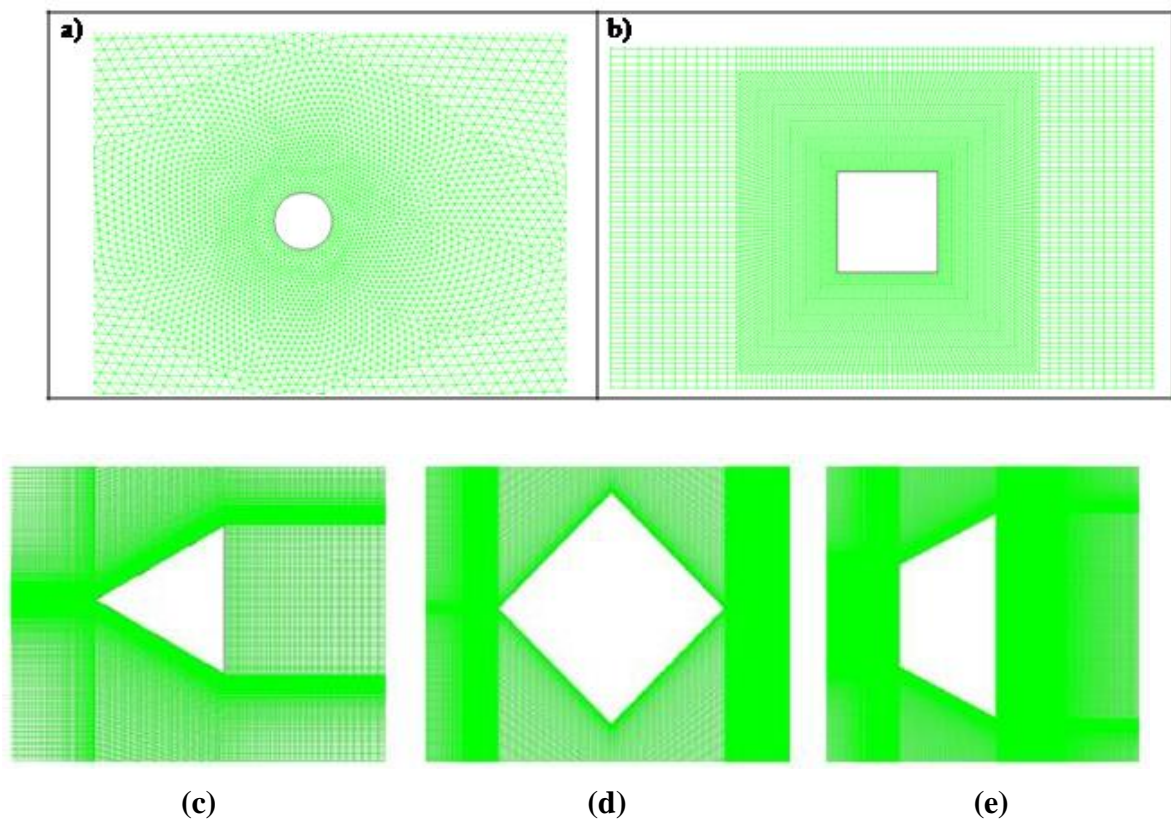**(c)**   **(d)**   **(e)**

Figure 4.2: Close up view of grids (a) circular cylinder (b) square cylinder (c) equilateral triangular prism (d) diamond and (e) small edge facing trapezoidal cylinder

4.5 Results and Discussion

Simulation results obtained for different Reynolds numbers are discussed in this section. The simulations are conducted for Reynolds numbers up to 200,000. The variation of average Nusselt number with the increase of Reynolds number at particular turbulence intensity is investigated and the increase in heat transfer coefficient with the increase in turbulence intensity is reported. The turbulence intensity varies from 5% to 40%.

4.5.1 Circular Cylinder

Average Nusselt number is obtained by integrating this value over the surface of the cylinder, which is defined as

$$\text{Nu} = \frac{1}{\pi} \int_0^\pi Nu(\theta) d\theta \qquad (3.29)$$

"Sparrow et al (2004)" had summarized correlations for both circular and non-circular cylinders in cross-flow. In this work, "Zukauskas, (1978)" and "Whitaker, (1976)" correlation for the external flow have been used in this study for verification of SST model simulation results for heat transfer coefficient calculation over the circular cylinders.

$$\overline{Nu}_D = 0.25 + \left(0.4 Re^{\frac{1}{2}} + 0.06 Re^{2/3}\right) Pr^{0.37} * \left(\frac{\mu}{\mu_w}\right)^{\frac{1}{4}} \qquad (3.30)$$

Where μ is the dynamic viscosity of the air and μw is the dynamic viscosity at the wall.

Figure 4.3 shows a variation of Nusselt number for a fixed value of turbulence intensity of 5%. The CFD simulation is performed for Reynolds number of 500 to 200,000 and the results show good agreements with the correlation mentioned above.
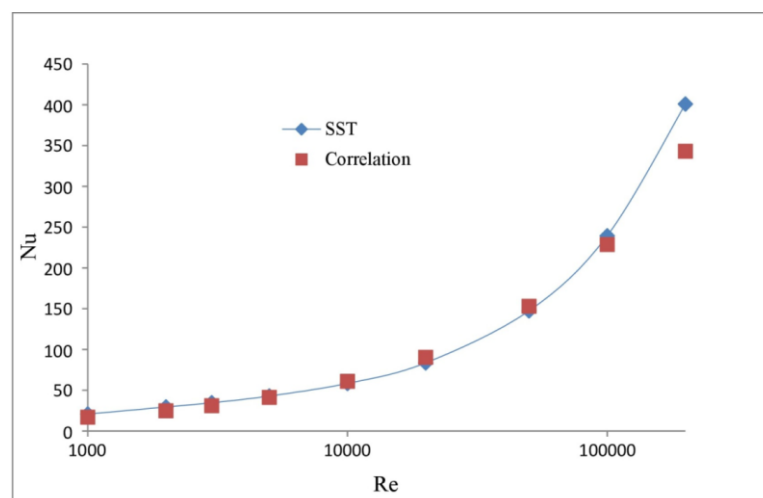

Figure 4.3: Validation of average Nusselt number with correlation

The predicted heat transfer rate is in good agreement with the experimental correlation prediction with a quantitative error of not more than 10% up to Reynolds number of 5,000. whereas at so higher value of Reynolds numbers the results show less error with experimental correlation prediction and almost merge with the data from experimental correlation prediction.

Influence of turbulence intensity on Nu

The influence of turbulence intensity on Nusselt number had been studied by Kondjoyan and Daudin (1995), who worked out the dependence of Nusselt number on turbulence intensity for a lower range of Reynolds number albeit for a circular cylinder. In this present work, the increase in Nusselt number has been recorded with an increase in Reynolds number for the turbulence intensity levels of 5%, 10%, 15%, 20%, and 40%. From figure 4.4 it is clear that for a low value of Reynolds number the turbulence intensity is not affecting significantly the heat transfer rate but when the value of Reynolds number is more than 20,000 there is a noticeable increase in heat transfer coefficient. The Nusselt number is more or less the same up to Reynolds number 8,000. But beyond this value of Re, Nusselt number increases prominently with increasing turbulence intensity. For example, at Re= 20,000 Nu increases from 75 to 100 when TI changes to 40% from 5% respectively. However at Re = 100, 000, Nu changed from 220 to 420 when TI changes from 5% to 40%. Thus the level of enhancement can be as high as 80% with the imposition of high turbulent intensity. This is in agreement with the results of Kondjoyan and Daudin (1995) though they have worked till Re of up to 50,000.
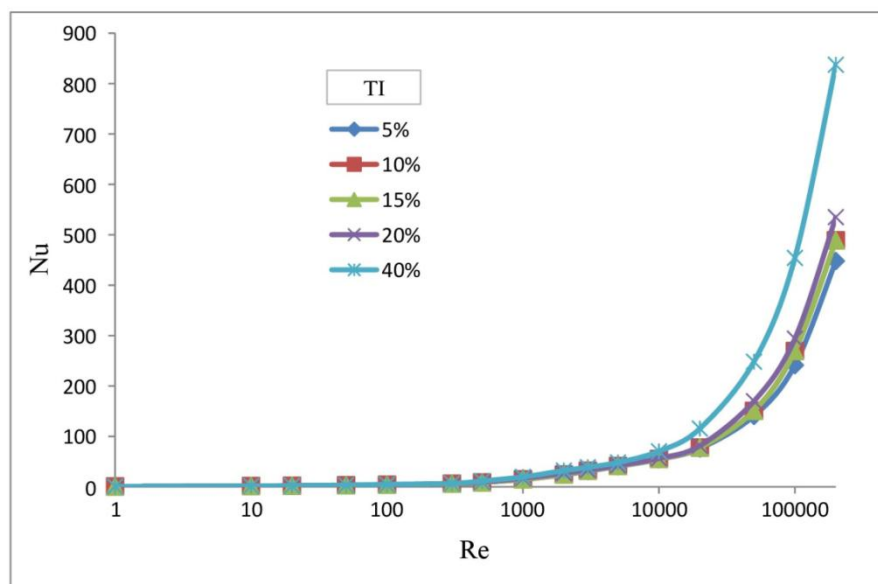

Figure 4.4: Effect of turbulence intensity on Nu

Variation of local Nusselt number over the cylinder surface

Figure 4.5 shows the variation of local Nusselt number over the cylinder for the value of Reynolds number 1,000 to 100,000 with a turbulence intensity of 5%. The distribution is plotted for one half of the cylinder. .For all levels of Reynolds number, the stagnation Nusselt number has local minima (Θ=0) though it increases slightly nearer to 600 to 900 beyond that this value very sharply drop. It is also seen that with increasing Reynolds number the separation point observed by looking at the local minima is shifting towards the rear side of the cylinder.
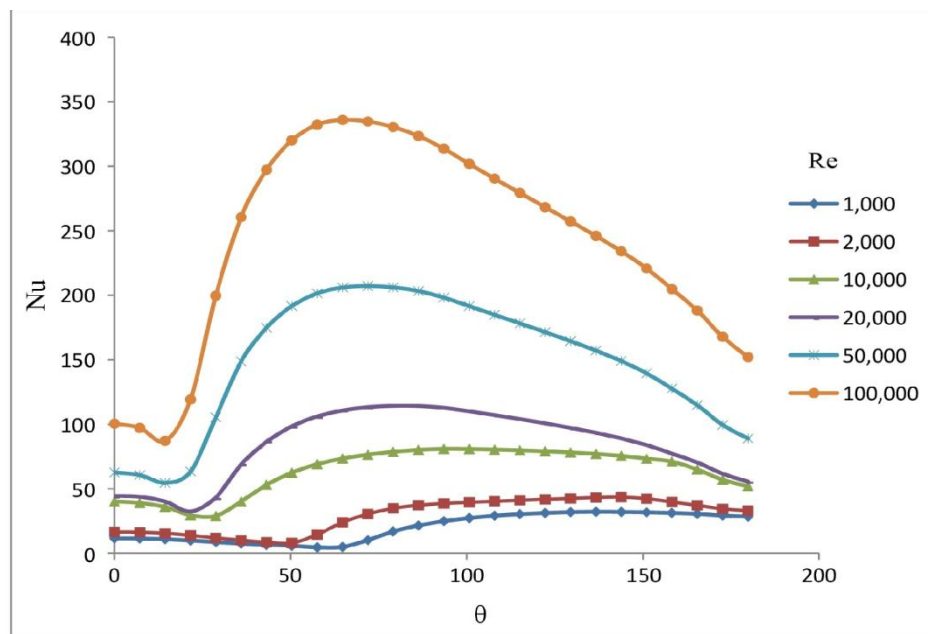

Figure 4.5: Variation of local Nusselt number over the cylinder surface at TI = 5%

Variation of local Nusselt number with turbulence intensity

The variation of local Nusselt number over the cylinder at a particular Reynolds number with the increase in turbulence intensity has been shown in figure 4.6. Figure 4.6 (a) shows the variation of local Nusselt number at a Reynolds number of 10,000 with turbulence intensity of between 5% to 40%. From the figure, it is observed that with the increase in turbulence intensity the point of separation does not change much but the value of local Nusselt number at stagnation point increases rapidly. The same type of graphical agreement found for all Reynolds numbers simulated. To see this result whether the same pattern followed or not for higher Reynolds number, authors have plotted to show the variation of local Nusselt number at Reynolds number equals to 100,000. The effect of increasing turbulent intensity is found to

particularly affect the rear half of the cylinder (90 – 2700) where the magnitude of Nu increases significantly with an increase in inlet turbulence. The highest change is noticed at the rear stagnation point.
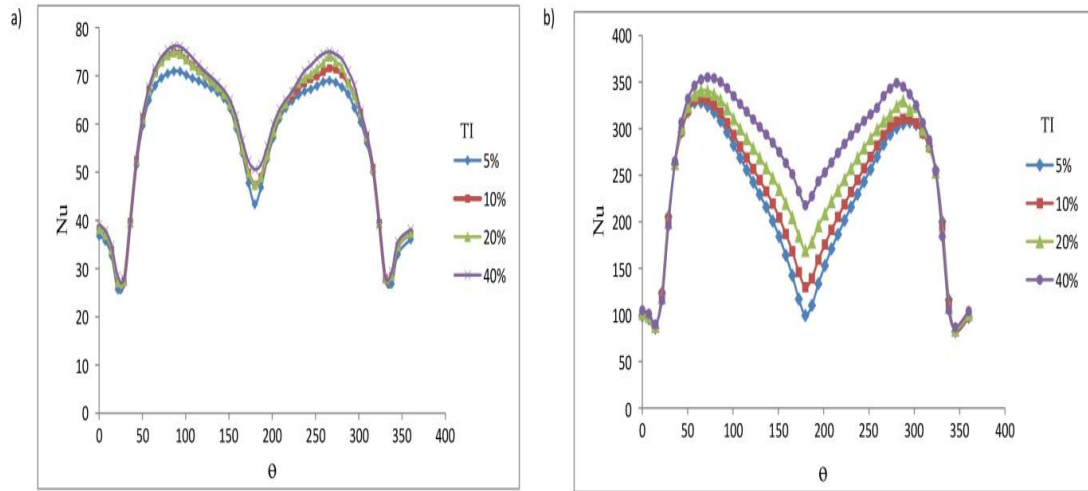

Figure 4.6: Local Nusselt number over the cylinder surface (a) Re=10,000 and (b) Re = 10^5

Azimuthally variation of C_p at different Reynolds number

Figure 4.7 shows the validation at low Re with the work of Park et al. (1998) which shows reasonably good agreement with the present computation for Re between 10 - 40. where the pressure coefficient is given by $C_P = \frac{(p-p_\infty)}{\frac{1}{2}\rho u_\infty^2}$. In figure 4.8, C_p is presented for higher levels of Re up to 2 x 10^5. At large Re about 50,000 to 200,000, C_p value over -2 can be observed at about 90^0.
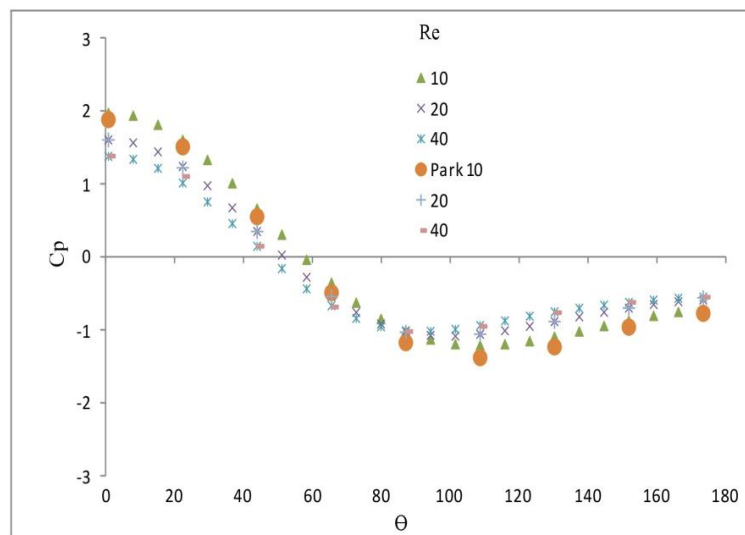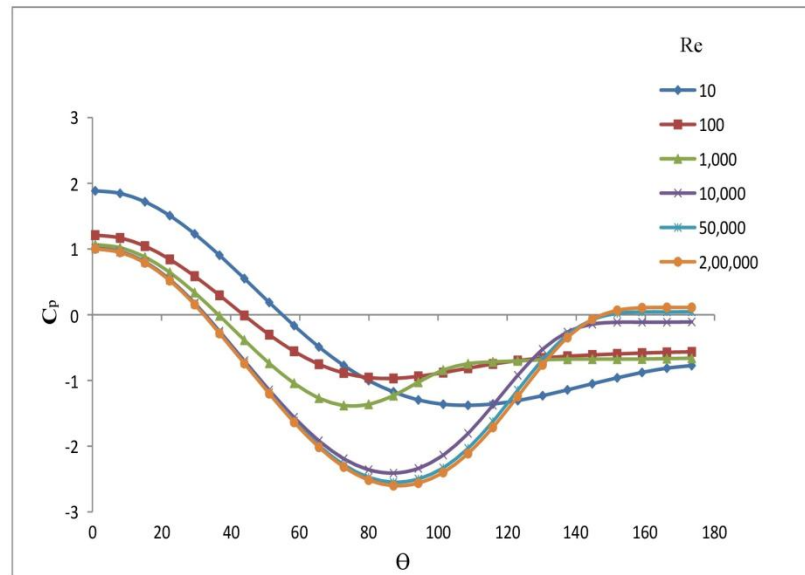

Figure 4.7: Validation of C_p

Figure 4.8: Variation of C_p over the cylinder at different Reynolds number

Effect of turbulent intensity over pressure coefficient

Looking at figure 4.9, it can be observed that C_p is about 1 at the stagnation point which gradually goes on reducing and at 900 it shows the maximum negative magnitude of around 2.5. After the topmost part i.e. 900, the Cp value starts increasing and reaches zero at about 1500. On increasing the value of TI there are insignificant changes in the local distribution of pressure coefficient.
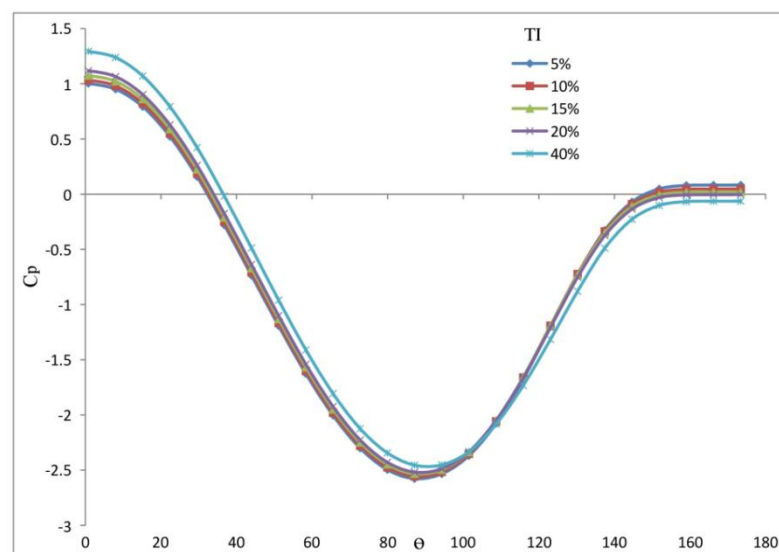

Figure 4.9: Azimuthal variation of C_p at different TI

Drag coefficient

The overall drag coefficient for the circular cylinder for various Reynolds number is shown in figure 4.10 which shows that for a lower value of Reynolds number the drag coefficient decreases up to Re=100. Further on increasing Re value beyond 100, again C_d values reduces up to Re 1,000 but with a lower slope. For Reynolds number beyond 10,000, the C_d value is almost the same up to 100,000. For example, while Re changes from 1 to100, the C_d value decrease from 5.698 to 1.498. However C_d values are 0.581 to 0.167 for Re 2,000 and 100,000 respectively. It is also seen that the present result is slightly higher compared to that of Park et al. (1998) up to Re 80 beyond which C_d is almost constant at about 1.7.
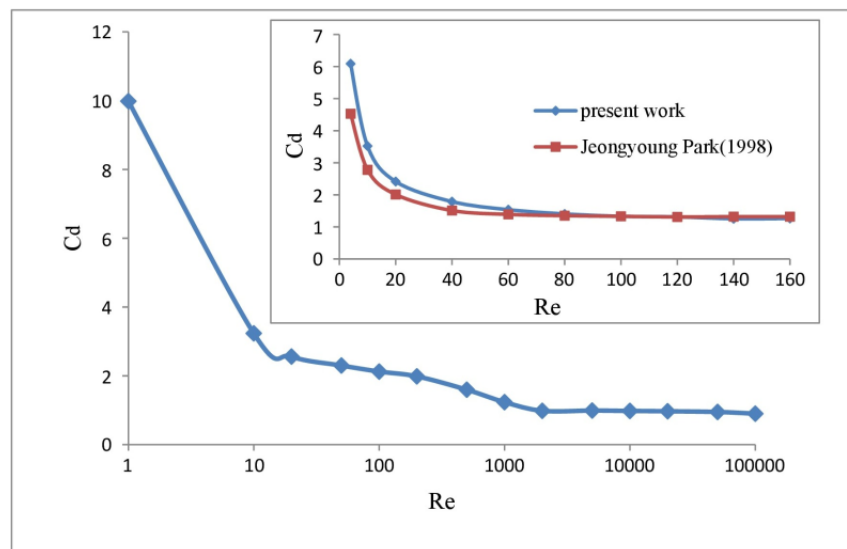

Figure 4.10: Effect of Reynolds number on C_d for circular cylinder

4.5.2 Square Cylinder

Influence of turbulence intensity on the heat transfer coefficient

The influence of turbulence intensity on Nusselt number had been studied by Kondjoyan and Daudin (1995) for circular cylinders only. In this present work, the increase in Nusselt number has been recorded with an increase in Reynolds number for the turbulence intensity of up to 40% for a square cylinder. From figure 4.11 it is clear that for a low value of Reynolds number the turbulence intensity is not much increasing the heat transfer rate but when the value of Reynolds number is more than 20,000 there is a higher increasing rate in heat transfer coefficient. The Nusselt number is more or less the same up to Reynolds number 10,000. But beyond this value of Re, Nusselt number increases prominently with increasing

turbulence intensity. For example, at Re= 20,000 Nu increases from 77 to 110 for TI of 5% and 40% respectively. However at Re = 1 00, 000, Nu changed from 248 to 450 when TI changes from 5% to 40%.
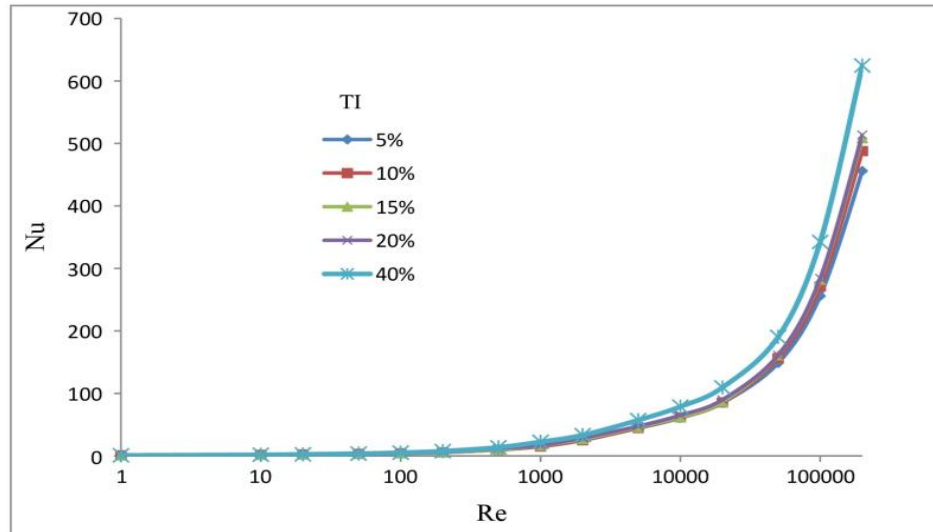

Figure 4.11: Effect of turbulence intensity on overall heat transfer

Variation of local Nusselt number with Reynolds number

Figure 4.12 shows the variation of local Nusselt number over the cylinder surface for the value of Reynolds number 100 to 200,000 with a turbulence intensity of 5%. At low turbulence intensity, Nusselt number is increasing gradually and it is maximum at the rear surface of the cylinder which can be attributed to the strong vertical flow structure at the rear wake. As such at low levels of Re (e.g. 100) heat transfer at the rear surface is rather marginal.
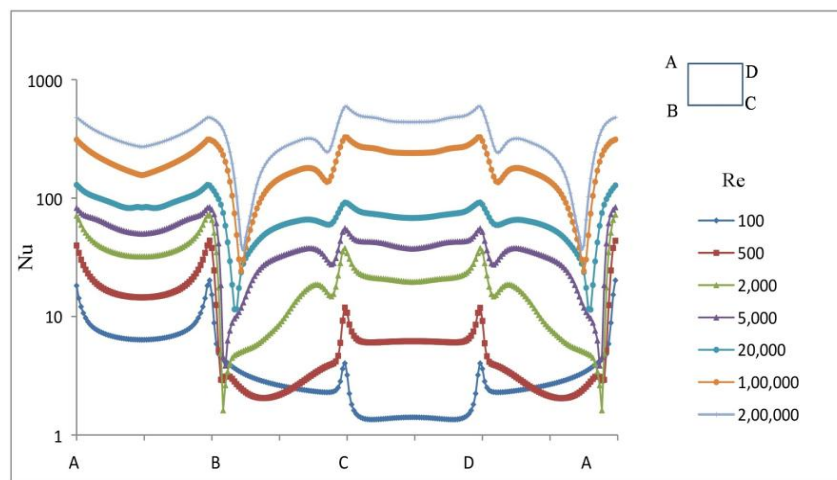

Figure 4.12: Variation of local Nusselt number over the square cylinder at TI = 5%

Variation of drag co-efficient with Reynolds number

The overall drag coefficient for the square cylinder for various Reynolds number is shown in figure 4.13 which shows that for a lower value of Reynolds number the drag coefficient decrease up to Re=100. Further on increasing Re value beyond 100, again C_d values gradually increase up to Re 1,000. But beyond that Reynolds number C_d values is almost the same up to Re=200,000. For example, Re=1-100, the C_d value decrease from 5.698 to 1.498. However C_d values from 1.614 to 1.757 for Re 2,000 and 200,000 respectively.

The inset figure here shows the variation of the drag coefficient with Re in the low range of Re up to 40. It is observed that the drag coefficient obtained in the present work is slightly upper up to Re 15 compared to Sharma (2004)" and Okajima (1997) after that for all the Re value the C_d value is almost same. The capability of the model is thus demonstrated for the laminar regime.
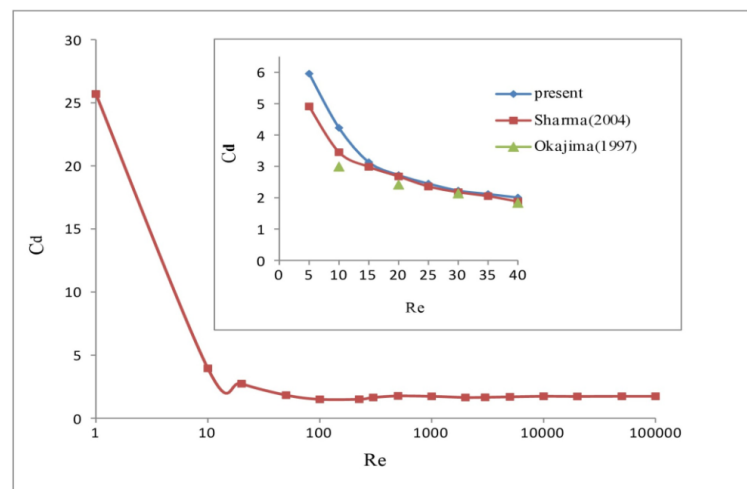

Figure 4.13: Variation of drag co-efficient with Reynolds number for square cylinder

Variation of local Nusselt number over the cylinder length with turbulence intensity

The variation of local Nusselt number around the cylinder at a particular Reynolds number with the increase in turbulence intensity has been shown in the figure given below. Figure 4.14(a) shows the variation of local Nusselt number at a Reynolds number of 10,000 with a turbulence intensity of 10%, 15%, 20%, and 40%. The local values of the Nusselt numbers are the highest on the front surface (concerning the incoming flow) of the cylinder for all turbulence intensity, indicating the highest heat transfer on the front surface compared to other surfaces of the cylinder. A symmetric Nu number distribution is observed on the bottom (BC) and top(DA) surfaces of the cylinders. The corresponding Nu is minimum at the

76

midpoint and maximum close to the corners. Since the heat transfer rate is closely related to the flow field, the local heat transfer rate is minimum where the velocity magnitudes are relatively small.
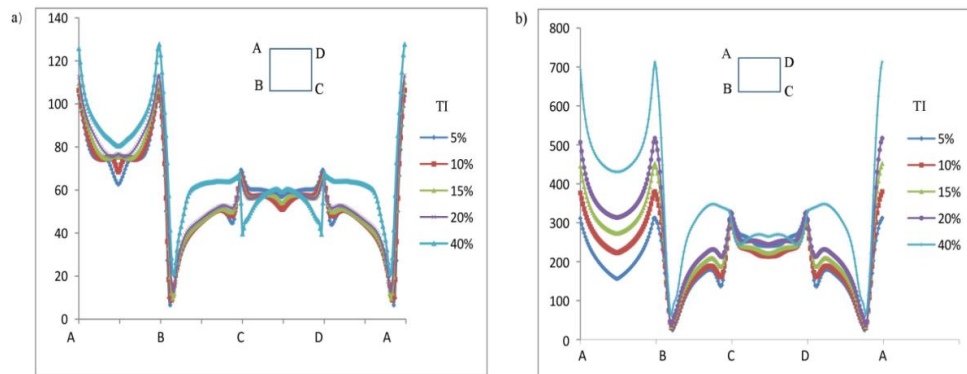

Figure 4.14: Variation of local Nusselt number over the cylinder with turbulence intensity at (a) Re=10,000 and (b) Re=100,000

The same type of graphical agreement found for all Reynolds numbers simulated. Another curve showing the variation of local Nusselt number over the entire cylinder at Reynolds number equals to 100,000 which is shown in figure 4.14(b) above.

Variation of drag coefficient with Re at different turbulence intensity

The drag coefficient C_d vs. Re is plotted in figure 4.15 which shows that initially there is strong descent in C_d value up to Re about 10. After that, there is a gradual decrease in drag coefficient while moving up to around Re 100 and on further increase in Re value there is no such commendable variation of C_d value, i.e. C_d value becomes more or less constant. It is also observed that with varying percentage of TI there are no appreciable changes in C_d value at all Re as observed for the case of pressure coefficient of the circular cylinder also.
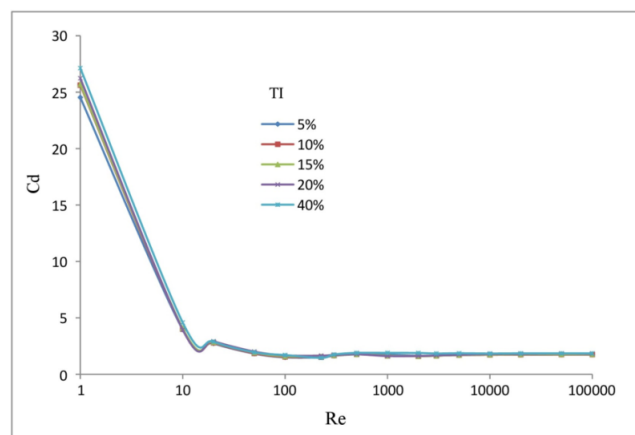

Figure 4.15: Variation of C_d vs. Re at different TI for square cylinder

77

Variation of C_p over the cylinder

The C_p value as seen in figure 4.16 shows a parabolic curve for flow over surface AB which depicts a gradual symmetrical rise in C_p value from its minimum range around -1.5 to its maximum magnitude of about 1.2 in the positive x-y plane. After reaching this maximum, the C_p value again decreases gradually. it has been observed that the C_p value pattern is similar while flow takes place over the surface AD and BC. In the rear surface CD, the variation is not strong as it has a low level of local velocity.
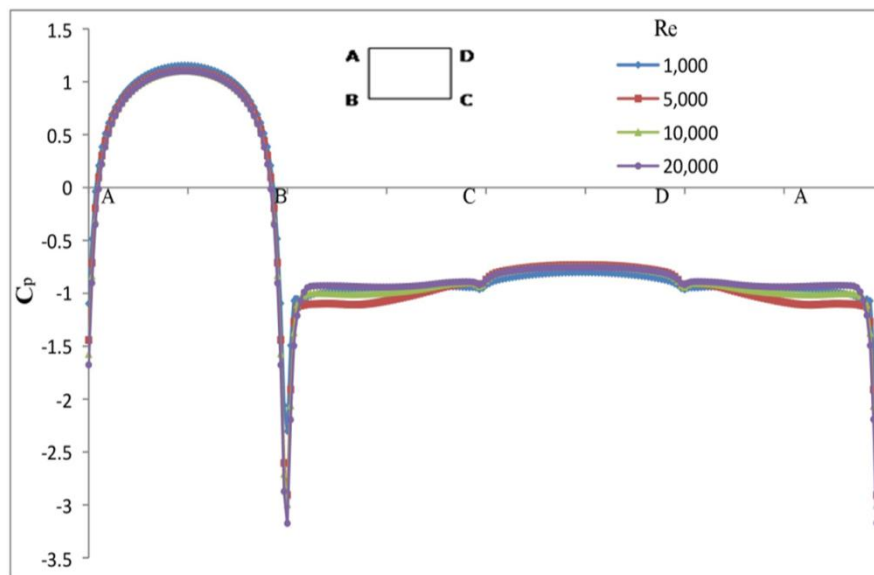
Figure 4.16: Variation of C_p over the cylinder at different Re

Variation of intermittency at outlet boundary

It has been mentioned that the present methodology of Menter (2013) can cover all flow regimes seamlessly. For this, an intermittency value at the inlet is prescribed which is dampened to near-zero value for predominantly laminar flows and approaches unity for turbulent flow. In figure 4.17 intermittency value at the central point of the exit plane is monitored. It can be seen that the intermittency value gradually increasing and the value of intermittency is 1.0 for Re above 10,000.
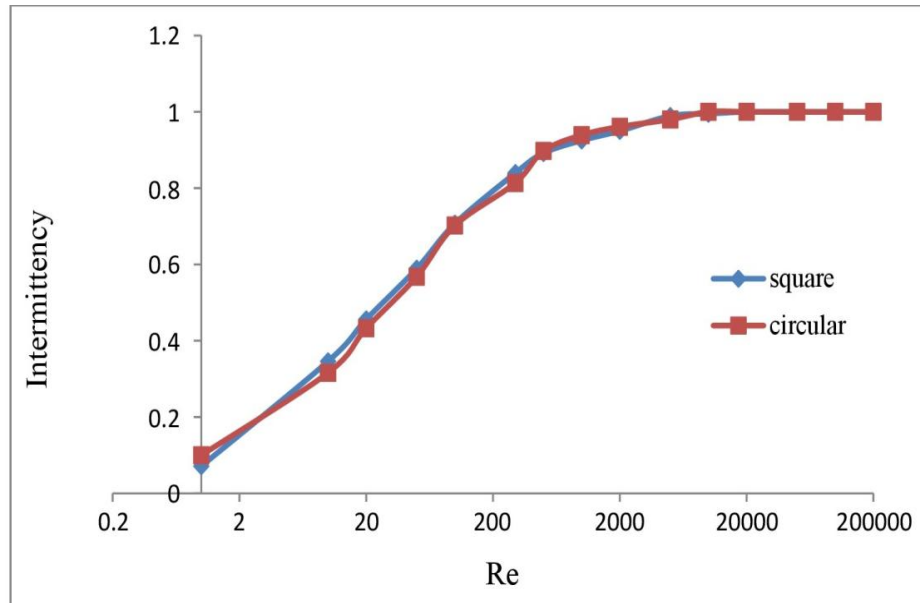
Figure 4.17: Variation of intermittency with Re

Effect of confinement

We have performed simulation for unconfined cases by using vanishing derivatives on top and bottom surfaces. However, the effect of confinement sometimes may be important particularly when the H/D is low. In the present case of H/D = 10, as seen in figure 4.18, confinement does not change the result. To simulate confinement, on top and bottom no-slip condition was prescribed. Figure 18 shows the variation of the Nusselt number for a fixed value of turbulence intensity of 5%. The CFD simulation is performed for Reynolds number of 1 to 200,000 and the curve shows perfect agreement between the case of confined flow and unconfined flow. Thus for the given blockage ratio of 10.0, confinement does not affect.

Figure 4.18: Effect of confinement on Nu-Re curve

4.5.3 Triangular prism

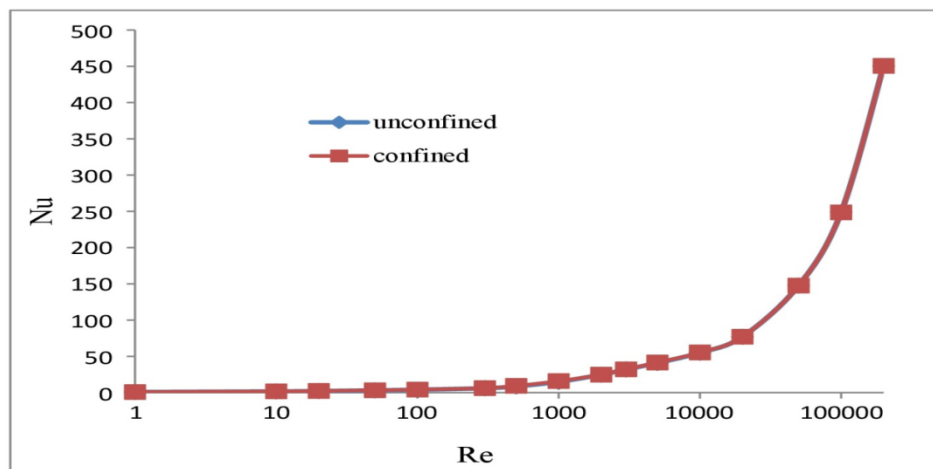Figure 4.19 provides the validation of Nu concerning Re that ranges from 50-150. From earlier works of literature, it has been observed that the Nu of the present work is following Dhiman, Shyam (2011) and Dalal (2006). It shows a gradual increasing Nu as Re increased.
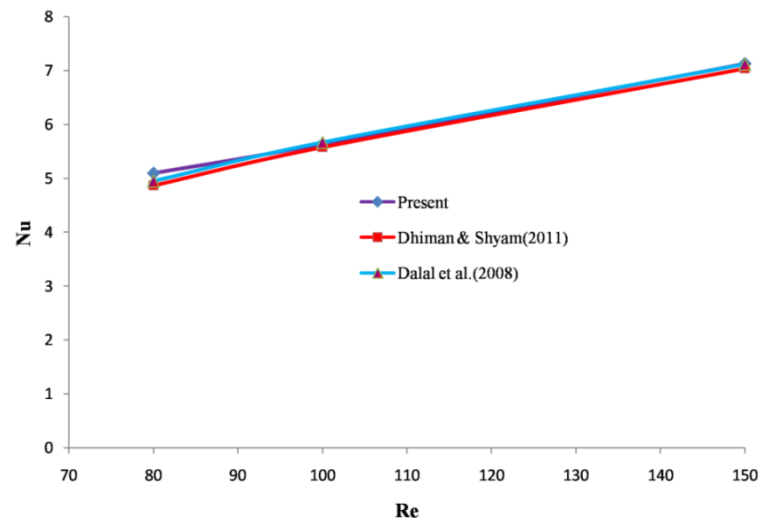
Figure 4.19: Validation of Nusselt number

The influence of turbulence intensity on Nusselt number had been studied by Kondjoyan and Daudin (1995), who worked out the dependence of Nusselt number on turbulence intensity for a lower range of Reynolds number. In this present work, the increase in Nusselt number has been recorded with an increase in Reynolds number for the turbulence intensity levels of 5%, 10%, 15%, 20%, and 40%. From figure 4.20 it is clear that for a low value of Reynolds number the turbulence intensity is not affecting significantly the heat transfer rate but when the value of Reynolds number is more than 10,000 there is a noticeable increase in heat transfer coefficient. The Nusselt number is more or less the same up to Reynolds number 8,000 at all levels of inlet turbulent intensity. But beyond this value of Re, Nusselt number increases prominently with increasing turbulence intensity.
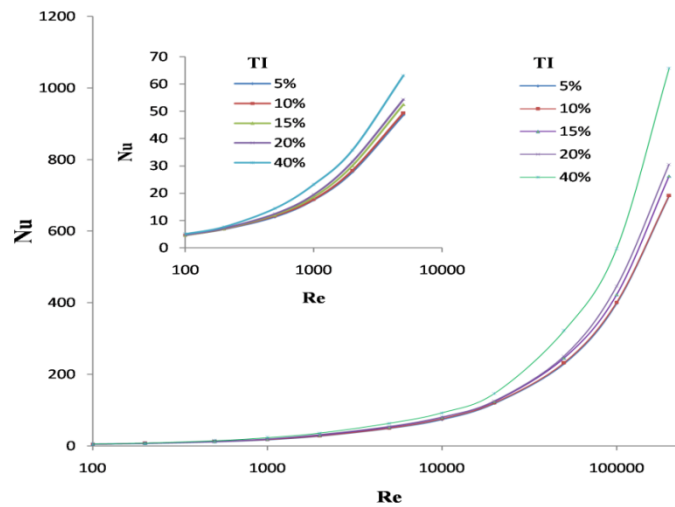
Figure 4.20: Effect of turbulence intensity on Nu

Figure 4.21 depicts the variation of local Nu over the triangular cylinder for lower Reynolds number. At the point, A Nu has been observed to be maximum. In the face BC the Nu falls sharply and then again rises parabolically and gradually falls up to point C. From C to A it has been observed that there is in a steep rise in Nu then again the pattern of variation follows the reverse path as A to B point. It has been also observed that the Nu shows higher value at each corner of the triangle relative to their adjacent sides. On considering different values of Re the Nu for each case increases slightly.

Figure 4.21: Variation of local Nusselt number over the triangular cylinder at low Reynolds number

In fig 4.22. the variation of Nu of the flow across the triangular cylinder has been plotted for a range of Re from 500-100,000. As increasing the Re the Nu also increases. As the flow moves A to B there is a gradual fall of Nu and the same pattern of the plot has been observed

when moving from C to A. As the flow reaches closer to B. There is a steep rise in Nu and it more or less remains unchanged from 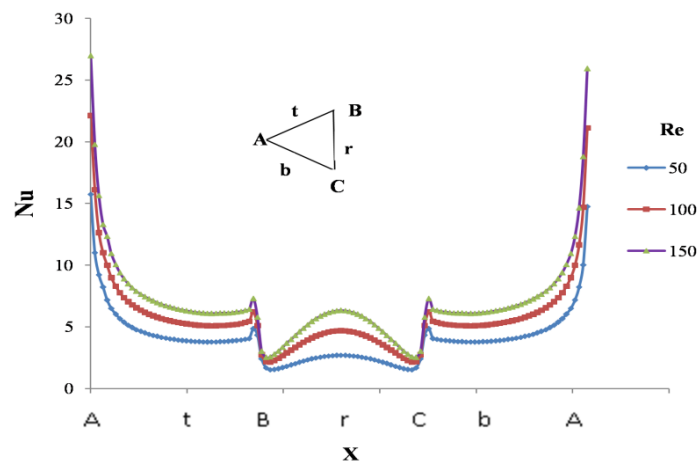B to C likewise as the flow comes closer to point C there is again symmetrical steep fall in Nu as seen in the case of point B. It has been documented that the heat transfer rate is higher of rare face BC due to vortex formation.
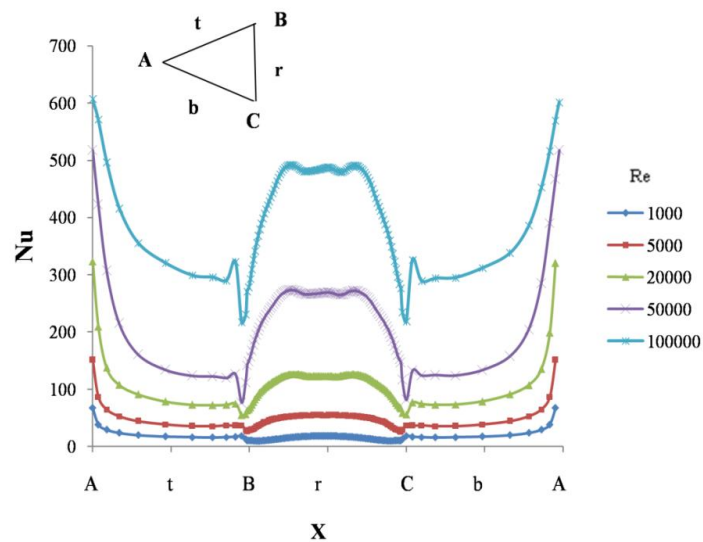
Figure 4.22: Variation of local Nusselt number over the triangular cylinder at TI = 5% with different Re

Figure 4.23 depicts variation of surface Nusselt number along the prism surface of different TI at low Reynolds number. It is observed that heat transfer increased in the entire TP surface as turbulence intensity increases. The rate of enhancement is similar through upper and lower slant sides (i.e. AB and AC) but maximum change is observed at the rear side of the TP.
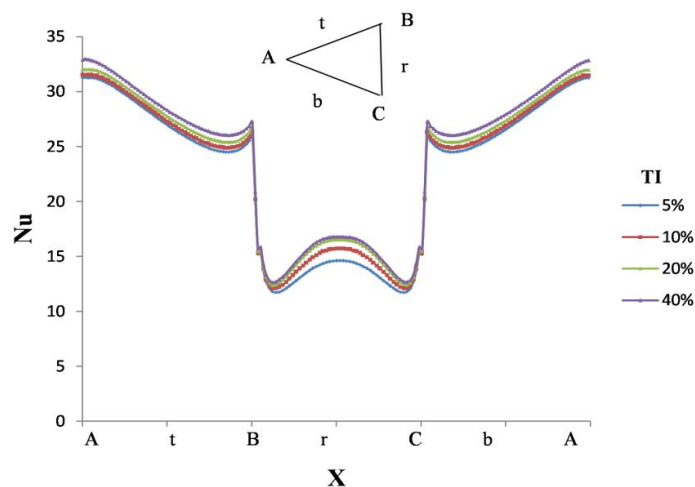
Figure 4.23: Variation of local Nusselt number over the triangular cylinder of different TI at Re=1,000

Fig. 4.24 shows the Nusselt number distribution over the triangular prism with different turbulence intensity at fixed Re=20,000. The Nu value gradually decreases before point B, after that heat transfer suddenly decreases close to point B. It is very interesting to note that unlike the case at Low Re, now at the slant surface BC the Nu value decreases with increasing turbulence intensity. A similar pattern is observed in the face of CA being a symmetric surface. It is also seen that Re is proportionally varying with turbulence intensity in the face AB and AC
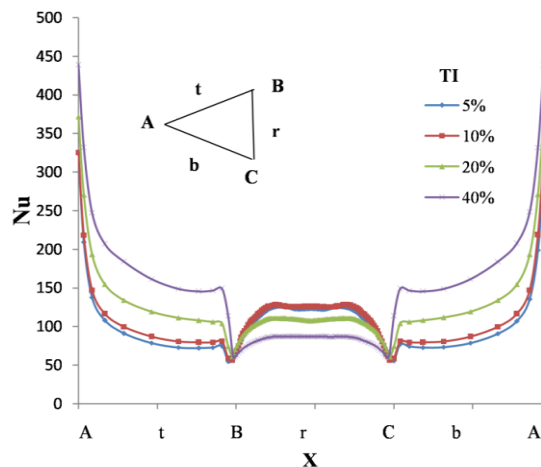
Figure 4.24: Variation of local Nusselt number over the triangular cylinder of different TI at Re=20,000

The plots in Fig. 4.25 shows the surface Nusselt number distribution over the triangular prism at different turbulence intensity at high Reynolds number (Re=200,000). The curves show the high heat transfer on rare face BC due to vortex interaction. Heat transfer increases with increasing Re at all the surfaces
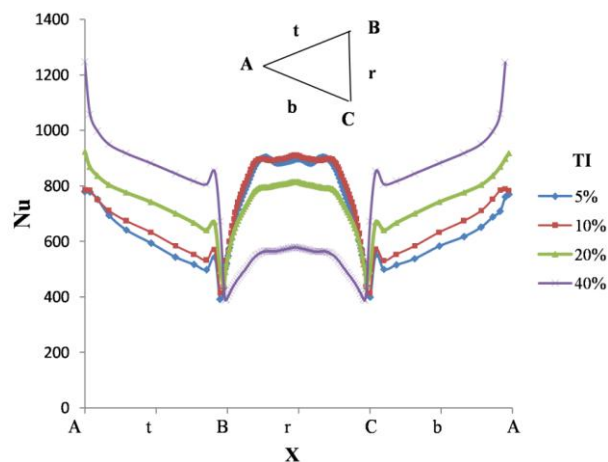
Figure 4.25: Variation of local Nusselt number over the triangular cylinder at different TI with Re=200,000

83

The drag coefficient C_d vs. Re is plotted in figure 4.26 which shows for different turbulent intensity. It is also observed that with varying percentage of TI there are appreciable changes in C_d value at all Re observed.
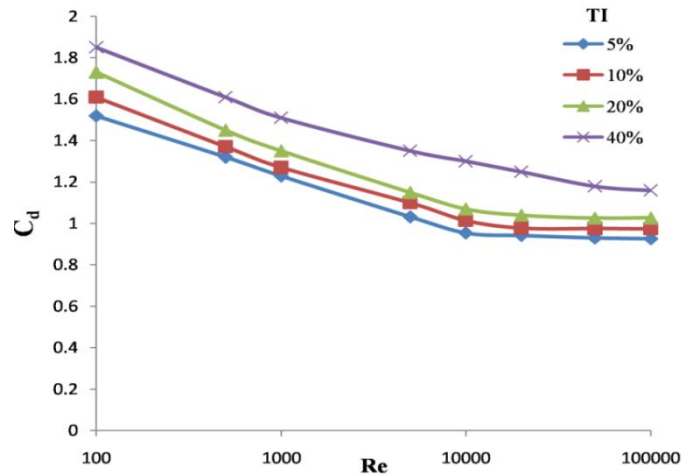
Figure 4.26: Variation of drag coefficient with Re at different turbulence intensity for triangular prism

4.5.4 Diamond

In fig. 4.27 shows the effect of turbulence intensity on Nusselt number at a different range of turbulence intensity. The value of Reynolds number is more than 10,000 there is a noticeable increase in the heat transfer coefficient. The Nusselt number is more or less the same up to Reynolds number 5,000. But beyond this value of Re, Nusselt number increases significantly with increasing turbulence intensity.
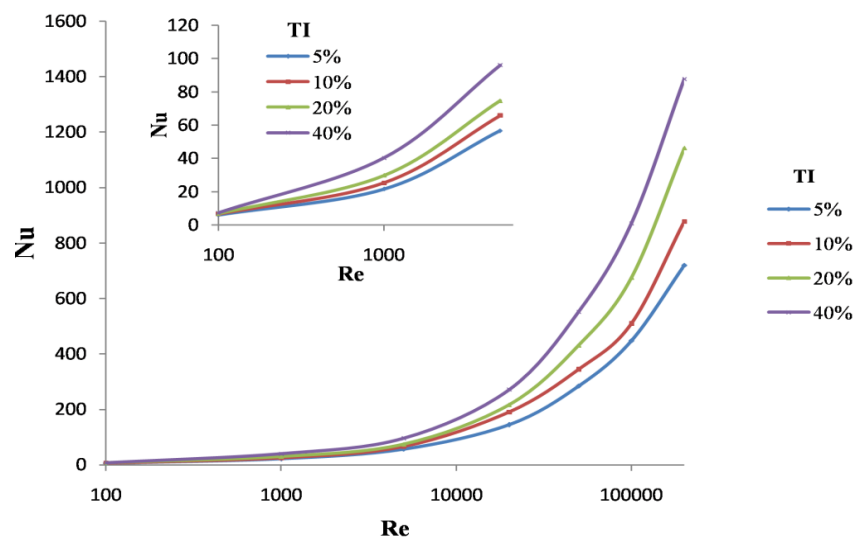
Figure 4.27: Effect of turbulence intensity on Nu

In fig Figure 4.28 the variation of Nu of the flow across the diamond cylinder has been plotted for the range of Re from 500-100,000. As increasing the Re the Nu also increases. As the flow moves A to B there is a gradual rise of the Nu. The same pattern of the entire plot has been observed when moving from D to A. As the flow reaches closer to B, there is a steep rise in Nu which again slightly decreases and gradually fall closer to C, likewise as the flow comes to point C there is again steep rise in Nu. The entire plot of the upper half is symmetric with the lower half. Beyond point B and D, there is a higher heat transfer due to vortex formation.
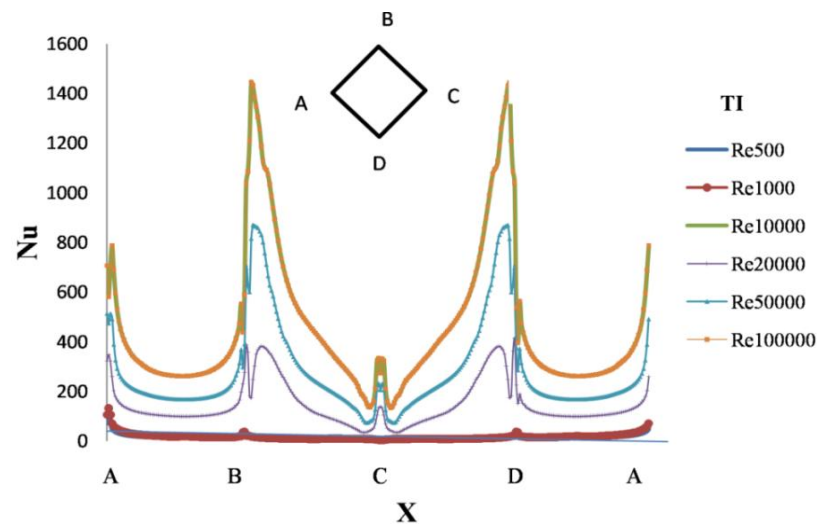
Figure 4.28: Distribution of Nu along channel in presence of diamond shape bluff body at different Re.

In fig 4.29 shows the variation of Nu with changing TI, keeping Re constant at 100,000. With increasing TI from 5-40%, it has been accentuated that the Nu value for the face A-B increases, while completely reverse happens for D to A. In face A to B there is a steep negative slope of Nu value and again rises gradually up to point B. After point B there are sudden decreases in the value and while gradually moving from B to C, It again rises close the point D. The plot of B to C would show the completely reverse nature of the plot as C to D and would coincide with this plot thus implying symmetry.
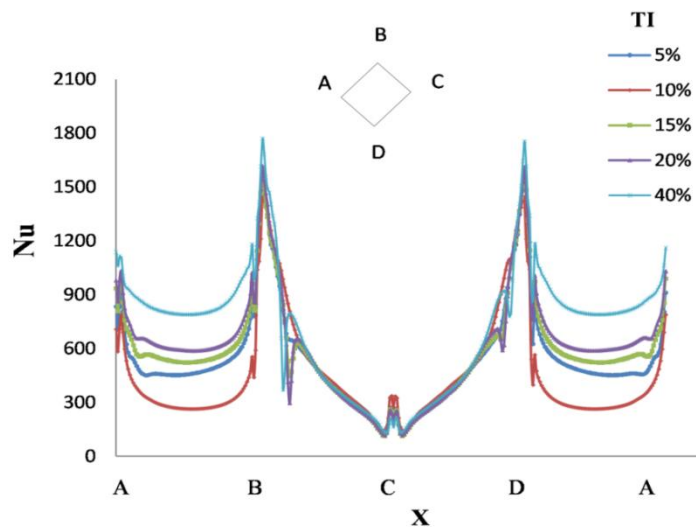
Figure 4.29: Variation of local Nusselt number over the curve length with turbulence intensity at Re=100,000.

Figure 4.30 depicts the relationship of average intermittency at the outlet plane at different Reynolds number. Fully turbulent flow has unit intermittency. In our case, the flow becomes completely turbulent at approximately 8,000 Reynolds number.
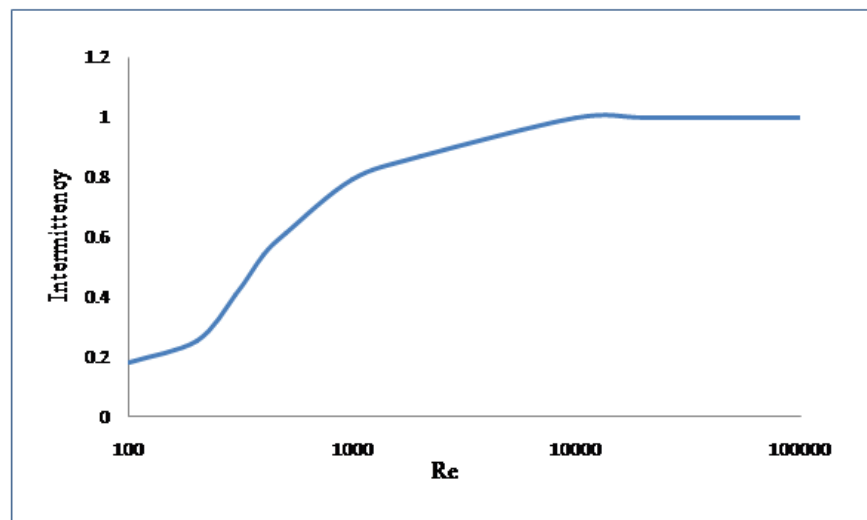
Figure 4.30: Intermittency at exit.

In figure 4.31 drag coefficient has been depicted. As in the case of a circular or square cylinder, the drag coefficient is decreased, here also the drag coefficient is inversely related to Re
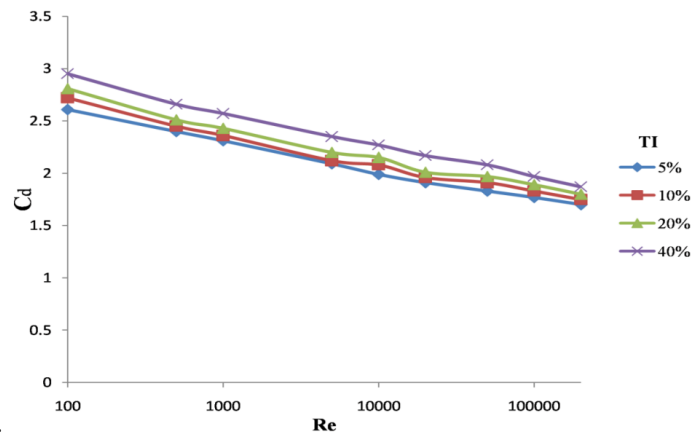
Figure 4.31: Variation of drag coefficient with Re for diamond

4.5.5 Small edge facing Trapezium

Figure 4.32 shows the distribution of heat transfer around the trapezium surface. While ABCD is the surface of the trapezium, R is in the middle of surface BC. As AB and CD are symmetrically placed and should show similar distribution. Ad and BC surfaces should exhibit different natures of distribution as the former is the frontal side and the latter is the rear surface. From fig. below it could be observed that there is a gradual fall in Nu while the flow is moving from A to B except in the case of Re 1,000 where there is a sudden rise in Nu and it gradually drops. As the flow reaches near to B there is a steep rise of Nu due to a sudden increase in pressure and the value of Nu steeply drop and reaches near to zero while the flow reaches point R the same symmetrical behavior of Nu is observed for the symmetrical part RCD of the trapezium. On surface DA the Nu shows an inverse parabolic pattern for all sets of Re with lowest heat transfer at the stagnation point. Nu depends strongly on Re.
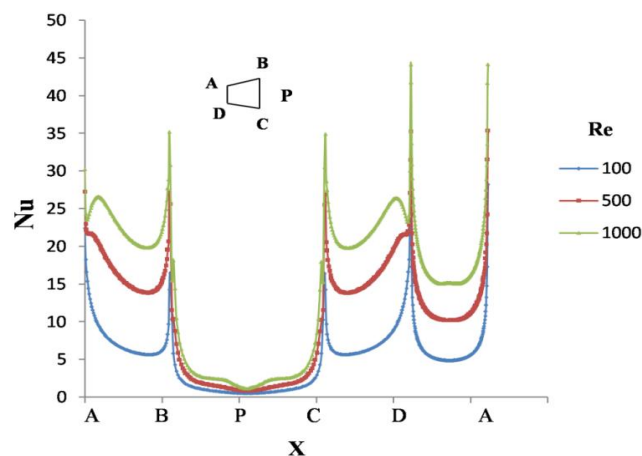
Figure 4.32: Distribution of local Nusselt number along the short side trapezoidal surface at laminar region at 5% TI

Figure 4.33 is a plot of Nu for various regions of the bluff body at relatively higher Re at 5% TI. As the flow moves A to B there is a sudden rise and fall of Nu due to proportional pressure variation. As the flow reaches toward B there is a slight increase in Nu but a steep drop in Nu value is noticed. For three lower values of Re, the Nu is gradually decreasing as it reaches the midpoint R of surface BC but for Re=200,000 the pattern is just the reverse due to strong vertical interaction of the flow. The symmetrical pattern of the Nu plot is observed for the symmetrical part of the bluff body. The nature of Nu on the surface DA is similar to that is observed in fig.16.
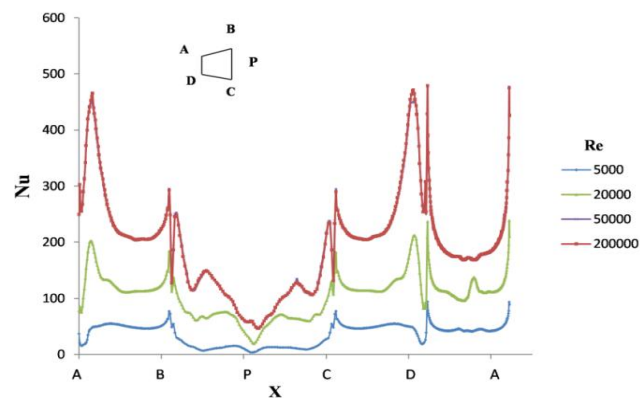
Figure 4.33: Distribution of local Nusselt number along the short side trapezoidal surface at different Reynolds number at 5%TI

Figure. 4.34 below shows the distribution of Nu along the trapezoidal surface at fixed Re=20,000 at different TI varying within 5 -40% TI. The graph shows a steep rise in Re in the vicinity of the corner (A, B, C, D). This nature is observed due to an increase in pressure of the flow. The surfaces of the bluff body show much lower values of Nu as the pressure in these regions is considerably low. It is also been observed that TI percentage positively affects the Nu value. The presence of a bluff body introduces higher vorticity level/prevents fluid mixing/increases turbulence. Thereby enhancing heat transfer is more.
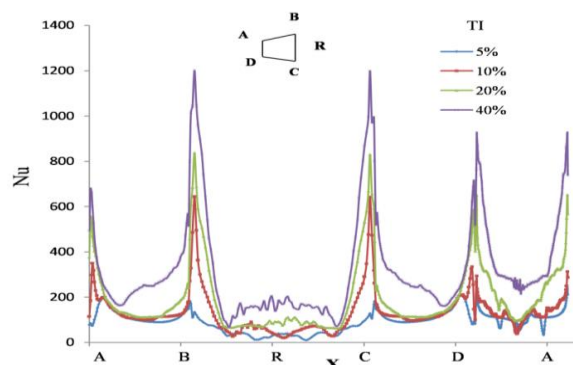
Figure 4.34: Distribution of local Nusselt number along the short side trapezoidal surface at different TI(Re=20,000)

88

Figure 4.35 shows the distribution of Nu along the trapezoidal surface at fixed higher Re=50,000 at different TI 5 -40% TI. The plot shows that The curve is almost similar to that curve in fig.5.3.16 above. But for the higher TI of 40%, the Nu value steeply increases and gradually drops while the flow reaches R from B due to fully development of the at higher TI.
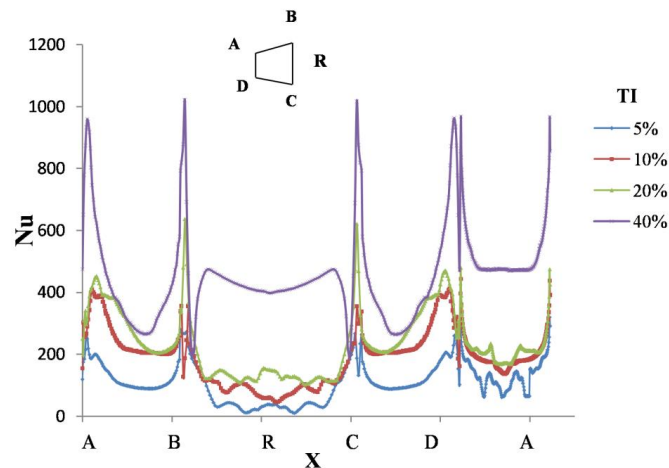
Figure. 4.35: Distribution of local Nusselt number along the short side trapezoidal surface at different TI(Re=50,000)

Heat transfer around the trapezium surface is presented now. The influence of turbulence intensity on Nusselt number had been studied by "Kondjoyan and Daudin (1995)", who worked out the dependence of Nusselt number on turbulence intensity for a lower range of Reynolds number. In this present work, the increase in Nusselt number has been recorded with an increase in Reynolds number for the turbulence intensity levels of 5%, 10%, 15%, 20%, and 40%. From figure 4.36 it is clear that for the low value of Reynolds number the turbulence intensity is not affecting significantly the heat transfer rate but when the value of Reynolds number is more than 9,000 there is a noticeable increase in heat transfer coefficient.
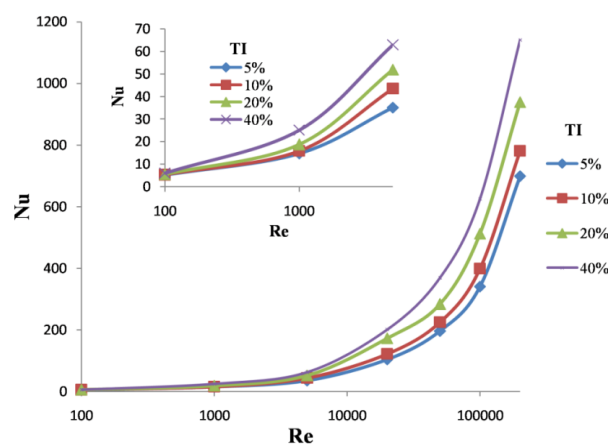
Figure 4.36: Effect of turbulence intensity on Nu

The drag coefficient C_d vs. Re is plot is shown in figure 4.37 which shows that initially there is strong descent in C_d value up to Re about 1,000. After that, there is a gradual increase in the drag coefficient while moving up to around Re 8,000 and on further increase in Re value there is also a gradual decrease of C_d value. It is also observed that with varying percentage of TI there is an appreciable change in C_d value at all Re as observed.
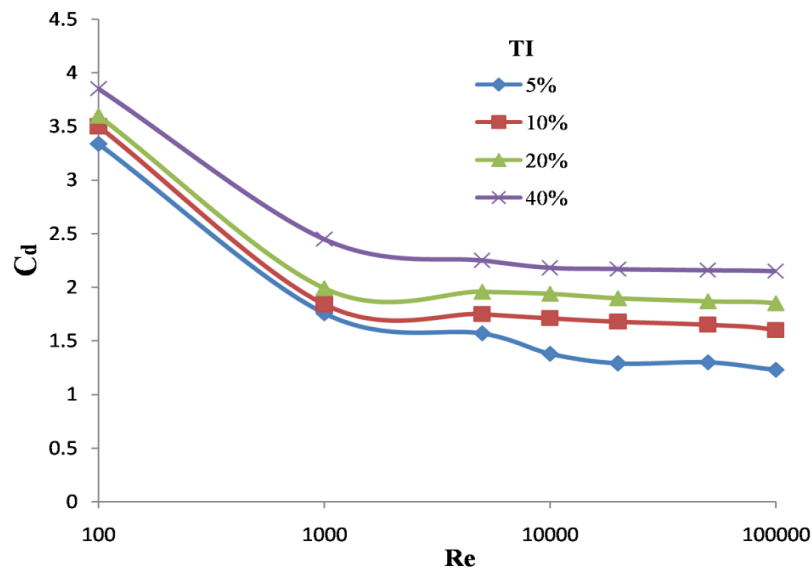
Figure 4.37: Variation of C_d vs. Re at different TI for small edge facing trapezium cylinder

Table 1 shows the heat transfer distribution for three different shape geometry at a different turbulent intensity and compares with correlation values. It is seen that for diamond heat transfer is higher compared to the other two bluff bodies.

Table 3: **Averaged Nusselt number for different bluff body**

Re	Triangular prism				Small edge facing trapezium				Diamond				Correlation values
	TI				TI				TI				
	5%	10%	20%	40%	5%	10%	20%	40%	5%	10%	20%	40%	
100	4.50	4.54	4.64	4.99	5.25	5.35	5.55	6.1	6.1	6.7	6.94	7.33	4.99
1,000	17.5	17.7	19.4	23.1	14.8	15.8	18.7	25.1	21	25	29.8	40.3	16.94
5,000	48.6	49.3	54.3	63.1	35.1	43.5	52.1	62.9	56	65	74.6	96.1	41.23
20,000	118	119	125	146	104.	122	190	321	144	190	216	271	90.32
50,000	210	231	250	321	196	216	283	477	284	345	430.8	551	152.89
100,000	298	401	446	550	375	512	473	518	447	510	675.	871	228.61
200,000	499	698	787	1055	530	722	810	1141	720	878	1142	1391	343.47

4.6 Summary

Convective heat transfer around different bluff bodies in the design of circular, square cylinder, triangular prism, diamond and trapezoidal cylinder has been studied in this work in a large range of Reynolds number. The transition SST model has been used for present simulation which provides excellent results in predicting heat transfer under all situation i.e., laminar, transition and turbulent conditions suggested by "Abraham et. al. (2009)". The heat transfer forecast was obtained smoothly from laminar to turbulent region using the above model. The investigation evaluates the effect of turbulent intensity on both local and the averaged Nusselt number. The present simulations results (averaged Nusselt number) are found in good agreement with published results. It is observed that, the drag coefficient value is decreased with increasing the Reynolds number. The drag coefficients are significantly affected by increasing inlet turbulent intensity for all bluff bodies.

Chapter

5

Augmentation Heat Transfer In Presence Of Triangular Prism, Diamond And Trapezoidal Bluff Body

5.1 Introduction

The primary area of the work is to show the augmentation of heat transfer in a channel due to the insertion of a bluff body. The fundamental governing equations of continuity, momentum, and energy are solved along with the transition SST model. The variation of the Nusselt number along the length of the channel is plotted with varying Reynolds numbers from Re 2,500-2,00,000. The Augmentation is also expressed as a percentage increased of heat transfer from a similar system without the bluff body.

5.2 Computational domain

The present work considers the forced convection cross flow around three bluff bodies, an equilateral triangle prism, diamond shaped and trapezoidal shaped shown in figure 5.1 for all the cases. The hydraulic diameter D of the prism, diamond, trapezoidal cylinder is the non-dimensional length. The trapezium can here three different orientations-(i) the larger base at the upstream(ii) the small base at the upstream and (iii) symmetrical placed as depicted through figure 5.1(c)-(e). The non-dimensional distance between the inlet plane and the front surface of the cylinder is 15D and the non-dimensional distance between the rear surface of the cylinder and exit plane is 35D with the total non-dimensional length of the computational domain 50D. The ratio of the width of the cylinder to the vertical distance between the upper and lower walls, H=4D has been used in this work. The problem is considered to be two-dimensional. Air is considered as a working fluid for which Prandtl number of 0.71.
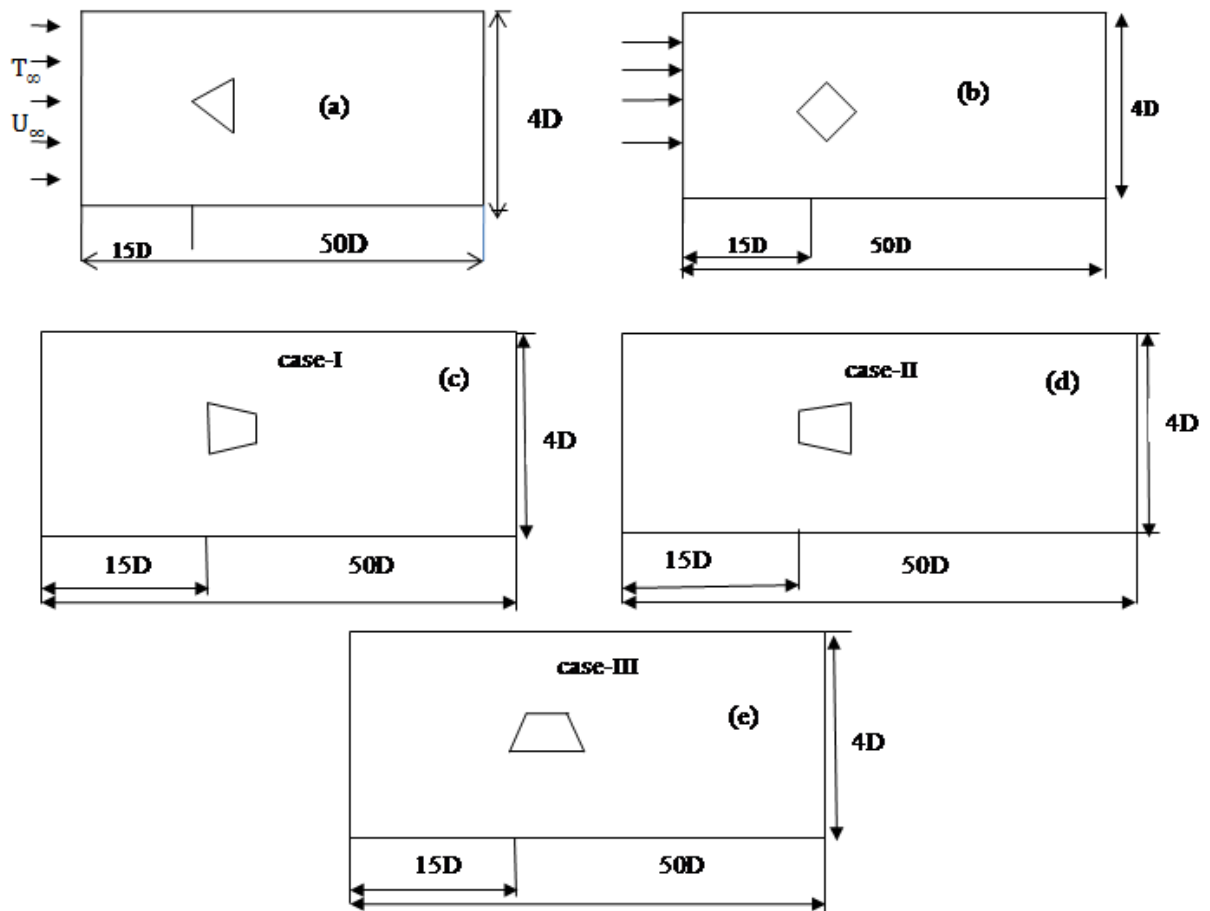
Figure 5.1: Computational domain for flow around bluff body (a) triangular Prism (b) diamond (c) trapezium large facing (d) small facing (e) symmetry

5.3 Boundary conditions

Fluid approaches to the bluff body with a uniform inlet velocity of U_∞ and uniform temperature of the inlet fluid is T_∞. The fluid is deciding to be air with fixed physical properties (Pr=0.71) with an inlet temperature of 298 K. The bluff bodies are kept at adiabatic condition so that $\frac{\partial T}{\partial n}$=o where n is the normal direction to the bluff body surface. The top and bottom walls are heated up(by adding temperature). The domain size is fixed and the fluid properties are also considered to be constant thus the variation of Reynolds number is done by changing the inlet velocity.
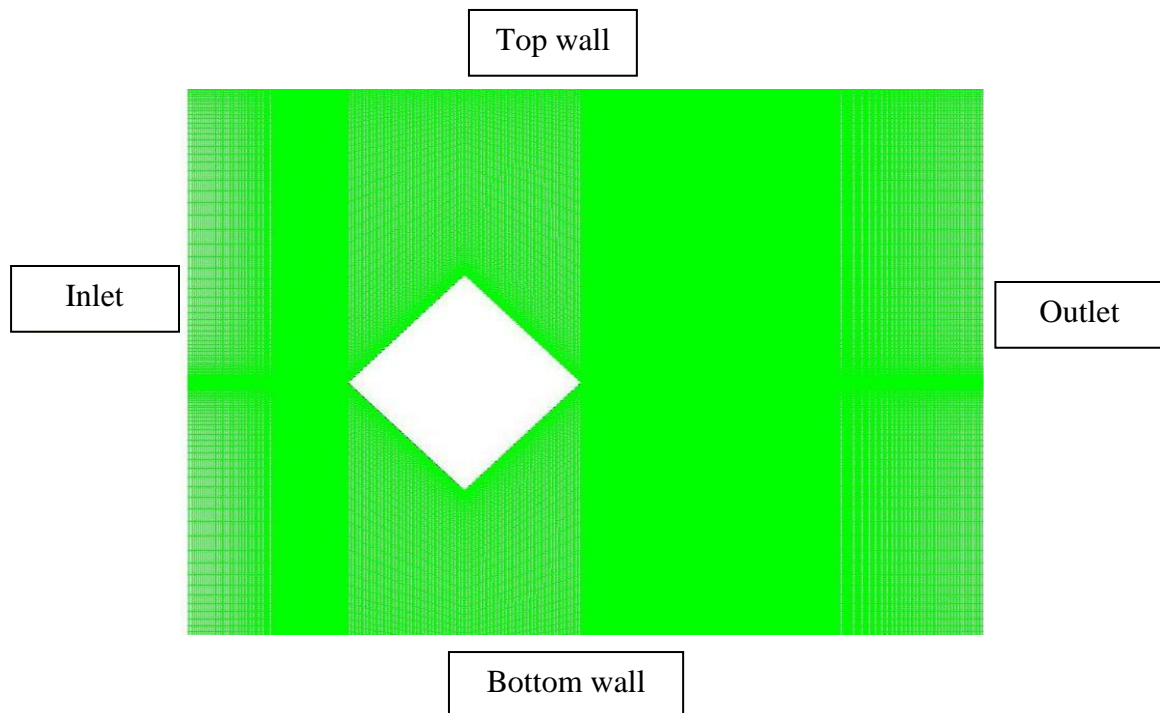
Fig.5.2: Closed up view of boundary condition for heat transfer augmentation

5.4 Solution procedure

The two-dimensional governing equations of continuity, momentum, and energy equations are solved using the Transition SST model proposed by "Abraham et. al. (2009)" was discussed in chapter 3. The governing equations are discretized on a non-uniform structured grid using a finite volume method. The velocities and pressures were predicted using a semi-implicit pressure linked equations (SIMPLE) scheme ("Patankar, 1978"). The interpolation of the gradients of velocities and temperature used the third-order accurate MUSCL scheme ("Van Leer, 1979"), while the gradients for intermittency ($\Box$), turbulent kinetic energy, specific dissipation rate, and momentum thickness used the second-order accurate upwind scheme. The discretized equations are then linearized using an implicit scheme and solved iteratively using Ansys Fluent 16.2, 2d double precision solver. The convergence criteria for energy, momentum, and continuity are 10^{-6}, 10^{-4} and 10^{-4} respectively.

The fig.5.3 show some close view of the different bluff body. After performing a rigorous check for grid independence, adequate numbers of cells were used. The number of nodes is 57,368 and 40,311 for the case with TP and without TP respectively. In both cases structure

meshes are used throughout the domain. The number of nodes is 3,48,080 and 5,02,200 for the case of diamond and trapezium respectively. A part of the grid is shown in figure 5.3.
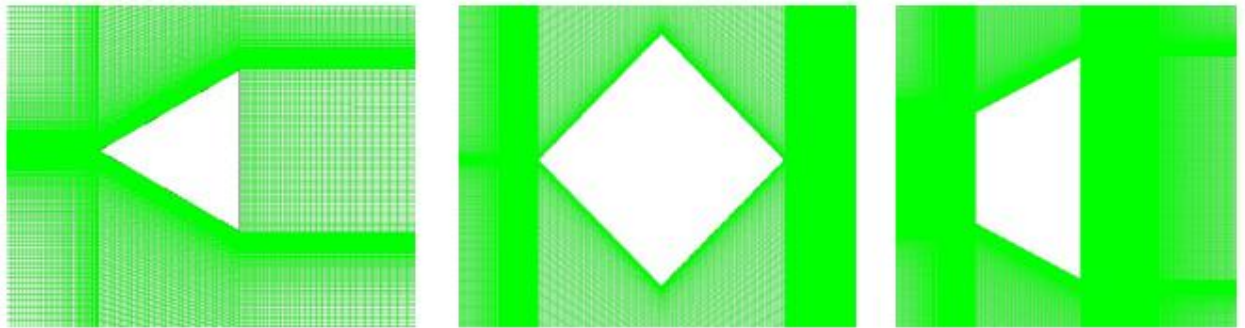
Figure5.3: Close up view of grids (a) triangle prism, (b) diamond, and(c) trapezoidal shape bluff body

5.5 Results and discussions

The results obtained after the simulation performed with the several Reynolds numbers with different turbulence intensity are discussed in this section. The simulations are conducted for Reynolds numbers ranging from 2,500- 2,00,000. The variation of Nusselt number with the increase of turbulence intensity at particular Reynolds number is investigated. The turbulence intensity varies from 5% to 40%.

5.5.1 Triangular Prism

Figure 5.4 shows the validation at high Re with the work of Benim (2011) which shows reasonably good agreement with the present computation for Re between 2,500 - 25,000. It is seen that the present Nu_{avg} which is found out by RANS model and Without TP is in good agreement with Benim et al. (2011).
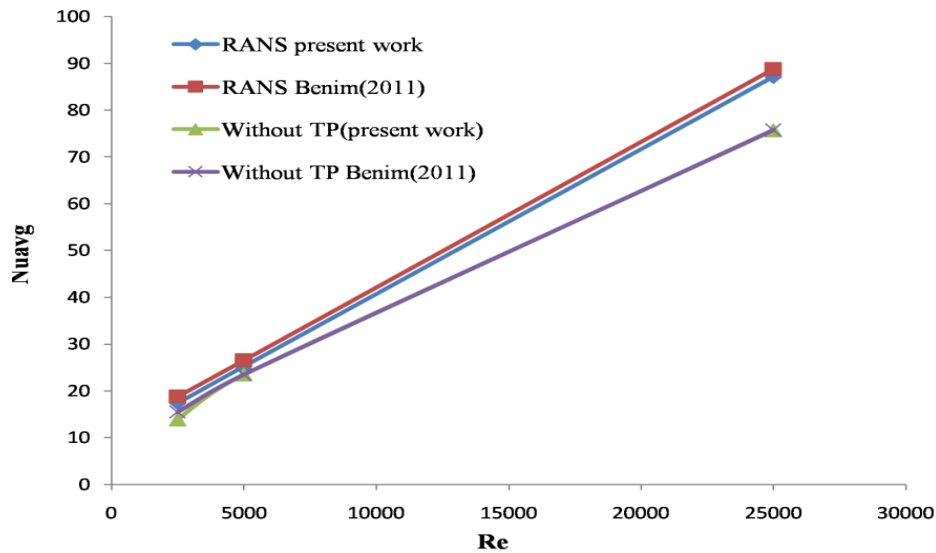
Figure 5.4: Validation of Averaged Nusselt number

Table 4 has shown the heat transfer data for the case with a triangular prism. The table shows the avg. value in the channel as well as asymptotic value. It can be observed that averaged Nusselt number as well as Nu_{asy} increases by about 10% in the channel when TP is present. The asymptotic values are almost the same with all the Reynolds number. The heat transfer enhanced is about 10-14% which is higher at high Re.

Table.4 **Heat transfer data for triangular prism**

Re_D	Nu_{avg}	$Nu_{avg,TP}$	Enhancement (%)	Nu_{asy}	$Nu_{asy,TP}$	Enhancement (%)
10,000	23.89	26.55	11.13	20.53	22.69	10.52
20,000	43.20	48.52	12.31	32.13	35.70	11.12
40,000	78.09	86.47	10.73	64.26	71.46	11.20
1,00,000	170.75	192.59	12.79	131.196	146.69	11.80
2,00,000	306.92	345.14	12.45	242.45	276.48	14.03

Figure .5.5 shows the Nu for the case with TP is compared with the case of the plane channel at Re-20,000 with a fixed 10% turbulence intensity. The plot shows that Nu value increases immediately after the location of TP. When the TP is present the asymptotic Nu value is found to be higher at the exit region.
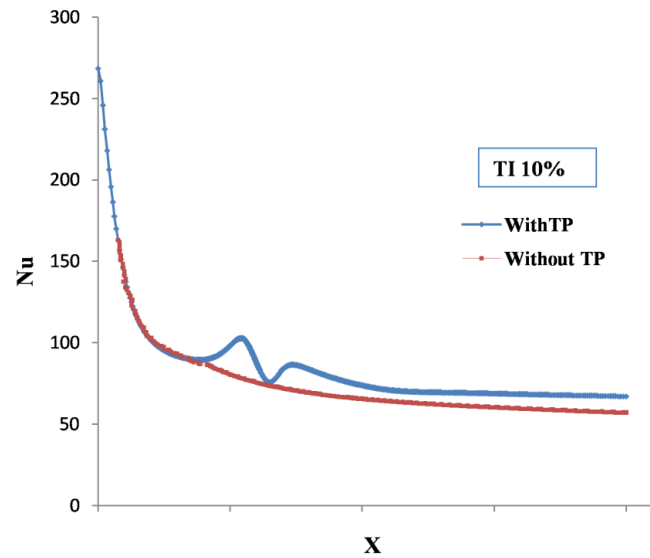
Figure 5.5: Nusselt number distribution at Reynolds number 20,000

Nusselt number distribution at different Re in presence of TP at turbulence intensity 10% is shown in Figure 5.6. From the graph, it can be observed those Nusselt number distribution patterns are similar. Though the magnitude of heat transfer increases with increasing the Reynolds number. The first peak is higher in magnitude compared to the second peak following the TP at Reynolds number 10,000, 20,000 and 40,000.
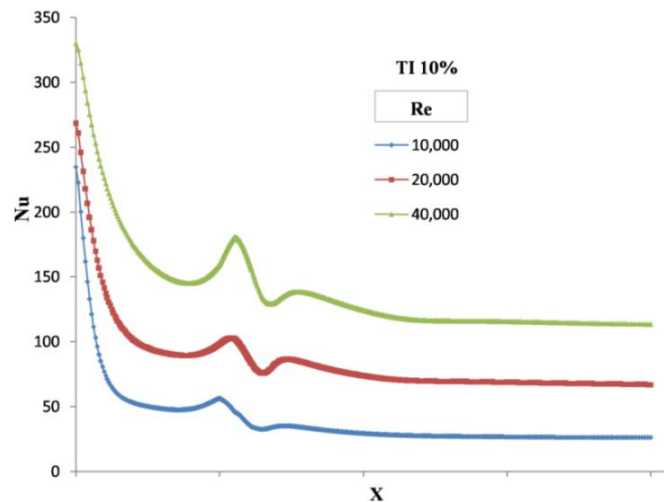
Figure 5.6: Nusselt number distribution along the channel wall

Earlier work by Kodjoan et al. (1995) shows the variation of turbulent intensity can lead to an increase in heat transfer. Accordingly, we calculated for different TI at the inlet. In figure 5.7, the Nu for the case with TP is compared with the case of the plane channel at Re 2,00,000

with different turbulence intensity. It can be seen that Nu increases immediately after the location of the TP with increasing the inlet turbulent intensity. There occurs a primary peak and crest further downstream. There is a change of 480-580 in average Nusselt number when TI changes from 5%-40%.
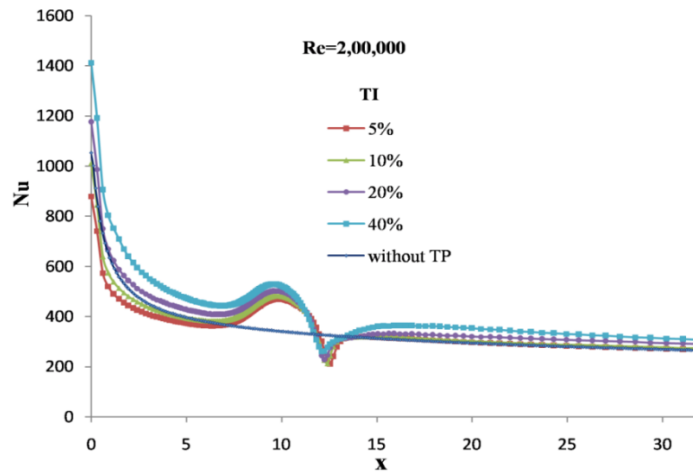
Figure 5.7: Nusselt number distribution along the channel wall at difference turbulence intensity

It is well known that the enhancement in heat transfer is associated with a penalty in terms if increase skin friction coefficient reading to higher pressure drop. Figure 5.8 presents the distributions of C_fRe, where it is evident that the presence of the TP involves increased the value of surface friction on the channel wall. Also, the rise of C_f following the TP persists even at far downstream locations.
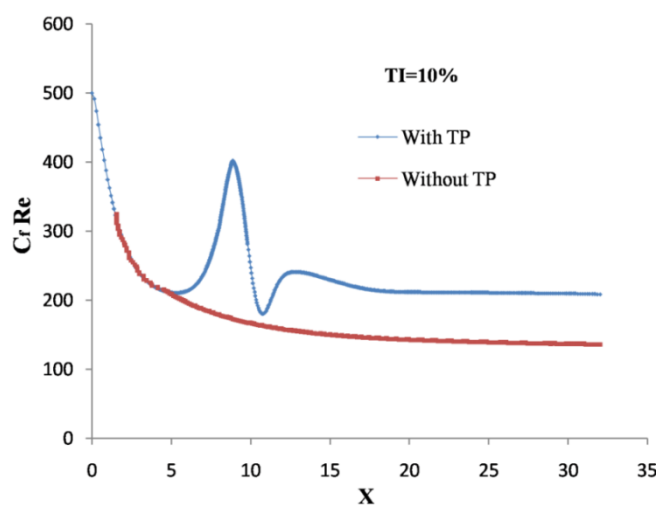
Figure 5.8: Distribution of skin friction coefficient at Reynolds number 20,000

In table 5 the effect of TI is present. The average Nu value is increased with increasing the TI for the case of a prism. For example, in the case of TP, the Nu value increases from 480 to 580 (as 20%) So it quantifies the TI effect on the TP shape bluff body is effective.

Table.5 **Effect of turbulence intensity for triangular prism**

Re_D	$Nu_{avg,TP}$		
	5% TI	**40% TI**	**% increase**
10,000	24.16	33.34	37
20,000	44.05	64.83	47
50,000	99.30	129.55	30
1,00,000	182.92	233.06	27
2,00,000	480	580	20

5.5.2 Diamond

The Nusselt number distributions at different Reynolds number in the presence of diamond is shown in figure 5.9. It is shown that the patterns are almost similar. However, the magnitude of heat transfer increases with increasing Re. The magnitude of the heat transfer is shifted towards downstream of the diamond. The second peak is higher compared to the first peak.
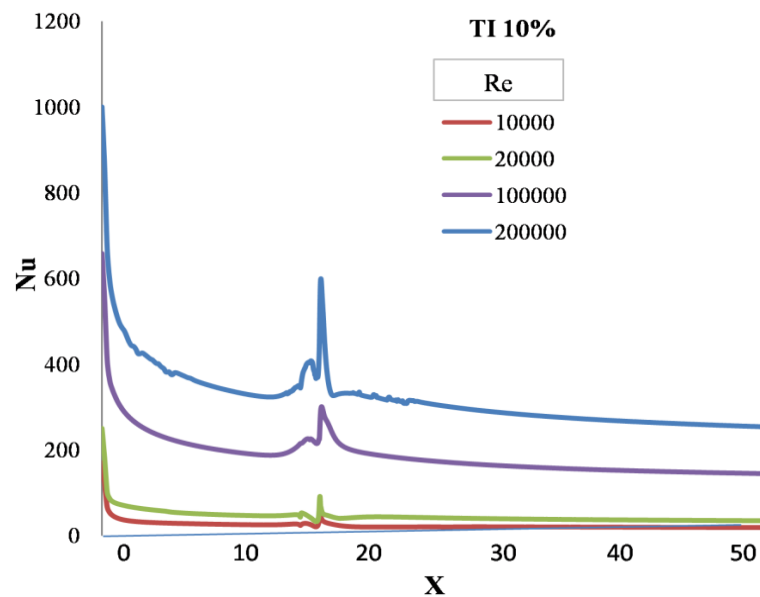
Figure 5.9: Distribution of Nu along channel in presence of diamond shape bluff body

Table 6 summarizes the heat transfer data. It can be observed from the table that the average Nu increases by about 4.6% in the duct when a diamond shaped bluff body is present.

Table.6 **Comparison of Heat Transfer for diamond**

Re_D	Nu_{avg_plane}	$Nu_{avg\_diamond}$	Enhancement(%)	Nu_{asy}	$Nu_{asy,diamond}$	Enhancement(%)
10,000	23.89	24.69	3.24	18.21	19.63	7.79
20,000	43.20	45.03	4.06	34.25	36.05	5.25
1,00,000	172.15	188.26	8.57	143.60	148.30	3.27
2,00,000	306.32	322.40	4.89	249.20	255.99	2.72

5.5.3. Trapezium

Figure 5.10 shows three different orientations of the trapezium. In the first case2(a) the short side is facing the flow, in case 1 (b) large side is facing flow and in case of 3 (c), the trapezium is symmetrically placed.

Figure 5.10: (a) small facing (case2) (b) large facing (case1) (c) symmetric (case3)

Nu number distribution at Re 2,00,000 with 10% turbulent intensity is shown in figure 5.11. It shows that the placement of trapezium affects the heat transfer pattern. The largest peak of heat transfer is seen for the short side facing the flow. For the vertically symmetric trapezium present, the enhancement is least.
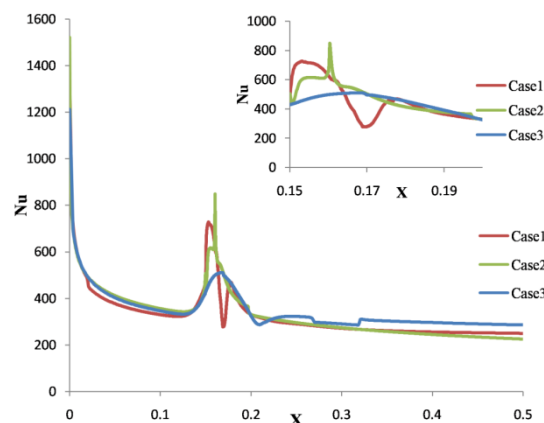
Figure 5.11: Distribution of Nu along channel wall in presence of trapezoidal shape bluffs body

101

In table 7 summaries of results are present. The average Nu number values are summarized for Re 20,000, 1,00,000, 2,00,000. Nu number value is higher in the case of TP compare to the diamond and trapezium. For example, the Nu value is 345.14 for TP compare to that diamond is 337.40 for fixed Re 2,00,000.

Table.7 **Comparison of Heat Transfer for different shape bluff body**

Re_D	$Nu_{avg,trapezium}$			$Nu_{avg,TP}$	$Nu_{avg,diamond}$
	Case1	Case2	Case3		
20,000	44.09	45.50	43.43	48.52	45.67
1,00,000	96.73	99.14	95.23	192.59	188.26
2,00,000	330.04	332.02	327.66	345.14	337.40

Figure 5.12 shows the distribution of friction factor vs. Reynolds number for three different shape bluff bodies. The curve shows that the friction factor is gradually decreasing up to Reynolds number approx 8,000. Beyond this point, the friction factor is almost the same. It is also seen that the friction factor is higher for the case of triangular prism compared to the other two bluff bodies.
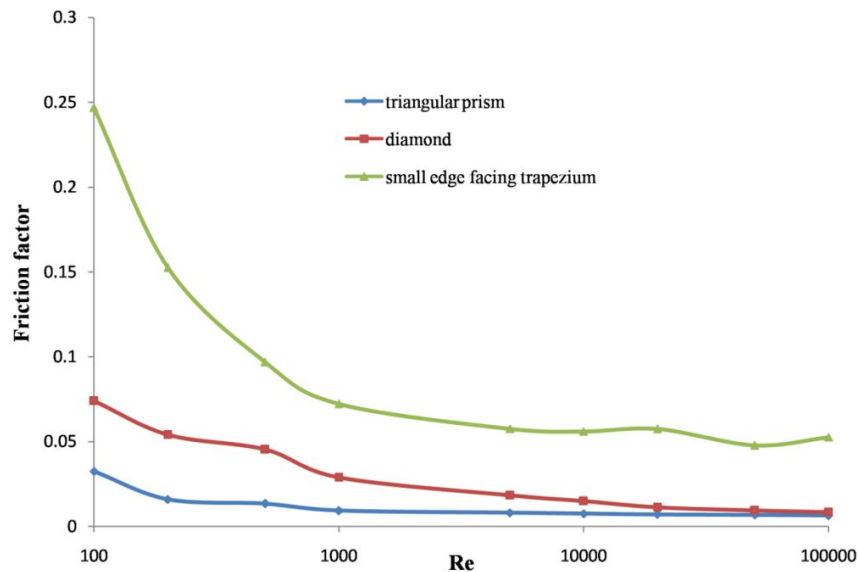
Figure 5.12: Distribution of friction factor against the Re in presence of different shape bluffs body

In figure 5.13, the distribution of the thermo hydraulic efficiency is shown against the Re. Here three orientation of trapezoidal shape bluff body is compared. The cases are a) small edge facing flow, b) large edge facing flow and c) symmetrically placed trapezium. When increasing the Reynolds number the thermo hydraulic performance steeply falls up to Re 1,000 for the symmetrically placed trapezium and Re=approx. 500 for large edge facing flow. Beyond that point, the thermo hydraulic efficiency gradually falls up to Re=about. 8000 and after that, the η is almost the same for the symmetrically placed trapezium. Beyond the Re of 500, in the case of the large edge facing flow, the thermo hydraulic efficiency gradually falls up to Re= 800, beyond that point the term hydraulic efficiency is almost the same.
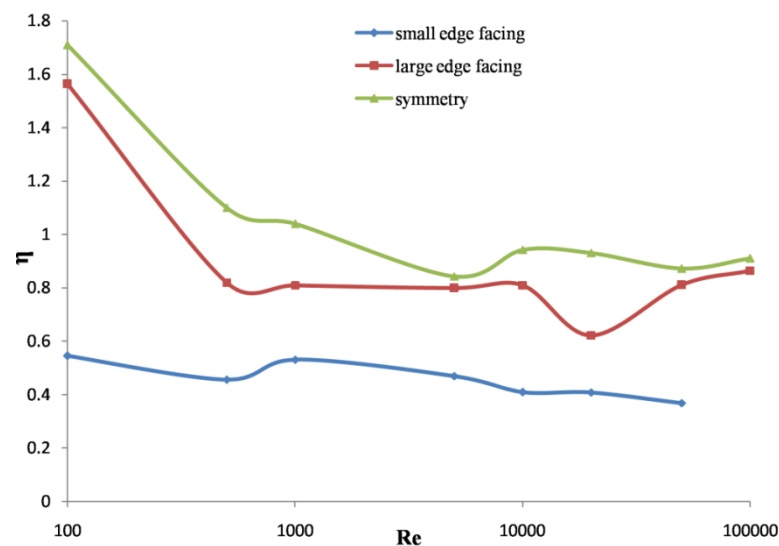
Figure 5.13: Distribution of thermo hydraulic efficiency vs. Re in three orientation of trapezoidal shape bluff body

It has been already mentioned that heat transfer is accompanied with an increase in pressure drop and hence a performance parameter (η) which combines heat transfer with pressure drop has been defined (see eq. 3.14, in chapter 3). A value over unity indicates that the pressure drop penalty does not overshadow the enhancement in heat transfer. In figure 5.14 an improvement of the thermo-hydraulic performance is only observed for very small Reynolds numbers up to about 1000 in the laminar region. With increasing Reynolds number, the thermo-hydraulic performance deteriorates rapidly up to Re = around1000. After that, a mild increase up to Re = approx. 1200 is observed. Beyond this point, the curve is almost the same up to Re=1,00,000. In this case, the frictional effects seem to play a dominant role and lead to a generally inferior thermal performance. It is, of course, obvious that for bluff bodies

pressure drop penalty is always high. The results indicate that among the bluff bodies used, triangular prism provides better performance.
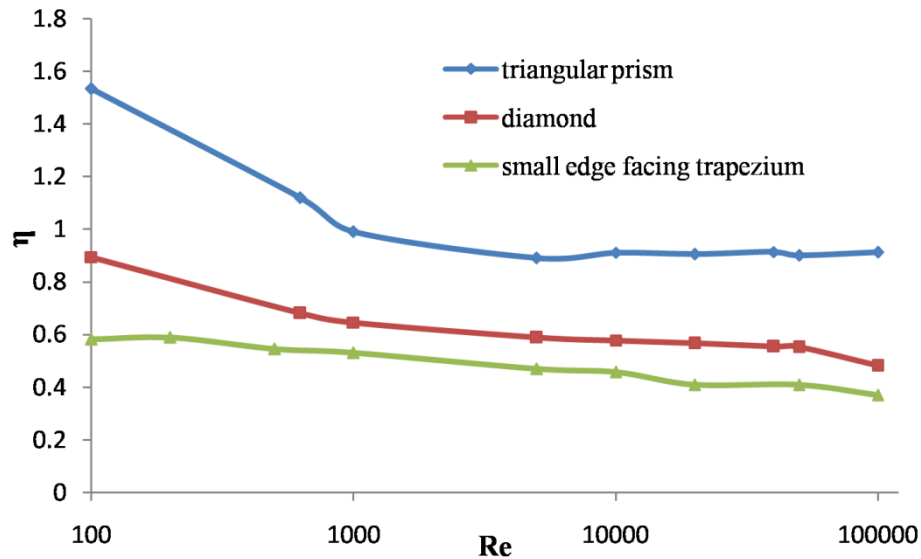
Figure 5.14: Distribution of thermo hydraulic efficiency vs. Re in three different shape bluff body

5.6 Summary

Heat transfer enhancement is estimated in a channel due to the presence of different types of bluff bodies using numerical simulation. The order of enhancement is higher (about 10%) in the case of triangular prism compare to the diamond and trapezoidal shape bluff body. Though augmentation is associated with enhanced skin friction coefficient, a comparative study using performance parameter combining friction and heat transfer shows triangular prism provided the best performance.

CHAPTER- 6

CONCLUSIONS AND FUTURE PROSPETCS

In the present work, heat transfer and fluid flow over bluff bodies of different shapes in a channel are investigated. Heat transfer augmentation on the wall due to the presence of bluff bodies is also investigated. The investigation was carried out for all three regimes encompassing laminar, transitional and turbulent flows using transition SST model. The particular focus of the work is the effect of inlet turbulent intensity on transport performance.

Bluff bodies of different forms have been considered in this work. These includes i) square cylinder, ii) circular cylinder, iii) triangular prism, iv) diamond, v) trapezium. For trapezoidal bodies, three different orientations are examined, they are large edge facing trapezoidal, small edge facing trapezoidal and symmetrical placed.

Convective heat transfer around different bluff bodies has been studied in this work in a large range of Reynolds number up to 2,00,000. The investigation evaluates the effect of turbulent intensity on both local and the averaged Nusselt number. The value of turbulent intensity is varied in the range of 5- 40%. Nusselt number is found to increase with increasing value of turbulent intensity but the distribution pattern around the bluff body is different at different levels of Re. Quantitative values of Nusselt number and drag coefficient have been tabulated for different shapes. The present simulations results (averaged Nusselt number) are found in good agreement with published results. It is observed that, the drag coefficient value is decreased with increasing the Reynolds number. The drag coefficients are significantly affected by increasing inlet turbulent intensity for all bluff bodies.

Heat transfer enhancement is estimated in a channel due to the presence of different types of bluff bodies using numerical simulation. The order of enhancement is higher (about 10%) in the case of triangular prism compare to the diamond and trapezoidal shape bluff body. As augmentation is associated with enhanced skin friction coefficient, a comparative study using performance parameter combining friction and heat transfer shows triangular prism provided the best performance. Trapezium with the small side facing upstream performs poorly over the diamond shaped cylinder. The gain in performance is higher at moderate Reynolds number level.

6.3 Future prospects

The research work is a primary attempt to analysis transport phenomena around the bluff bodies in cross flow at varying inlet turbulent intensity. This study also examines the possibility of heat transfer augmentation on channel walls by introducing bluff body of different shapes. The study is limited to two-dimensional computations which is of course an important limitation of the work.

Further improvement and advancement may consider the following aspects:

➢ Future extension of the work involves the computation of three -dimensional flow field as the present work is done in two -dimensional only.

➢ The extension of work can be carried out for bluff bodies will different orientations.

➢ The effect of Prandtl number is not included in this work. So, further computations at different Pr reveal the performance for other fluids like water, polymers or mineral oils.

➢ Unsteady RANS and simulations using LES may be carried out which can shed light on the turbulent structures and detailed turbulent statistics.

References

Abdollah, S., Mahdi, A., Noorallah, R., (2008), Experimental study of near wake flow behind a rectangular cylinder, American J. Applied Sciences, vol.5, pp. 917-926.

Abraham, A.P., Sparrow, E.M. and Tong, J.C.K., (2009), Heat transfer in all pipe flow regimes: laminar, transitional/ intermittent, and turbulent, Int. J. Heat and Mass Transfer, vol. 52, pp. 557–563.

Achenbach, E., (1968), Distribution of local pressure and skin friction around a circular cylinder in cross-flow up to Re $=5\times10^{6}$, J. fluid mech.,vol.34, part 4, pp. 625-639.

Ahmadi Motlagh, A.H. and Hashemabadi, S.H., (2008), CFD based evaluation of heat transfer coefficient from cylindrical particles, International Communications in Heat and Mass Transfer , vol. 12(35), pp. 674–680.

Ai, Y., Feng, D., Ye, H., Li, L., (2013), Unsteady numerical simulation of flow around 2-D circular cylinder for high Reynolds numbers, Application, vol. 12, pp. 2,180–184.

Bearman, P.W., Trueman, D.M., (1972), Aeronautical Quarterly, vol.23, pp. 229.

Bearman, P.W., Morel T., (1983), Effect of free stream turbulence on the flow around bluff bodies, Prog. Aerospace Sci. vol. 20, pp. 97-123.

Bearman, P.W., (1969), On vortex shedding from a circular cylinder in the critical Reynolds number regime, J. Fluid Mech, vol. 37, pp. 577–585.

Bearman, P.W., Trueman, D.M., (1972), An investigation of the flow around rectangular cylinders, Aeronaut. Quart., vol. 23, pp. 229-237.

Benim, A.C., Chattopadhyay, H. and Navahandi, A., (2011), Computational analysis of turbulent forced convection in a channel with a triangular prism, Int. J. Thermal Science, vol. 50, pp. 1973-1983.

Benim, A.C., Cagan M., Nahavandi, A., Pasqualotto, E., August 25-27., (2007), RANS Predictions of Turbulent Flow Past a Circular Cylinder over the Critical Regime, 5th IASME / WSEAS international Conference on Fluid Mechanics and Aerodynamics, Athens, Greece.

Benim, A.C., Pasqualotto, E. and Suh, S.H., (2008), Modelling of turbulent flow past a circular cylinder by RANS, URANS, LES and DES', Progress in Computational Dynamics, vol. 8(5), pp. 299-307.

Bergles, A.E., (1983), Techniques to augment heat transfer, in: Handbook of Heat Transfer Applications, McGraw-Hill, New York, pp. 31-80.

Bergles, A.E., (2011), Recent developments in enhanced heat transfer, Heat Mass Transfer, vol. 47(8), pp. 1001–1008.

Berger, E., Wille, R., (1972) Periodic flow phenomena. Annu. Rev. Fluid Mech. vol.4, pp. 313.

Berrone, S., Garbero, V., Marro, M., (2011), Numerical simulation of low-Reynolds number flows past rectangular cylinders based on adaptive finite element and finite volume methods. Comput. Fluids vol. 40, pp. 92–112.

Bhattacharyya, S., Chattopadhyay, H., Benim, A.C., 2017, Simulation of heat transfer enhancement in duct flow with twisted tape insert, Progress in Computational Fluid Dynamics, an International Journal, vol. 17, no. 3, pp. 193-197.

Biswas, G. and Chattopadhyay, H., (1992), Heat-transfer in a channel with built-in wing-type vortex generators, Int. J. Heat Mass Transfer, vol.35, no.4, pp. 803–814.

Breuer, M., Bernsdorf, J., Zeiser, T., and Durst. F., (2000), Accurate computations of the laminar flow past a square cylinder based on two different methods: Lattice-Boltzmann and finite volume, Int. J. Heat Fluid Flow, vol. 21, pp. 186–196.

Buresti, G., Lombardi,G. and Talamelli, A., (1998), Low aspect-ratio triangular prisms in cross-flow: measurements of the wake fluctuating velocity field, J. Wind Eng. Ind. Aerodynamic, vol. 74–76 , pp. 463–473.

Buresti, G. and Lombardi, G., (1998), Experimental analysis of the free-end and upper wake flow fields of finite triangular prisms, in: G. Diana, F. Cheli, A. Zasso (Eds.), Proceedings of the Seventh National Congress on Wind.

Camarri, S., Salvetti, M., Buresti, G., (2006), Large-eddy simulation of the flow around a triangular prism with moderate aspect ratio, vol. 94(5), PP. 309-322.

Cantwel, L. B., Coles, D., (1983), An experimental study of entrainment and transport in the turbulent near wake of a circular cylinder, J. Fluid Mech., vol. 136, pp. 321-374.

Catalona, P., Wang, Laccarina, P., Moin, P G., (2003), Numerical simulation of the flow around a circular cylinder at high Reynolds numbers, Int. J. of Heat and Fluid Flow, vol. 24, Issue 4, pp. 463–469.

Chaterjee, D. and Mondal, B., (2012), Effect of thermal buoyancy on the two-dimensional upward flow and heat transfer around a square cylinder, Heat Transfer Engineering, vol.33(12), pp. 1063-1074.

Chatterjee, D. Mondal, B. and Halder, P., (2013), Unsteady forced convection heat transfer over a semicircular cylinder at low Reynolds numbers, Int. J. Computation and Methodology, vol. 6(63), pp. 411-429.

Chattopadhyay, H., (2007), Augmentation of heat transfer in a channel using a triangular prism, Int. J. Thermal Sciences, vol.46, pp. 501-505.

Chen, O. M., Utnes, T., Holmedel, L. E., Pettersen, D. M. B., (2009), Numerical simulation of flow around a smooth circular cylinder at very high Reynolds numbers, marine structures, vol. 22, pp. 142-153.

Chen, Z., Li, Q., Meier, D., Warnecke, H. J., (1997), Convective heat transfer and pressure loss in rectangular ducts with drop-shaped pin fins, Heat and Mass Transfer, vol. 33 (3) , pp. 219–224.

Chen, X.B., Yu, P., Winoto, S.H., (2009), Numerical analysis for the flow past a porous trapezoidal-cylinder based on the stress-jump interfacial-conditions, International Journal of Numerical Methods for Heat and Fluid Flow, vol.19(2), pp. 223-241.

Dalal, A., Eswaran, V., Biswas, G., (2008), A Finite-Volume Method for Navier-Stokes Equations on Unstructured Meshes, Numerical Heat Transfer, Part B, pp. 54238–259.

Dalton, C. and Zheng, W., (2003), Numerical solutions of a viscous uniform approach flow past square and diamond cylinders, J. of Fluids and Structures, vol. 18, pp. 455-465.

Courchesne, J., Leneville, A., (1997), J. of Fluid Eng., Trans. ASME 101, vol. 101, pp. 506.

Davis, R. W., and Moore, E F., (1982), A numerical study of vortex shedding from rectangles, J. Fluid Mech., vol. 116, pp. 475–506.

Dhiman. A., Ghosh. R., (2013), Computer simulation of momentum and heat transfer across an expanded trapezoidal bluff body, Int. J. Heat and Mass Transfer, vol.59, pp. pp. 338–352.

Dhiman, A. Radhe, S., (2011), Unsteady Heat Transfer from an Equilateral Triangular Cylinder in the Unconfined Flow Regime, International Scholarly Research Network , ISRN Mechanical Engineering, Article ID 932738, 13pages.

Davenport, AG., (1962), Buffeting of a suspension bridge by storm winds. J Struct Div ASCE vol. 88(ST3), pp. 233–68.

Djeridi, H.,Braza, M., Perrin, R., Harran, G., Cid, E., Cazin, S., (2003), Near-Wake Turbulence Properties around a Circular Cylinder at High Reynolds Number, Flow,vol.71(1), pp. 19–34.

Ding, H., Shu, C., Yeo, K. S and Xu, D., (2004), Simulation of incompressible viscous flow past a circular cylinder by hybrid FD scheme and meshless least square-based finite difference method, Computer Methods in Applied Mechanics and Engineering, vol.193, pp. 727-744.

Doi, K. and Komai, H. T., (1977), Heat/mass transfer in Taylor vortex flow with constant axial flow rates. Int. J. Heat and Mass Transfer, vol. 20, pp. 57–63.

Dutta, S., Panigrahi, P. K., Muralidhar, K., (2004), Effect of orientation on the wake of a square cylinder at low Reynolds numbers, Indian J. of Engineering & Materials Sciences, vol. 11, 447-459, Steady and unsteady regimes, Asia-Pac. J. Chem. Eng., in press.

Edwards, F.J. and Alker, G.J.R., (1974), The improvement of forced convection surface heat transfer using surface protrusions in the form of (a) cubes and (b) vortex generators. Proceedings of the Fifth International Heat Transfer Conference Tokyo , pp. 2,2244–2248.

Elghnam, R. I., (2014), Experimental and numerical investigation of heat transfer from a heated horizontal cylinder rotating in still air around its axis, Ain Shams Eng., vol. 5, pp. 177-185.

Farouk, B., Guceri, S. I., (1982), Natural and Mixed Convection Heat Transfer Around a Horizontal Cylinder Within Confining Walls, Num. Heat Transfer , vol. 5, pp. 329–341.

Fan, A.W., Deng, J.J., Nakayama, A. and Liu, W., (2012), Parametric study on turbulent heat transfer and flow characteristics in a circular tube fitted with louvered strip inserts, Int. J. Heat and Mass Transfer, September, vol. 55, no. 19–20, pp.5205–5213.

Fujii, K., (2005), Progress and future prospects of CFD in aerospace − wind tunnel and beyond. Progr Aero Sci , vol.41: pp. 455–70.

Gartshore, I, S., (1973), The effects of free stream turbulence on the drag of rectangular two-dimensionalprisms, Boundary Layer Wind Tunnel Laboratory 4-73, The University of Western Ontario.

Garcia, A. A., Gutiérrez-Torres, C., Del, C., Jiménez-Bernal, J. A., Barbosa-Saldaña, J G., Mollinedo-Ponce de León, H. R., Martínez-Delgadillo, S. A., (2013), Numerical simulation of the subcritical flow over a circular cylinder with u and v grooves, Proceedings of the ASME 2013 Int. Mechanical Engineering Congress and ExpositionIMECE2013,San Diego, California, USA.

Gupta, A.K, Sharma, A, Chhabra, R.P, Eswaran, V.B., (2003), Two-dimensional steady flow of a power-law fluid past a square cylinder in a plane channel: momentum and heat-transfer characteristics, Industrial and Engineering Chemistry Research, vol. 42, pp. 5674–5686.

Golani, R., Dhiman, A. K., (2014), Fluid flow and heat transfer across a circular cylinder in the unsteady flow regime, Int. J. Eng. And Science, vol. 3, pp. 08-19.

Goujan-Durand, S., Renffer, K., Wesfried, JE., (1994), Downstream evolution of the Benard-von-Karman instability, Phys Rev E, vol.50, pp. 308.

Haan, Jr. F. L., Kareem, A., Szewczyk, A. A., (1998), The effects of turbulence on the pressure distribution around a rectangular prism, J. of Wind Eng. and Industrial Aerodyn., vol. 77 and 78, pp. 381-392.

Hasan, M., Dhiman, A., (2010), Flow and heat transfer over a trapezoidal cylinder, 37th National & 4th International Conference on Fluid Mechanics and Fluid Power, At IIT Madras, India.

Hiravennavar, S.R., Tulapurkara, E.G. and Biswas, G., (2007), A note on the flow and heat transfer enhancement in a channel with built-in winglet pair, Int. J. Heat Fluid Flow, vol. 28, no. 2, pp. 299–300.

Igarashi, T., (1987), Int. J. Heat Mass Transfer, vol.30, pp. 893.

Isaev, S. A., Leontiev, A. I., Kudryavtsev, N. A., Baranova, T. A., Lysenko, D. A., (2005) , Numerical simulation of unsteady state heat transfer under conditions of laminar transverse flow past a circular cylinder, High Temperature, vol. 43 , pp. 746 − 759.

Islam, T., Hassan R.M.S., (2013), Experimental and Numerical Investigation of Flow over a Cylinder at Reynolds Number 105, J. Modern Science and Technology vol. 1, pp. 52-60.

Islam, U.S., Abbasi, S.W., Rahman, H., (2014), Force Statistics and Wake Structure Mechanism of Flow around a Square Cylinder at Low Reynolds Numbers International Journal of Mechanical, Aerospace, Industrial, Mechatronic and Manufacturing Eng., vol. 8, pp. 1405-1410.

Islam, U.S., Zhou, C.Y., Shah, A., Xie , P., (2012), Numerical simulation of flow past rectangular cylinders with different aspect ratios using the incompressible lattice Boltzmann method, J. of Mechanical Science and Technology, vol. 26 (4), pp. 1027-1041.

Kahawita, R., Wang, P., (2002), Numerical simulation of the wake flow behind the trapezoidal bluff bodies, Computers and fluids, vol. 31, pp. 99-112.

Kato, M., Launder, B. E., (1993), The modeling of turbulent flow around stationary and vibrating square cylinders. Ninth Symposium on Turbulent Shear Flows, Paper 10-4, Kyoto, Japan.

Kawamura, T., Kuwahara, K., (1984), Computation of high Reynolds number flow around circular cylinder with surface roughness, AIAA Paper 84-0340, vol. 4, pp. 450-480.

Kelkar, K.M., Patankar, S.V., (1992), Numerical prediction of vortex shedding behind a square cylinder, Int. J. Numerical Methods for Fluids, vol. 14, pp. 327–341.

Kadiyala, P.K., Chattopadhyay, H., 2017, Numerical Analysis of Heat Transfer from a Moving Surface Due to Impingement of Slot Jets, Heat Transfer Engineering, pp. 1-7.

Kim, D.H., Yang, K.S., Senda, M., (2004), Large-Eddy Simulation of Turbulent Flow Past a Square Cylinder Confined in a Channel, Comput. Fluids, vol. 33(1), pp. 81–96.

King, JPC., (2003), The aerodynamics of long-span bridges. Ph.D. Thesis, Faculty of Engineering, University of Western Ontario.

Kondjoyan, A., and Daudin, J.D., (1995), Effects of free stream turbulence intensity on heat and mass transfers at the surface of a circular cylinder and an elliptical cylinder, axis ratio 4, Int. J. Heat Mass Transfer, vol. 10(38), pp. 1735- 1749.

Knisely, C.W., J. of Fluid and Structures, (1990), vol.4, pp. 371.

Lehmkuhl, O., Rodríguez, I., Borrell, R., Chiva, J., Oliva, A., (2014), Unsteady forces on a circular cylinder at critical Reynolds numbers, physics of fluids, vol. 26, pp. 110-125.

Leonard, B.P., Mokhtari, (1990), S.ULTRA-SHARP Nonoscillatory Convection Schemes for High-Speed Steady Multidimensional Flow. NASATM1-2568 (ICOMP-90-12).NASA, Lewis Research Center.

Li, Q., Chen, Z., Flechtner, U., Warnecke, H.J., (1998), Heat transfer and pressure drop characteristics in rectangular channels with elliptic pin fins, Int. J. Heat and Fluid Flow, vol. 19 (3), pp. 245–250.

Li, Q. S., Melbourne, W.H., (1995), Effects of turbulence on surface pressures of a flat plate and rectangular cylinders in separated and reattaching flows, Papers for the 9th Int. Conf. on Wind Engineering, vol. 1,Wiley Eastern Limited, New Delhi.

Liu, G., Kopp, G.A., (2011), High-resolution vortex particle simulations of flows around rectangular cylinders. Comput. Fluids, vol. 40, pp. 2–11.

Liu, X., Wei, A., Luo, K., Fan, J., (2015), Numerical study of the effects of particles on the near wake around a circular cylinder, Int. J. of Computational Fluid Dynamics, vol. 29(2), pp. 150-160.

Menter, F.E., Kubacki, T.S.E., (2013), Transition modeling based on local variables in: Fifth International Symposium on Engineering Turbulence Modeling and Measurements, Mallorca, Spain.

Mittal, R., Balachander, S., (1995), Effect of three-dimensionality on the lift and drag of nominally two-dimensional cylinders, Phy. of Fluids, vol. 7, pp. 1841- 1865.

Mochida, A., Murakami, S., Tominaga, Y., Kobayashi, H., (1996), Large eddy simulation of turbulent vortex shedding flow past 2-D square cylinder using Dynamic SGS model (Part 1), J. of Architecture Planning and Environmental Engineering (Transactions of Architectural Institute of Japan) No. 479, pp. 41-47.

Motlagh, A. H. A., Hashemabadi, S. H., (2008), CFD based evaluation of heat transfer coefficient from cylindrical particles, Int. Comm. in Heat and Mass Transfer, vol. 12(35), pp. 674–680.

MurakamI S. Mochida A., (1995), On turbulent vortex shedding flow past 2-D square cylinder predicted by CFD, J. of wind Eng. and Industrial Aerodyn. vol. 54/55, pp. 191-211.

Najjar, F.M., Balachandar, S., (1998), Low frequency unsteadiness in the wake of a normal flat plate, J. of Fluid Mech., vol. 370, pp. 101–147.

Nakagawa, S., Nitta, K., Senda, M., (1999), An experimental study on unsteady turbulent near wake of a rectangular cylinder in, channel flow, Experiments in Fluids, vol.27, pp. 284-294.

Nakagawa, S., Senda, M., Hiraide, A., Kikkawa, S., (1999), Heat transfer characteristics in a channel flow with a rectangular cylinder. JSME Int J B, vol.42(2), pp. 188–96.

Nakaguchi, H., Hasimoto, K., and Muto, S., (1968), J. Japan Soc. Aero. Space Sci, vol. 16(1).

Nakamura, H., Igarashi, T., (2004), Variation of Nusselt number with flow regimes behind a circular cylinder for Reynolds numbers from 70 to 30,000, Int. J. Heat and Mass Transfer, vol.47(23), pp. 5169 –5173.

Nakaguchi, H., Hashimoto, K., Muto, M., (1968), An experimental study on aerodynamics drag of rectangular cylinders, J. Japan Society of Aeronautical and Space Sci., vol.16, pp. 1-5.

Nakamura, Y., Ozono, S., (1987), The effects of turbulence on a separating and reattaching flow, J. Fluid Mech., vol. 178, pp. 477-490.

Nakamura, Y., Mizota, T., (1975), J. Eng. Mech, Div., Proc. ASCE,101:EM2,125.

Norberg, C., (1993), Flow around rectangular cylinders: Pressure forces and wake frequencies, J. of Wind Eng. and Industrial Aerodyn., vol. 40, pp. 187-196.

Nozawa, K., Tamura, T., (1998), An appropriate approach to the application of large-eddy simulation to complex turbulent flow past a square cylinder, J. of Struc. Mech. and Earthquake Eng., vol. I-43, 591, pp. 151-161.

Okajima, A., (1982), Strouhal number of rectangular cylinders, J. of Fluid Mech., vol.123, pp. 379-398.

Okajima A., (1990), Numerical simulation of flow around rectangular cylinders, J. of Wind Eng. and Industrial Aerodyn., vol. 33, pp. 171-180.

Okajima, A., Nagahisa, T., and Rokugoh, A., (1990), A numerical analysis of flow around rectangular cylinders, The Japan Society of Mechanical Engineers, Series II, vol.33 No.4, pp. 702-721.

Okajima, A., Sakuda, Yi. A., and Nakano, T., (1997), Numerical study of blockage effects on aerodynamics characteristics of oscillating rectangular cylinder, J. Wind Engg. Ind. Aerodyn, vol. 67-68, pp. 91-102.

Olawore, A.S., Odesola, I.F., (2013), 2D Flow around a Rectangular Cylinder a Computational Study, An Int. J. of Science and Technology, vol. 2 (1), pp. 1-26.

Paliwal, B, Sharma, A, Chhabra, R.P, Eswaran, V., (2003), Power law fluid flow past a square cylinder: momentum and heat transfer characteristics. Chemical Eng. Science, vol.58, pp. 5315–5329.

Ponta, L. F., Aref, H., (2004), Strouhal-Reynolds number relationship for vortex streets, Phys. Review Letters, vol. 93, No. 8, pp. 1-4.

Posdziech, O., Grundmann, R., (2007), A systematic approach to the numerical calculation of fundamental quantities of the two-dimensional flow over a circular cylinder, J. Fluids Struct., vol. 23, pp. 479 – 499.

Prasad, A., and Williamson, C.H.K., (1997), The instability of the shear layer separating from a bluff body, J. Fluid Mech., vol. 333, pp. 375–492.

Pal, T.K., Chattopadhyay, H., and Mandal, D.K., (2018), Flow and heat transfer due to impinging annular jet, Int. J. Fluid Mechanics Research. (in press).

Park, J., Kwon, K. and Choi, H., (1998), Numerical solutions of flow past a circular cylinder at Reynolds number up to 160.KSME , Int. J. 12, pp. 1200-1205.

Rajani, B. N., Kandasamy, A., Majumdar, S., (2008), Numerical simulation of laminar flow past a circular cylinder, Applied Mathematical Modelling, vol. 33, pp. 1228 - 1247.

Robichuax, J., Balachandar, S., Vanka, S.P., (1999), Three-dimensional floquet instability of the wake of square cylinder, Phys. of Fluids, vol. 1, pp. 560-578.

Rodriguez, I., Lehmkuhl, O., Borrell, R., Oliva, A., (2012), Flow dynamics in the wake of a sphere at sub-critical Reynolds numbers. Computers & Fluids, vol. 80, pp. 223-243.

Rodriguez, I., Lehmkuhl, O., Borrell, R., Paniagua, L., Perez-Segarra, C. D., (2013), High Performance Computing of the flow past a circular cylinder at critical and supercritical Reynolds numbers, Parallel Comp. Fluid Dynamics Conference, Procedia Engineering, vol. 61, pp. 166 – 172.

Rogers, SE., Roth, K., Cao, HV., Slotnick, JP., Whitlock, M., Nash, SM., (2001), Computation of viscous flow for a Boeing 777 aircraft in landing configuration. J Aircraft, vol. 38(6), pp 1060–8.

Rokugou, A., Okajima, A., and Kamiyama, K., (2002), Numerical Analysis of Flow around Rectangular Cylinders with Various Side Ratios. Japan.

Roshko, A., (1954), On the development of turbulent wakes from vortex streets. NACA Rep.,1191.

Roshko, A., (1961), Experiments on the flow past a circular cylinder at very high Reynolds number, J. Fluid Mech, vol. 10, pp. 345–356.

Saha, A. K., Biswas, G., Muralidhar, K., (1999), Numerical study of turbulent unsteady wake behind a partially enclosed square cylinder using RANS Computer Methods, Applied Mechanics and Eng., vol.178(3), pp. 323-341.

Saha, A. K., Biswas, G., Muralidhar, K., (2001), Two-dimensional study of the turbulent wake behind a square cylinder subject to uniform shear, J. Fluids Eng., vol. 123, pp. 595–603.

Saeedi, M., LePoudre, P.P., Wang, B.C., (2014), Direct numerical simulation of turbulent wake behind a surface-mounted square cylinder, Journal of Fluids and Structures, vol. 51, pp. 20–39.

Samani, M., Bergstrom, D.J., (2015), Effect of a wall on the wake dynamics of an infinite square cylinder, Int. J. Heat and Fluid Flow, vol. 55, pp. 158–166.

Sanitjai, S and Goldstein, R.J., (2004), Forced convection heat transfer from a circular cylinder in cross flow to air and liquids, Int. J. Heat and Mass Transfer, vol. 12(47), pp. 4795–4805.

Sen, S., Mittal, S., Biswas, G., (2011), Flow past a square cylinder at low Reynolds numbers, Int. J. Numer. Meth. Fluids, vol. 67, pp. 1160–1174.

Scholeten, J.W. and Murray, D.B., (1998), Unsteady heat transfer and velocity of a cylinder in cross flow- I. Low free stream turbulence, Int. J. Heat Mass Transfer, vol. 10(41), pp. 1139-1148.

Sharma, A. and Eswaran, V., (2004), Heat and fluid flow across a square cylinder in the two-dimensional laminar flow regime, Numerical heat transfer , vol. 45, pp. 247-269.

Shang, J.S., (2004), Three decades of accomplishments in computational fluid dynamics. Progr Aero Sci, vol. 40(3), pp. 173–97.

Shimada, K., Ishihara, T., (2002), Application of a modified k-εmodel to the prediction of aerodynamic characteristics of rectangular cross-section cylinders, J. of Fluids and Struct., vol. 16(4), pp 465-485.

Shu, C., Qu, K., Niu, X.D. and Chew, Y.T., (2005), Numerical simulation of flow past a rotational circular cylinder by Taylor-series-expansion and least squares-based lattice Boltzmann method, Int. J. of Modern Physics C, vol. 16, pp. 1753-1770.

Singh, S.P., Mittal, S., (2005), Flow past a cylinder: shear layer instability and drag crisis numerical., Int. J. numer. meth. fluids, vol. 47, pp. 75–98.

Singh, D., Premachandran, K.B.S., (2015), Effect of nozzle shape on jet impingement heat transfer from a circular cylinder, Int. J. of Thermal Sciences, vol. 96, pp. 45–69.

Smyth, R., Zurit, P., (1994), Heat transfer at the outer surface of a rotating cylinder in the presence of axial flows, Transactions on Eng. Sciences, vol. 5, WIT Press, UK.

Suzuki, K., Suzuki, H., (1994), Unsteady Heat Transfer in a Channel Obstructed by an Immersed Body, Annu. Rev. Heat Transfer, vol.5, pp. 177–206.

Sparrow, E.M., Abraham, J.P. and Jimmy, C.K., (2004), Tong. Archival correlations for average heat transfer coefficients for non-circular and circular cylinders and for spheres in cross-flow, Int. J. Heat and Mass Transfer, vol. 47, pp. 5285–5296.

Srikant, S., Dhiman, A.K. and Bijjam, S., (2010), Confined flow and heat transfer across a triangular cylinder in a channel, Int. J. of Thermal Science, vol. 49, pp. 2191-2200.

Taned, T., (1965), Experimental investigation of vortex streets, J. Phys. Soc. Jpn. vol. 20, pp. 1714–1721.

Tamura, T., Ito, Y., (1996), Aerodynamic characteristics and flow structures around a rectangular cylinder with a section of various depth/breadth ratios. J. of Structure. and Construction Eng., (Rans actions of Architectural Institute of Japan) vol. 486, pp. 153-162.

Taylor, Ian J. (1999), Study of bluff body flow fields and aero elastic stability using a discrete vortex method, Phd thesis.

Thompson, M.C., Leweke, T., Williamson, C.H.K., (2001), The physical mechanism of transition in bluff body wakes, J. of Fluids and Struct.,vol.15, pp. 607-616.

Torii, S., Yang, W.J. and Umeda, S., (2000), Evolution of vortices behind single Diamond-shaped Cylinders in a free stream flow. Proceedings of the ASME/IMECE conference, Orlando.

Valencia, A., (1995), Heat transfer enhancement in a channel with a built-in rectangular cylinder, Heat Mass Transfer, vol.30, pp. 423–427.

Van Leer, B., (1979), Towards the ultimate conservative deference scheme. V. A second-order sequel to Godunoy's method, J. Computational Physics , vol. 32, pp. 101-136.

Venugopal, A, Agrawal, A, Prabhu, S.V., (2015), Spanwise correlations in the wake of a circular cylinder and a trapezoid placed inside a circular pipe, J. of Fluids and Struct. vol. 54, pp. 536–547.

Wang, F., Zhang, J., Wang, S., (2012), Investigation on flow and heat transfer characteristics in rectangular channel with drop-shaped pin fins, Propulsion and Power Research, vol. 1(1): pp. 64–70.

Wang, H., Zhou, Y., Chan, C., Zhou, T., (2009), Momentum and heat transport in a finite-length cylinder wake. Experiments in Fluids, vol. 46, pp. 1173–1185.

Werner, H., Wengle, H., (1989), Large-eddy simulation of turbulent flow over a square rib in a channel. Adv. Turbul., vol. 2, pp. 418–423.

Wang, X. K., Tan, S. K., (2008), Near-wake flow characteristics of a circular cylinder close to a wall, J. Fluids Struct., vol. 24, pp. 605–627.

Williamson, C.H.K., (1996), Vortex Dynamics in the Cylinder Wake, Annual Review of Fluid Mechanics, vol. 28(1), pp. 477–539.

Webb, R.L. and Kim, N.H., (2005), Principles of Enhanced Heat Transfer, Taylor& Francis, New York .

Whitaker, A., (1976), Elementary Heat Transfer Analysis, Pergamon Press, Inc, New York.

Williamson, CHK., (1988a), Defining a universal and continuous Strouhal-Reynolds number relationship for the laminar vortex shedding of a circular cylinder. Phys. Fluids vol. 31: pp. 2742.

Williamson, CHK., (1988b), The existence of two stages in the transition to three dimensionality of a cylinder wake. Phys. Fluids, vol. 31: pp. 3165.

Yoon, D.H., Yang, K.S. and Choi, C.B., (2009), Heat transfer enhancement in channel flow using an inclined square cylinder, J. Heat Transfer – Trans. ASME, vol. 131, no. 7.

Yoon, D.Y., Yang, K.S., Choi, C.B., (2009), Heat Transfer Enhancement in Channel Flow Using an Inclined Square Cylinder, J. of Heat Transfer, vol. 131 / 074503-4.

You, J.Y. and Kwon, O.J., (2012), Numerical assessment of turbulent models at a critical regime on unstructured meshes, J. Mechanical Science and Technology, vol. 26 (5), pp. 1363~1369.

Zheng, D.D., Zheng, T., (2011), Comparison study on flow fields in vortex flow sensors with circular cylinder and trapezoidal cylinder bluff bodies, Proceedings of the International Conference on Machine Learning and Cybernetics, Guilin, 10-13 July.

Zukauskas, A., (1978), Heat transfer from tubes in cross flow in: J.P. Harnett, T.F. Irvine Jr. (Eds.), Advances in Heat Transfer, vol. (8), Academic Press, Inc, New York.